

INFORMATION TO USERS

This manuscript has been reproduced from the microfilm master. UMI films the text directly from the original or copy submitted. Thus, some thesis and dissertation copies are in typewriter face, while others may be from any type of computer printer.

The quality of this reproduction is dependent upon the quality of the copy submitted. Broken or indistinct print, colored or poor quality illustrations and photographs, print bleedthrough, substandard margins, and improper alignment can adversely affect reproduction.

In the unlikely event that the author did not send UMI a complete manuscript and there are missing pages, these will be noted. Also, if unauthorized copyright material had to be removed, a note will indicate the deletion.

Oversize materials (e.g., maps, drawings, charts) are reproduced by sectioning the original, beginning at the upper left-hand corner and continuing from left to right in equal sections with small overlaps.

Photographs included in the original manuscript have been reproduced xerographically in this copy. Higher quality 6" x 9" black and white photographic prints are available for any photographs or illustrations appearing in this copy for an additional charge. Contact UMI directly to order.

ProQuest Information and Learning
300 North Zeeb Road, Ann Arbor, MI 48106-1346 USA
800-521-0600

UMI[®]

University of Alberta

**Effects of Trapped Air on Flow Transients in Rapidly
Filling Sewers**

by

Fayi Zhou



A thesis submitted to the
Faculty of Graduate Studies and Research
in partial fulfillment of the requirements for the degree of
Doctor of Philosophy

in

Water Resources Engineering
Department of Civil and Environmental Engineering

Edmonton, Alberta

Fall 2000



**National Library
of Canada**

**Acquisitions and
Bibliographic Services**

**395 Wellington Street
Ottawa ON K1A 0N4
Canada**

**Bibliothèque nationale
du Canada**

**Acquisitions et
services bibliographiques**

**395, rue Wellington
Ottawa ON K1A 0N4
Canada**

Your file Votre référence

Our file Notre référence

The author has granted a non-exclusive licence allowing the National Library of Canada to reproduce, loan, distribute or sell copies of this thesis in microform, paper or electronic formats.

The author retains ownership of the copyright in this thesis. Neither the thesis nor substantial extracts from it may be printed or otherwise reproduced without the author's permission.

L'auteur a accordé une licence non exclusive permettant à la Bibliothèque nationale du Canada de reproduire, prêter, distribuer ou vendre des copies de cette thèse sous la forme de microfiche/film, de reproduction sur papier ou sur format électronique.

L'auteur conserve la propriété du droit d'auteur qui protège cette thèse. Ni la thèse ni des extraits substantiels de celle-ci ne doivent être imprimés ou autrement reproduits sans son autorisation.

0-612-59706-7

Canada

University of Alberta

Library Release Form

Name of Author: Fayi Zhou

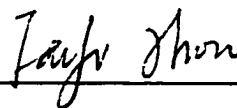
Title of Thesis: Effects of Trapped Air on Flow
Transients in Rapidly Filling Sewers

Degree: Doctor of Philosophy

Year this Degree Granted: 2000

Permission is hereby granted to the University of Alberta library to reproduce single copies of this thesis and to lend or sell such copies for private, scholarly or scientific research purposes only.

The author reserves all other publication and other rights in association with the copyright in the thesis, and except as herein before provided, neither the thesis nor any substantial portion thereof may be printed or otherwise reproduced in any material form whatever without the author's prior written permission.



449G, Michener Park

Edmonton, Alberta

Canada, T6H 4M5

Date: Sept 28, 2000

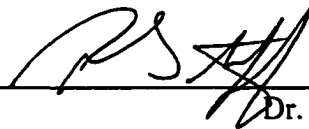
University of Alberta

Faculty of Graduate Studies and Research

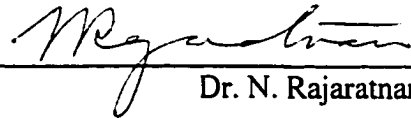
The undersigned certify that they have read, and recommended to the Faculty of Graduate Studies and Research for acceptance, a thesis entitled "Effects of Trapped Air on Flow Transients in Rapidly Filling Sewers" submitted by Fayi Zhou in partial fulfillment of the requirements for the degree of Doctor of Philosophy in Water Resources Engineering.



Dr. F.E. Hicks
(Supervisor)



Dr. P.M. Steffler
(Co-Supervisor)



Dr. N. Rajaratnam



Dr. I.D. Buchanan



Dr. L. Sigurdson



Dr. J.A. McCorquodale
(External Examiner)

Date: Sept. 27, 2000

Abstract

This thesis presents the results of experimental and analytical investigations on the effects of trapped air on flow transients in pipelines, especially for sewer trunks during the rapid filling stage.

The experimental study consists of rapid filling of different pipeline configurations containing trapped air, including a single horizontal pipe which was initially empty, a single horizontal pipe which initially had a tailwater, and a horizontal pipe with a vertical pipe segment positioned at different locations along the horizontal pipe. The pipe end was outfitted with orifices of different sizes to study the effects of air leakage on the pressure. The effects of varying the driving head, initial water column length, and orifice size on the maximum pressure peaks and pressure oscillation patterns were investigated. The air-water flow patterns in a horizontal pipe during rapid filling stage were also observed with a high speed camera. Pressure histories synchronously recorded illustrate the relation between the air-water phase evolution and the pressure oscillation pattern.

The experimental study revealed three types of pressure oscillation patterns in a rapidly filling pipe system, depending on the size of the orifice. When no air is released or when orifice sizes are small, waterhammer effects are negligible because of the cushioning effect of the air pocket. When the orifice size is very large, the air cushioning effect vanishes and the waterhammer pressure is dominant. For intermediate orifice sizes, the pressure oscillation pattern consists of long period oscillations followed by short period pressure oscillations. The maximum peak

pressure under no air release condition could be 4 times the driving head. Under air leakage condition, this peak pressure could be up to 15 times the upstream head. The pressure oscillation pattern and magnitude of peak pressure in an L-shape pipe system were close to those in a single horizontal pipe. It was found that the T-shape pipe system could mitigate the peak pressure significantly when the air release through the end of horizontal pipe was significant.

An analytical model, based on rigid water column theory, was developed to simulate the pressure transients in rapidly filling pipe systems containing trapped air. The model integrates the calculation of air pocket pressure oscillation with the magnitude of maximum waterhammer peak pressure. The analytical model was calibrated using the experimental data and was found to be able to predict pressure oscillation patterns for no or small air release situations. The model also is able to predict the maximum pressure magnitude for a wide air leakage range. The model study verified the ability of rigid water column theory in exploring the trapped air induced pressure transients during rapid filling.

To my parents

ACKNOWLEDGEMENTS

I would like to express my sincere gratitude to my supervisors Dr. F.E. Hicks and Dr. P.M. Steffler for their patience, support, and continuous encouragement throughout the course of this study. They devoted their time and efforts to make this study a success.

I wish to extend my thanks to Dr. N. Rajaratnam, Dr. J.A. McCorquodale, Dr. I. D. Buchann, and Dr. L. Sigurdson, for serving on the examining committee and for their time and efforts in reading this thesis thoroughly and making many helpful comments and suggestions.

I would like to acknowledge the financial support for this research provided by the Drainage Services, City of Edmonton and would like to thank Chris Ward who administered the contract and provided valuable technical advice over the course of the investigations. I also gratefully acknowledge the video instrumentation which was purchased through an NSERC equipment grant to Dr. F.E. Hicks. I express my sincere appreciation to Sheldon Lovell for designing and building the experimental apparatus and to Perry Fedun for setting up and maintaining the instrumentation.

Special thanks are to my wife, Christy, and my daughter, Lunning, for their love, understanding, and support during this study.

Table of Contents

1.0 Introduction	1
1.1 General.....	1
1.2 Reasons of Flow Transients in Urban Drainage Sewers.....	2
1.3 Effect of Air on Hydraulic Transients	3
1.3.1 Definition of air forms in water lines	3
1.3.2 Effects of air on hydraulic transients	3
1.4 Literature Review of the Effect of the Presence of Entrapped Air in Liquid Pipelines	4
1.5 Mathematical Models of Air Pocket Effects on Transient Flows.....	7
1.5.1 Limit of models based on the method of characteristics	8
1.5.2 Models based on rigid water column theory	8
1.5.3 Water-Gas separated flow model	10
1.6 Research Objectives.....	11
1.7 Content and Organization of the Dissertation.....	13
1.8 Reference	13
2.0 Transient Flow in A Rapidly Filling Horizontal Pipe Containing Trapped Air	20
2.1 Introduction	20
2.2 Theoretical Analysis.....	23
2.2.1 Governing equations.....	24
2.2.2 Numerical solution approach.....	26
2.3 Sensitivity Analysis	29
2.3.1 Effects of the friction factor	29
2.3.2 Effects of the orifice	30
2.3.3 Effects of the polytropical component k	31
2.4 Experimental Program.....	31
2.5 Experimental Results.....	33

2.5.1 Pressure oscillation patterns within the air pocket during rapid filling.....	34
2.5.2 Magnitude of peak pressures as a function of the orifice ratio and water column length	38
2.5.3 Magnitude of peak pressures as a function of the driving pressure ...	39
2.5.4 The speed of the waterhammer pressure wave.....	40
2.6 Analytical Model Verification.....	40
2.6.1 Comparison of the calculated and measured pressures	41
2.6.2 Martin's (1976) model	43
2.7 Conclusion and Discussion.....	43
2.8 Reference	45

3.0 Observation of The Air-Water Interaction in A

Rapidly Filling Horizontal Pipe	60
3.1 Introduction	60
3.2 Experimental Apparatus and Operations.....	61
3.3 Results of Observations.....	63
3.3.1 Zero or minimal air release – waterhammer effects negligible.....	64
3.3.2 Large air release – waterhammer effect dominated	66
3.3.3 Intermediate air release – mitigated water hammer effect	68
3.4 Implications for the Analytical Model	70
3.4.1 Shape of the air-water interface.....	70
3.4.2 Effects of air Entrainment	71
3.5 Conclusions	74
3.6 References	76

4.0 Effect of Trapped Air during Rapid Filling

of Partially Full Pipes	92
4.1 Introduction	92
4.2 Experimental Investigations	93
4.2.1 Experiment apparatus	93
4.2.2 Cases studied	94

4.3 Experimental Results.....	94
4.3.1 No or small air release situations	95
4.3.2 Large air release situations	95
4.3.3 Intermediate air release situations	97
4.4 Theoretical Considerations.....	97
4.4.1 Governing equations.....	97
4.4.2 Comparison between calculation and experiment.....	100
4.5 Conclusions	102
4.6 References	103

5.0 Pressure Surges in A Rapidly Filling Horizontal

Pipe with A Downstream Vertical Pipe Branch	119
5.1 Introduction	119
5.2 Theoretical Analysis.....	120
5.2.1 Configuration.....	120
5.2.2 Governing equations.....	120
5.2.3 Non-dimensional equations.....	122
5.4 Experimental Results.....	124
5.4.1 Pressure oscillation patterns within the air pocket during rapid filling	125
5.4.2 Magnitude of peak pressures as a function of the orifice ratio and initial water column length	126
5.5 Analytical Model Verification.....	127
5.6 Conclusions and Suggestions	129
5.7 References	130

6.0 Pressure Surges in A Rapidly Filling T-Pipe with

A Vertical Pipe Branch Containing Trapped Air	139
6.1 Introduction	139
6.2 Experimental Program.....	139
6.3 Theoretical Analysis.....	140
6.3.1 Configuration.....	140

6.3.2 Governing equations	141
6.3.3 Non-dimensional equations.....	142
6.4 Experimental Observations	143
6.4.1 Magnitude of peak pressures.....	143
6.4.2 Pressure oscillation patterns	145
6.5 Comparison of Experimental and Analytical Model Results	146
6.6 Conclusions and Suggestions	147
7.0 Conclusions and Recommendations for Future Work.....	158
7.1 Conclusions	158
7.1.1 Rapidly filling horizontal pipe which is initially dry	158
7.1.2 Rapidly filling horizontal pipe which is partially full	160
7.1.3 Rapid filling horizontal-vertical pipeline	161
7.2 Surge Controls for Sewage Systems.....	161
7.3 Suggestions for Further Studies.....	163
8.0 Appendix – CD-ROM.....	166
8.1 What’s On the CD-ROM.....	166
8.2.Analytical Model	166
8.3 Experimental Data	167
8.4 Declaration	168

List of Tables

Table	Title	Page
2.1	Pressure pattern for different orifice size.....	49
2.2	Comparison between measured and calculated peak pressure values	50
4.1	Error analysis for the analytical model	104
5.1	Comparison of calculated maximum pressure magnitudes between LP case and HP case (shown in Fig. 5.8)	138

List of Figures

Figure	Title	Page
1.1	(a) Manhole cover blow-off (City of Edmonton, 1995)	19
	(b) Sewer pipe rupture (City of Edmonton, 1995).....	19
2.1	The trunk profile at Gallagher Hill Park.....	51
2.2	Defining sketch for the theoretical analysis.....	51
2.3	Defining sketch for the impact pressure calculation.....	51
2.4	Effects of discharge coefficient of the orifice.....	52
2.5	Effects of polytropical component k.....	53
2.6	Diagram of the experimental apparatus	53
2. 7(a)	Pressure oscillation patterns: type 1- negligible waterhammer effect, $d/D = 0$	54
2. 7(b)	Pressure oscillation patterns: type 2- mitigate waterhammer effect, $d/D = 0.114$	54
2. 7(c)	Pressure oscillation patterns: type 3- waterhammer effect dominated, $d/D = 0.2$	55
2. 7(d)	Pressure oscillation patterns: type 3- waterhammer effect dominated, $d/D = 0.34$	55
2. 8	The relation between maximum pressure and relative orifice size for different types of behavior.....	56
2.9	The relation between maximum pressure and relative orifice size ($H^*_0/H^*_b = 3.86$).....	57
2. 10(a)	A comparison between calculated and experimental pressure oscillations (Type 1, $H^*_0/H^*_b = 4.57$, $\lambda_0 = 0.8$, $d/D = 0.028$).....	58
2. 10(b)	A comparison between calculated and experimental pressure oscillations (Type 2, $H^*_0/H^*_b = 3.86$, $\lambda_0 = 0.5$, $d/D = 0.114$).....	58
2. 10(c)	A comparison between calculated and experimental pressure oscillations (Type 3, $H^*_0/H^*_b = 3.86$, $\lambda_0 = 0.5$, $d/D = 0.18$).....	58
2. 11	A comparison between computed and measured maximum pressures.....	59
3. 1	Diagram of experimental apparatus	77
3. 2	No air release case, type 1 behavior ($P_0 = 137$ kPa, $x_0 = 5$ m, $d = 0$ mm).....	78
3. 3	Small air release case, type 1 behavior($P_0 = 137$ kPa, $x_0 = 8$ m, $d = 2$ mm) ...	79

3. 4	Small air release case, type 1 behavior ($P_0 = 275$ kPa, $x_0 = 8$ m, $d = 2$ mm) .	80
3. 5	Large air release case, type 3 behavior ($P_0 = 275$ kPa, $x_0 = 5$ m, $d = 7$ mm) ..	81
3. 6	Large air release case, type 3 behavior ($P_0 = 275$ kPa, $x_0 = 5$ m, $d = 7$ mm) ...	83
3. 7	Intermediate air release case, type 2 behavior ($P_0 = 275$ kPa, $x_0 = 0.48$ m, $d = 4$ mm).....	85
3. 8	Intermediate air release case, type 2 behavior ($P_0 = 275$ kPa, $x_0 = 5$ m, $d = 4$ mm).....	88
3. 9	The measured speed of pressure wave.....	90
3. 10	Air fraction relation with orifice size.....	91
4. 1	Diagram of the experimental apparatus-stagnant flow.....	105
4. 2	Maximum peak pressure relation with tailwater depth.....	106
4. 3	Pressure oscillation pattern ($H^*_o/H^*_b = 2.43$, $\lambda_0 = 0.56$, $d/D=0$).....	107
4. 4	Pressure oscillation pattern ($H^*_o/H^*_b = 2.43$, $\lambda_0 = 0.89$, $d/D=0$).....	108
4. 5	Pressure oscillation pattern ($H^*_o/H^*_b = 2.43$, $\lambda_0 = 0.56$, $d/D=0.171$).....	109
4. 6	Pressure oscillation pattern ($H^*_o/H^*_b = 2.43$, $\lambda_0 = 0.89$, $d/D=0.171$).....	110
4. 7	Pressure oscillation pattern ($H^*_o/H^*_b = 2.43$, $\lambda_0 = 0.56$, $d/D=0.114$).....	111
4. 8	Pressure oscillation pattern ($H^*_o/H^*_b = 2.43$, $\lambda_0 = 0.89$, $d/D=0.114$).....	112
4. 9	Comparison between calculated and measured maximum pressure magnitudes ($y/D=0$).....	113
4. 10	Comparison between calculated and measured maximum pressure magnitudes ($y/D=0.2$).....	114
4. 11	Comparison between calculated and measured maximum pressure magnitudes ($y/D=0.4$).....	115
4. 12	Comparison between calculated and measured maximum pressure magnitudes ($y/D=0.6$).....	116
4. 13	Comparison between calculated and measured maximum pressure magnitudes ($y/D=0.8$).....	117
4. 14	Equivalent dry-front model.....	118
5. 1	Defining sketch for the theoretical analysis.....	131
5. 2	Diagram of the experimental apparatus - L-pipe.....	131
5. 3	Pressure oscillation patterns.....	132
5. 4	Average maximum pressure magnitude.....	134

5. 5	Measured speed of pressure wave ($H^*_o/H^*_b = 3.86$)	135
5. 6	A comparison of calculated and measured pressure oscillation	136
5. 7	A comparison of calculated and measured maximum pressure magnitudes.....	137
5. 8	Effects of relative vertical pipe length on the maximum air pressure ($\lambda_0 = 0.8, L/D = 200, f = 0.035$)	138
6. 1	Diagram of the experimental apparatus - T-pipe	148
6. 2	Defining sketch for the theoretical analysis.....	148
6. 3	A comparison of measured maximum pressure magnitude between HP case and TP case.....	149
6. 4	A comparison of pressure oscillation patterns between a TP case and a HP case($H_0 = 275$ kPa, $\lambda_0 = 0.60, d/D = 0$).....	150
6. 5	Pressure oscillation patterns at three transducer locations ($H_0 = 275$ kPa, $\lambda_0 = 0.96, d/D = 0$).....	151
6. 6	Pressure oscillation patterns at three transducer locations ($H_0 = 275$ kPa, $\lambda_0 = 0.96, d/D = 0.171$).....	152
6. 7	Pressure oscillation patterns at three transducer locations ($H_0 = 137$ kPa, $\lambda_0 = 0.60, d/D = 0.171$).....	153
6. 8	A comparison of pressure history between cases with/without orifice on top of the vertical pipe (at location Tran.1, $H_0 = 275$ kPa, $\lambda_0 = 0.60, d/D = 0$)	154
6. 9	A comparison of pressure history between cases with/without orifice on top of the vertical pipe (at location Tran.1, $H_0 = 275$ kPa, $\lambda_0 = 0.60, d/D = 0.171$)	155
6. 10	A comparison of calculated and measured maximum pressure magnitude	156
6. 11	A comparison of calculated and measured pressure oscillation patterns ($H_0 = 275$ kPa, $\lambda_0 = 0.60, d/D = 0$).....	157
7.1.a	Possible scenario of air release pressure – flow backup	165
7.1.b	Possible scenario of air release pressure – rapid filling to a dead end.....	165

Nomenclature*

<u>Symbol</u>	<u>Description</u>
A	= cross section area of pipe [2],[4],[5],[6];
A_0	= area of orifice (leakage)[2],[4],[5],[6];
A_c	= cross-sectional area of tailwater[4];
A_s	= cross-sectional area of vertical pipe [5],[6];
a	= speed of pressure wave[2],[4],[5],[6];
a_a	= speed of sound in air alone[3];
a_m	= speed of air-water flow[3];
a_w	= speed of sound in water alone[3];
B	= coefficient [2],[4],[5],[6];
d	= diameter of the orifice [2],[3],[4],[5],[6];
C_d	= discharge coefficient of orifice [2],[3],[4],[5],[6];
C_0	= parameter representing combined effects of friction, pipe size, and initial water column length [2],[4],[5],[6];
D	= diameter of the pipe[2],[3],[4],[5],[6];
f	= Darcy-Weisbach friction factor[2],[4],[5],[6];
g	= acceleration due to gravity[2],[3],[4],[5],[6];
H_0	= upstream water head (or driving head, gauge value) [2], [3], [4], [5], [6];
H^*	= pressure head (absolute value) [2],[3],[4],[5],[6];
H^*_b	= initial air pressure head (absolute value) [2],[3],[4],[5],[6];
L	= length of pipe [2], [3], [4], [5], [6];
K	= bulk modulus of water [3]; minor losses of energy [5],[6];
P_a	= absolute air pressure [3];
P_0	= driving pressure [2],[4],[5],[6];
Q_a	= air discharge through orifice [2],[4],[5],[6];
S	= channel or conduit slope [4],[5],[6];

* The number in square brackets [] denotes relevant chapter number.

t	=	time[2],[3],[4],[5],[6];
U	=	velocity of water column [2],[3],[4],[5],[6];
U_0	=	the initial velocity of water column [2],[3],[4],[5],[6];
U_c	=	velocity of tailwater[4];
U_w	=	velocity of surge front[4];
V_a	=	air volume [2],[3],[4],[5],[6];
V_{a0}	=	initial air volume[2],[3],[4],[5],[6];
x	=	length of water column[2],[4],[5],[6];
x_0	=	initial length of the water column [2],[3],[4],[5],[6];
y	=	depth of tailwater [4];
α	=	ratio of cross-sectional area [4],[5],[6];
κ	=	polytropic component [2],[4],[5],[6];;
λ	=	non-dimensional length of water column [2],[3],[4],[5],[6];
η	=	non-dimensional air volume[2],[4],[5],[6];
ϕ	=	non-dimensional pressure head [2],[3],[4],[5],[6];
ψ	=	non-dimensional velocity of water column [2],[3],[4],[5],[6];
ρ_w	=	density of water [2],[3],[4],[5],[6];
ρ_a	=	density of air[2],[3],[4],[5],[6];
τ	=	non-dimensional time[2],[4],[5],[6].

1.0 INTRODUCTION

1.1 General

The main component of drainage sewer infrastructure is a system of pipes that collects storm run-off from the ground surface area and buildings in urban areas and distributes the runoff to points of treatment or disposal. There are two important aspects of the design of drainage sewers: hydraulic capacity and structural strength. Practical hydraulic design criteria include an expectation that the capacity of the system is limited to something in the order of a 1:5 to 1:10 year return period event (Yen, 1986). This means that the system is, in effect, designed to be hydraulically overloaded, including surcharging (the transition from open channel to pressure flow conditions), also known as flow transients. However, hydraulic overloading can have significant implications on the structural design of drainage sewer systems. In fact, anecdotal evidence (e.g. EHG, 1996) indicates that conventional structural design criteria for drainage sewer systems may be inadequate in situations where hydraulic overloading occurs. Sewer failures, such as combined sewers overflows (CSOs), basement flooding, manhole covers blowing off, pipe rupture, etc. have been reported in many cities (EHG, 1996; Guo and Song, 1990; Hamam and McCorquodale, 1982; Globe and Mail, 1999; McNarin, 1999; Weil, 1990). Fig. 1.1 shows two sewer failure pictures reported in the City of Edmonton, Alberta on July 15, 1995 (City of Edmonton, 1995).

Earlier research (e.g. Martin, 1976) suggests that trapped air may play a significant role in inducing large pressures within surcharging drainage sewers and

that it may also, in some cases, have the potential to mitigate waterhammer effects. The purpose of this research project was to investigate the effects of trapped air in rapidly filling pipes with a view to establishing a design protocol for aiding the structural design of drainage sewers under conditions of hydraulic overloading.

1.2 Reasons for Flow Transients in Urban Drainage Sewers

The reasons for flow transients in urban drainage sewers have been discussed by some researchers (Yen, 1986; Hamam and McCorquodale, 1982; Cardel and Song, 1988; Guo and Song, 1990). Generally, the following reasons have been attributed to the occurrence of flow transients in sewers:

1. Inflows exceed the capacity of pipelines(hydraulic over loading);
2. Pump start-up and shut-down;
3. Improper alignment of pipelines;
4. Blockage of pipelines;
5. Flow instabilities due to the existence of inverted siphons, weirs and interceptors;
6. Air pocket entrapment in pipelines.

The flow transients induced by pump operations in pressurized pipelines have been widely studied (Jonsson 1985; Muller, 1991; Chaudhry et al. 1990; Lee, 1994), in which the waterhammer is the main concern. The transition from gravity flow to pressurized flow during drainage sewer surcharging has also been investigated (Song et al., 1983; Cardel and Song, 1986; Hamam and McCorquodale, 1982; Capart et al., 1997). These studies either neglected the trapped air effect or just focused on the

the entrained air. The free air effect on transient flow is the least studied topic in sewer hydraulic transient problems.

1.3 Effect of Air on Hydraulic Transients

1.3.1 Definition of air forms in water lines

According to the *size* of the air component, Wisner et al. (1975) defined two basic types of air in water lines as: (1) *bubbles*, which are entrapped in water by turbulent action such as the impact of a falling nappe of water or in a hydraulic jump; and (2) *pockets*, which are formed as a result of a coalescence of bubbles or by entrapment of large quantities of air as occurs during the filling of a pipeline.

According to the *location* of the air in water, Lamb (1987) classified the air in a hydraulic system as: (1) *contiguous air*, which is partially bounded by the fluid, similar to air pockets in pipework and the air above the free surface in an open channel flow, (2) *entrained air*, which exists as individual bubbles separated by relatively thick films of liquid, (3) *foam*, in which the air bubbles are separated by relatively thin films and float on the liquid surface, and (4) *dissolved air*, which is dispersed within the molecular structure of the liquid. Dissolved air is invisible. Contiguous air and entrained air are commonly regarded as free air.

1.3.2 Effects of air on hydraulic transients

It is obvious that all of the forms of air discussed above may exist in pipelines, however, in transient flow studies, only *free air* is important. Among free air studies, entrained air has been intensively studied and many mathematical models have been proposed (Martin, 1979; Chaudhry, 1985, Chaudhry, et al, 1990; Lee 1991;

DeHenau and Gaithby, 1995; Boisson and Malin, 1996). These studies indicate that the entrained air increases the compressibility of water and reduces the speed of pressure wave and the pressure amplitude.

On the contrast, the contiguous air (called an air pocket hereafter) in pipelines may have detrimental effects such as reducing capacity, inducing surge and blowbacks, and reducing pump efficiency.

1.4 Literature Review of the Effect of the Presence of Entrapped Air in Liquid Pipelines

Kalinske and Robertson (1943) experimentally investigated the air entrainment due to a hydraulic jump in a circular pipe. Seven different pipe slopes and ratios of approaching water depth to diameter were tested. It was found that a hydraulic jump can entrain air in a circular pipe and that the rate of air entrainment depends on the water discharge and the intensity of agitation or turbulence of the jump, which can be expressed as a function of upstream supercritical Froude number. It was found that the air pressure within a specific pocket was almost constant and that the hydraulic grade line was parallel to the water surface.

Holley (1969), and Burton and Nelson (1971) investigated surges and air entrainment problems in some upstream controlled water conveyance systems. The pressure oscillation in a pipeline with pipe check structures spaced along the pipe in steady inflow condition was investigated. The check structures serve two purposes: (1) providing an air resource to keep negative pressures from developing when the discharge is less than design value, and (2) creating an overflow point high enough in

elevation to keep the pipe from draining when there is no inflow. It was found that huge pressure peak occurred when large bubbles along the top of the pipe were released from either the downstream air release vent pipe or the upstream check structures.

Albertson and Andrews (1971) conducted experimental and theoretical studies of pressure transients occurring through air release valves using two configurations. The first involved an air release valve on the top of a standpipe which was installed at the downstream end of a horizontal pipe. The pipe was initially pressurized and then an air pocket was introduced by injecting air into the standpipe with a compressor. Once the air valve was opened, pressure variations were recorded. The second configuration involved rising and falling pipe sections. An air release valve was installed at the peak between these two pipe sections, which was initially drained and separated from the pressurized upstream flow using a control valve. Once the valve was opened, rapid filling of the test section began and pressure variations were recorded using a transducer near the air release valve. They found that the maximum peak pressure could be 15 times the operating pressure.

Martin (1976), through an analytical model investigation, demonstrated that the entrapped air inside of pipelines could either be beneficial or detrimental, depending upon the amount of air, two-phase regime of the mixture, and the nature of the transient. The beneficial aspect is that a dispersed gas reduces the waterhammer pressure because of the increase of the elasticity of the mixture. On the other hand, his investigation suggests that, if the entrapped air is in the form of a large pocket, its impact would be detrimental. Air pockets store energy that maintains a high

acceleration force and therefore can lead to higher transient pressures and lower capacities of the pipelines.

Hope and Papworth (1980) analytically studied a fire main failure caused by high-pressures in a rapidly filled dry riser. In automatic fire protection systems, exposed pipeworks leading to the fire fighting devices are usually kept empty when not in use. In the case of a water demand, the pipework is rapidly primed and large pressure transients can be generated when the filling flow is obstructed by the fire-fighting device. The authors believed that the trapped air pocket in the previously empty pipework acts as a cushion, which can reduce the pressure peaks. It was found from the calculated pressure results that the magnitude of the maximum pressure was more than twice as high as the pressure head in the supply tank.

Valentin (1981) experimentally investigated the surcharging problems in sewage systems. His physical set up consisted of a 292 mm diameter, 35-m long Plexiglas conduit, connecting reservoirs at both upstream and downstream with a maximum slope up to 0.02. By closing the sluice gate at the downstream reservoir, the transition from free surface flow to pressurized flow was induced. It was found that when flow touched the crown, air was trapped in the flow and, when the trapped air pocket suddenly escaped a short and sharp pressure pulse occurred.

Jonsson (1985) conducted experimental and numerical studies on the impact of air pockets on transient pressures in the operation of a sewage pump stations. Both numerical and experimental studies indicated that an extreme pressure oscillation might occur when air is sucked into the conduit through the pump. He suggested that these strong pressure peaks must be considered at the design stage of the conduit.

Hamam and McCorquodale (1982), and Cardle, Song and Yuan (1989) observed air pocket motion and its effect on flow surges in their experimental investigations of transients in a mixed-flow condition. Their experiments illustrated the significance of air entrapment at the interface between the free surface and the pressurized flow. They found that air effects become important when the velocity of the air being forced ahead of the interface is large relative to the velocity of the water surface. Under such conditions, instabilities develop on the water surface and strong pressure oscillations occur.

Muller (1991) conducted experiments on the fluid transients in a large-scale parallel pumping system. The magnitudes of the fluid transients in the system were determined and the changes in the fluid transients due to the changes of amount of air trapped in the system prior to pump startup were observed. It is known from the experiments that the trapped air in the system serves two purposes. First, it acts as a cushion, helping to absorb the initial impact associated with the pump startup. However, if the amount of trapped air is reduced, the decay rate and the frequency of pressure oscillations may increase.

1.5 Mathematical Models of Air Pocket Effects on Transient Flows

In the past, the evaluation of drainage sewer hydraulics relied heavily on physical modeling. With the advance of computer technology, the computational modeling has become a common practice. The computer models for general hydraulic calculations such as steady flow for sewer systems are very common and reliable (Yen, 1986). One challenge in the numerical simulation is the flow transients in air-water two-phase flow.

1.5.1 Limit of models based on the method of characteristics

The Method of Characteristics (MOC hereafter) has been extensively used in transient flow studies. Boldy (1993) conducted an extensive literature review on numerical methods for solution of flow transients. Although the MOC has the advantage of being able to accurately predict the pressure amplitude, its application to air entrained flows is limited. The main reason is the difficulty of treating the speed of sound, which varies drastically with the pressure in air entrained flows (Chaudhry, 1987). Although great effort has been put into simulating the free air effects on flow transients using the MOC (Wylie and Streeter, 1979; Jonsson, 1985; Simpson et al, 1994; Swaffied and Boldy, 1993), the MOC can only be used to solve the cases where the air pocket volume is very small compared to the water volume. For a rapidly filling, or surcharging system containing trapped air, the MOC has difficulty in dealing with rapid varying flow boundary. Recently, algorithms for solving the moving boundary system have been developed (Chen, 1995). However, if such an algorithm is implemented in a rapidly filling pipeline, a very small time step has to be used to capture the rapid surge front, making the computation expensive and time consuming.

1.5.2 Models based on rigid water column theory

Models based on rigid water column theory have been developed and implemented in numerous transient flow studies (Johnson, 1913; Quick, 1933; Paramakian, 1963; Wood, 1973 and 1974; Wylie, 1981; Abreu, et al., 1999). The rigid water column model (RWCM) is based on the assumptions that the density of

water and the cross-sectional area of the pipe remain constant, that is, the storage of mass within the control volume is neglected.

Valentine (1965) compared the elastic and rigid water column approaches by studying the pressure transients in a frictionless pipe with uniform downstream gate closure. It was found that, when the ratio of the static head on the gate to the initial velocity of the flow was less than 50, the results of the two methods were practically identical. Karney (1991) used an energy approach to determine the effect of the rigid water column method. He proposed a compressibility index, which is equal to the ratio of total change in internal energy to the total change in kinetic energy to quantify the role of compressibility. He found that, when the compressibility index approaches zero, the rigid water column theory provides a good approximation of the transient behavior of the system. Rogalla and Wolters (1994) conducted intensive comparisons between the compressible fluid model and the rigid water column model. Their studies indicated that the rigid water column method is applicable when the inertial force is dominant.

Hamam and McCorquodale (1982) proposed a RWCM model to study the transition from free surface flow to pressurized flow in surcharging sewers. The entire surcharging process was divided into three stages: (1) free surface flow, (2) flow transition, and (3) pressurized flow. In the flow transition stage, an interface instability criteria was proposed to determine the air pocket entrapment. Later, Li (1986) improved this model by adding in the simulation of the air release from the drop shaft.

In summary, the study of air induced pressure in real sewer systems is difficult for several reasons. The first is the speed of pressure wave. In sewers, this speed can vary from below 100m/s to above 1200m/s, depending on the air content (which is difficult to quantify). Second, the manner of air pocket collapse can vary from an instantaneous closure to a slow release. Therefore, it is hard to capture air pocket behavior in mathematical models. The third reason is that the topology of a sewer system network is very complicated: the branches, loops, dropshafts, and other irregularities can greatly affect the potential for transient transmission or damping. Finally, the rapid transition from air-water flow to a surcharged condition can vary from a slow pipe-filling to a highly dynamic effect. These difficulties make mathematical studies based on simplified configurations a necessary starting point for the study of air pocket effects on flow transients.

1.5.3 Water-Gas separated flow model

Graze (1968) developed a rigid water column method to analyze the mitigating effects of an air chamber on pressure surges. In this model, the water column was assumed to be rigid and to be separated from the entrapped air which was to be collected as a large pocket and occupied the entire cross section. Later, Martin (1976) proposed a similar analytical model to investigate the effect of trapped air on the startup of liquid columns from rest. The effect of air release on the pressure surge was simulated using an orifice at the pipe end. Comparisons conducted by Martin (1976) and Jonsson (1985) indicated that the maximum pressures obtained with the rigid column model and the elastic model are very close except for the time of the

occurrence of the maximum pressure. It was also found that the liquid compressibility could not be ignored if pipes are very long.

More experimental studies are required to validate this type of model, especially when there is air release in the system. One limitation of Martin's (1976) model is its inability to calculate the air release pressure when the orifice size is large. This means that two separate models would have to be used to study the trapped air effect on transient pressures (one used to calculate no or small air release cases, and another for significant air release cases), which would be inconvenient to apply since one has to know under which conditions the air release is insignificant and under which it is. An integrated model, which can simulate both the air pocket pressure when the air release is small and the waterhammer pressure when the air release is significant, is therefore preferable.

Another limitation of Martin's (1976) water-air separated flow model is that the water column length is assumed to be a constant during the air pocket deformation process, which is only acceptable when the air volume is extremely small compared to the water volume. Although Cabrea et al. (1992) analytically proved that the constant water column length model has identical results with that of a varied length column under no air release conditions, no studies have been reported to date on the validity of the constant length model under air release conditions.

1.6 Research Objectives

The literature review revealed the complexity of air problems in flow transients in pipelines. It is impossible to establish a universal physical or theoretical

model to study all the possible air scenarios in even a simple pipeline. Therefore, the objectives of this research are: (1) to develop a methodology based on the rigid water column method which will enable the municipal design engineers to quantify the pressures that drainage system infrastructures must be expected to withstand and to explore the effects of mitigate devices on these design requirements; and (2) to investigate, in a physical model, the effect of the air pocket on rapidly filling under several simple flow configurations.

In terms of experiments, studies on a simple, rapidly filling horizontal pipe was first conducted. Although this configuration provides an idealized situation which may exist only under laboratory conditions and in numerical simulations, it provides an understanding of fundamental transient behavior in pipelines with air entrapment and release. The experimental study then considered those scenarios which are a step closer to real sewers, such as the vertical pipe and partially full pipe.

An analytical model was also developed, based on the rigid water column theory. The model calculates both the air pocket pressure and the air release pressure in an integrated way. The model has been validated with the experimental results.

The theoretical model obviously cannot provide the exact solutions to very complex industrial problems. It does, however, facilitate the first hand investigations on the subject, it gives apparent orders of magnitude, and it demonstrates the general manner in which changes occur. These were our purposes in developing analytical models to explain complicated air-water flow problems in sewer systems.

1.7 Content and Organization of the Dissertation

Chapter 2 studies the rapid filling in a horizontal pipe, including the experimental set up, instrumental calibration, analysis of the experimental data, rigid water column theory, derivation of governing equations, calculated results, and comparisons with experiments. Chapter 3 is an observation-based study of air-water interface development in a horizontal pipe that is subject to rapid filling, aiming to interpret the relation between pressure oscillation and air-water profile. Chapter 4 describes the study of rapid filling of a partially full pipe, with a purpose of interpreting the effect of the tailwater depth on pressures and explores the capabilities of the model developed in Chapter 2. Chapter 5 describes the effects of air release from a vertical pipe situated at the end of a horizontal pipe and Chapter 6 describes the effect of T-pipe on mitigating the pressure surge. The last chapter, Chapter 7, provides general conclusions and recommendations for further studies on this subject.

1.8 Reference

- Albertson, M.L., and Andrews, J.S. (1971). "Transients caused by air release." *Control of Flow in Closed Conduits*, (J.P.Tullis, ed.), pp.315-340, Colorado State University, Fort Collins, Colorado.
- Boisson, N., and Malin, M.R. (1996). "Numerical prediction of two-phase flow in bubble columns." *International Journal of Numerical Methods in Fluids*, Vol.23, pp.1289-1310.

- Boldy, A.P. (1993). "Numerical methods for solution of governing equations." *Computer Modeling of Free Surface and Pressurized Flows*, Chaudhry and Mays edited, NATO ASI Series, pp. 459-485.
- Burton, L.H., and Nelson, D.F. (1971). "Surge and air entrainment in pipelines." *Control of Flow in Closed Conduits (J.P.Tullis, ed.)*, pp.257-294, Colorado State University, Fort Collins, Colorado.
- Cabrera, E., Abreu, J., Perez, R. and Vela, A. (1992). "Influence of liquid length variation in hydraulic transients." *ASCE Journal of Hydraulic Engineering*, Vol.118, No.12, pp.1639-1650.
- Capart, H., Sillen, X. and Zech, Y. (1997). "Numerical and experimental water transients in sewer pipes." *Journal of Hydraulic Research*, Vol.35, No.5, pp. 695-672.
- Cardle, J.A., and Song, C.C.S. (1988). "Mathematical modeling of unsteady flow in storm sewers." *International Journal of Engineering Fluid Mechanics*, Vol.194, pp.495-518.
- Cardle, J.A and Song, C.C.S. and Yuan, M. (1989). "Measurements of mixed transient flows." *ASCE Journal of Hydraulic Engineering*, Vol.115, No.2, pp.169-181.
- Chaudhry, M.H. (1985). "Limitations of hydraulic—transient computations." *21st IAHR Congress*, Melbourne, Australia, 19-23 August, pp.132-136.
- Chaudhry, M.H., Bhallamudi, S.M., Martin, C.S., and Naghash, M. (1990). "Analysis of transient pressures in bubbly, homogeneous, gas-liquid mixtures." *ASME Journal of Fluids Engineering*, Vol.112, No.2, pp.225-230.

- City of Edmonton, (1995). *A report on the July 4, 1995 Storm Event*, a technical report prepared by the Drainage Branch of Transportation Department, City of Edmonton.
- Chen, X.Y. (1995). *Multi-Dimensional Finite Volume Simulation of Fluid Flows on Fixed, Moving and Deforming Mesh Systems*, A Thesis Submitted in Partial Fulfillment of the Requirements for the Degree of Doctor of Philosophy, University of Minnesota.
- DeHenau, V., and Raithby, G.D. (1995). "A transient two-fluid model for the simulation of slug flow in pipelines-I theory." *Int. J. Multiphase Flow*, Vol.21, No.3, pp336-349.
- EHG, (1996). *Hydraulic Transient Evaluations of the City of Edmonton Sewerage system*, Consulting report prepared for the City of Edmonton, Environmental Hydraulics Group.
- EHG, (1997). *Hydraulic Transient Analysis for the Western beaches Tunnel*, City of Toronto, Project Report by Environmental Hydraulics Group, Inc.
- Globe and Mail, (1999). "Sewage surf a beach summer." April 15, Toronto, Ontario, pp. A20.
- Graze (1968). "A rational thermodynamic equation for air chamber design." *The Third Australian Conference on Hydraulics and Fluid Mechanics*, Sydney, Australia, 25th to 29th November, pp. 55-61.
- Guo, Q. and Song, C.C.S. (1990). "Surging in urban storm drainage system." *ASCE Journal of Hydraulic Engineering*, Vol.116, No.12, pp.1523-1537.

- Hamam, M.A. and McCorquodale, J.A. (1982). "Transient conditions in the transition from gravity to surcharged sewer flow." *Canadian Journal of Civil Engineering*, Vol.9, No.2, pp.189-196.
- Holley, E.R. (1969). "Surging in laboratory pipeline with steady inflow." *ASCE Journal of Hydraulic Engineering*, Vol.95, No. 3, pp.961-979.
- Hope, P. and Papworth, M.U. (1980). "Fire main failures due to rapid priming of dry lines." *3rd International Conference on Pressure Surges, BHRA*, Bedford, England, March.
- Johnson, R.D. (1913). "Discussion of Warren's paper on penstock and surge tank problems." *Trans. ASCE*, Vol. 79.
- Jonsson, L. (1985). "Maximum transient pressures in a conduit with check valve and air entrainment." *International Conference on the Hydraulic of Pumping Stations*, Manchester, England, pp.55-69.
- Kalinske, A.A., and Robertson, J.M. (1943). "Closed conduit flow." *Transactions of ASCE, HY, 1943* .
- Lamb, W.S. (1987). *Cavitation and Aeration in Hydraulic Systems*, BHRA, The Fluid Engineering Center.
- Li, J. (1986). "Pressure transients during the transition from gravity to surcharged flow in storm sewers." *A thesis for degree of master of science at the University of Windsor, Canada*.
- Li, J. and McCorquodale, J.A. (1999). "Modeling mixed flow in storm sewers." *ASCE Journal of Hydraulic Engineering*, Vol. 125, No.11, pp.1170-1179.

- Martin, C.S. (1976). "Entrapped air in pipelines," *Proceeding of the Second International Conference on Pressure Surges*, London, England, F2-15.
- Martin, C.S. and Padmanabham, M.(1979). "Pressure pulse propagation in two-component slug flow." *Journal of Fluid Engineering*, ASME, Vol.101, pp.44-52.
- Martin, C.S. (1981). "Air entrainment." *Closed Conduit Flow* (edited by Chaudhry and Yevjevich), pp. 209-223.
- McNarin, K. (1999). "City grapples with mounting costs over river bank." *Start Phoenix*, September 18, Saskatoon, Saskatchewan, pp. A3.
- Muller, M.R. (1991). "An experimental study of fluid transients in a large scale parallel pumping system." *International Journal of Engineering Fluid Mechanics*, Vol. 4(1), pp. 57-70.
- Rogalla, B.U. and Wolters, A. (1994). "Slow transients in closed conduit flow." *Computer Modeling Free-Surface and Pressurized Flows* (Chaudhry and Mays edited), Kluwer Academic Publishers, pp. 613-671.
- Song, C.C.S., Cardel, J.A. and Leung, K.S. (1983). "Transient mixed-flow models for storm sewers." *ASCE Journal of Hydraulic Engineering*, Vol.109, No.11, pp.1487-1504.
- Streeter, V.L. and Wylie, E.B. (1967). *Hydraulic Transients*, McGraw-Hill Book Company.
- Swaffield, J.A. and Boldy, A.P. (1993). *Pressure Surge in Pipe and Duct System*, Avebury Technical Press.

- Valentine, H.R.(1965). "Rigid water column theory for uniform gate closure." *Proceedings of the American Society of Civil Engineering*, Vol.91, No.HY4, pp.27-33.
- Valentin, F. (1981). "Continuous discharge measurement for the transition between partially filled and pressurized conduit flow in sewerage systems." *Journal of Water Science and Technology*, Vol.13, pp.81-88.
- Weil G.J. (1990). "Remote infrared thermal sensing of sewer voids." *Proceedings of the 17th Annual Conference, Water Resources and Management Division*, ASCE, Houston, Texas.
- Wisner, P.E., Mohsen, F.N., and Kouwen, N. (1975). "Removal of air from water lines by hydraulic means." *ASCE Journal of Hydraulic Engineering*, Vol.101, No.2, pp.243-257.
- Wylie, E.B. and Streeter, V.L. (1978), *Fluid Transients*, McGraw-Hill, New York.
- Yen, B.C. (1986), "Hydraulics of sewers." *Advances in Hydroscience*, Vol.14, pp.1-123.
- Zech, Y. (1985), "Flow instabilities in culverts and storm sewers." *Proceeding of 21st IAHR Congress on Urban drainage Hydraulics*, Australia.



Fig. 1.1.a Manhole Cover Blow-off (City of Edmonton, 1995)



Fig. 1.1.b Sewer Pipe Rupture (City of Edmonton, 1995)

2.0 TRANSIENT FLOW IN A RAPIDLY FILLING HORIZONTAL PIPE CONTAINING TRAPPED AIR¹

2.1 Introduction

On July 4, 1995, an extreme storm occurred over the Bonnie Doon area of Edmonton, Alberta, during which rainfall amounts of nearly 90 mm were recorded over a 2 hour period. This event, estimated by the City of Edmonton to have a return period in excess of 1:300 years, surcharged storm and combined sewers and resulted in surface and basement flooding. In addition, severe infrastructure damage occurred at the Gallagher Hill Park manhole. Specifically, the entire manhole structure was blown off of the pipe, along with ancillary structures including a 300 mm force main, a 1200 mm trunk sewer, a 600 mm water main, and a 400 mm gas line (City of Edmonton, 1995). Fig. 2.1, showing the profile of Gallagher Hill Park Trunk System, illustrates the probable scenario during the storm event of July 4, 1995. Normally, flow would be from left to right, as the force main would bring flow to the trunk sewer. However, in this case, it is believed that the trunk sewer experienced a reverse flow, caused by downstream overloading in the drainage system, which in turn caused a rapid transition from gravity flow to surcharged conditions in the trunk sewer, as shown in the figure. The pressure head driving the reverse flow was estimated to have been about 12 to 15 m (EHG, 1996). It is believed by the authors of this paper that the air trapped ahead of the

¹ An abbreviated version of this chapter is currently under review with Journal of Hydraulic Engineering, American Society of Civil Engineers (originally submitted Nov. 15, 1999, and resubmitted after minor revision on July 2, 2000).

advancing surge wave was a significant factor in the dynamic loading which caused the structural failure.

Past studies reported in the literature suggest that entrapped air can induce pressure oscillations in pipelines. Holly's (1969) experiments suggested that the storage and release of entrapped air was the source of surge initiation in pipelines. Burton and Nelson (1971) investigated surge generation and air entrapment in water conveyance systems. Based on Holly's (1969) findings and their own field investigations they suggested that severe pressure surges may be induced by air trapped in the system. Albertson and Andrews (1971) conducted experimental and theoretical studies of pressure transients occurring through air release valves using two configurations. The first involved an air release valve on the top of a standpipe which was installed at the downstream end of a horizontal pipe. The pipe was initially pressurized and then an air pocket was introduced by injecting air into the standpipe with a compressor. Once the air valve was opened, pressure variations were recorded. The second configuration involved rising and falling pipe sections. An air release valve was installed at the peak between these two pipe sections, which was initially drained and separated from the pressurized upstream flow using a control valve. Once the valve was opened, rapid filling of the test section began and pressure variations were recorded using a transducer near the air release valve. They found that the maximum peak pressure could be 15 times the operating pressure. They also investigated the effects of filling velocity and orifice size on the peak pressures. However, due to the limitations of their instrumentation, the pressure oscillation history during the filling process was not

documented. Their theoretical study was based on a simple water hammer theory and was unable to describe the pressure variations during the filling process.

Martin (1976) developed a theoretical model to calculate the pressure oscillation within a trapped air pocket in a single pipe subject to instantaneous valve opening. The solutions showed that the peak pressure inside of the air pocket was much higher than the operational pressure; however, he did not have experimental data for model verification. Hamam and McCorquodale (1982) found through their experiments that air pockets are easily trapped in front of a surge interface in pipelines when surcharging begins. Jonsson (1985), in his experiments of flow transients in a sewerage pump subject to sudden shut down, found that a trapped air pocket in a conduit can induce a pressure 3 to 4 times the operational pressure. Jonsson compared his experimental data to a model equivalent to Martin's, with good agreement. He identified the need to consider the effects of air leakage in future studies. Cardle et al. (1989), in their experiment on pipe surcharging, observed a high frequency pressure oscillation when an air was forced out of the system by an advancing surge.

These earlier studies suggest that pressure oscillations within trapped air pockets, or high peak pressures induced by air release, may be important in the behavior of drainage systems under hydraulic overloading. To further investigate this phenomenon, an experimental investigation into the mechanics of flow transients in a rapidly filling pipe containing trapped air, and experiencing air leakage, was conducted. This configuration can be regarded as a simplified sewer trunk subject to rapid surcharging, similar to the case illustrated in Fig. 2.1. Building on the work of Martin

(1976), an analytical model was also developed to describe pressure transients within an air pocket trapped at the end of a horizontal pipe under rapid filling conditions. Comparisons between the results from the analytical model and the experimental observations are also provided.

2.2 Theoretical Analysis

Fig. 2.2 defines terms needed for the analytical model: H_0 is the upstream head, U is the velocity of the water column during rapid filling, V_a is the volume of air, H^* is the air absolute pressure head, x is the length of the water column, D is the inside diameter of the pipe, d is the diameter of the orifice, and L is the length of the pipe. The proposed analytical model extends beyond that presented by Martin (1976), in that it also considers high rates of air release, the changing water column length during pipe filling, and also incorporates the calculation of peak pressure when the water column impacts on the pipe end. This last feature is particularly important since it occurs at the final stage of the rapid filling process and, in some cases, may constitute the maximum pressure which might occur under air leakage conditions.

The following assumptions (Martin, 1976) were made in the development of this theoretical model: (1) the water column is incompressible. Cabrera et al. (1992) found that the difference in maximum pressure between the elastic model and rigid model for a rapid filling pipe is less than 2%; (2) the pipe is horizontal; (3) the air pocket occupies the entire cross section; (4) the water-air interface is vertical (i.e., it is assumed that the air pocket remains cylindrical in shape); (5) a polytropic law is applicable for the air phase; (6) the wall friction factor for steady flow is applicable for unsteady flow

conditions. Fok (1987) found that the difference in maximum pressure between the steady flow friction model and the unsteady flow friction model is less than 5%; and (7) air pocket has negligible flow resistance inertia and constant pressure throughout.

2.2.1 Governing equations

From the control volume shown in Fig. 2-2, the change in the volume of air within the horizontal pipe can be written as

$$\frac{dV_a}{dt} = -AU \quad (2-1)$$

where A is the cross-sectional area of the pipe and t is time.

The momentum equation of the water column is

$$\frac{dU}{dt} = -g \frac{H - H_0}{x} - f \frac{U|U|}{2D} - \frac{U^2}{2x} \quad (2-2)$$

where H is the air pressure head, f is the wall friction factor, and g is the gravitational acceleration (9.81 m/s²).

The governing equation for the air phase is (Martin 1976)

$$\frac{dH^*}{dt} = -k \frac{H^*}{V_a} \frac{dV_a}{dt} - k \frac{H^*}{V_a} Q_a \quad (2-3)$$

where Q_a is the air discharge out of the orifice A_o , and k is the polytropic exponent. Graze (1968) investigated the impact of varying the polytropic exponent, k , (from 1.0 to 1.4) for adiabatic air pressure oscillation in an air chamber. He found $k = 1.4$ gave the best fit to the experimental data. This value was adopted here.

Here the asterisk denotes the absolute pressure head. Q_a can be expressed by

$$Q_a = C_d A_0 Y \sqrt{2g \frac{\rho_w}{\rho_a} (H^* - H_b^*)} = C_d A_0 Y \sqrt{2g \frac{\rho_w}{\rho_{a0}} \frac{\rho_{a0}}{\rho_a} (H^* - H_b^*)} \quad (2-4)$$

where H_b^* is the absolute initial air pocket pressure head, which is assumed to be equal to atmospheric pressure in this study. C_d is the discharge coefficient, which can be taken from conventional hydraulic tables for compressible flows through orifices and nozzles; here $C_d = 0.65$ (American Gas Association, 1978). Y is an expansion factor which can be expressed as (Martin, 1976)

$$Y = \left[\frac{k}{k-1} \left(\frac{H_b^*}{H^*} \right)^{2/k} \frac{1 - (H_b^*/H^*)^{(k-1)/k}}{1 - H_b^*/H^*} \right]^{1/2} \quad (2-5)$$

If H^*/H_b^* is greater than 1.89, the orifice is choked (Binder, 1950) and the discharge can be calculated by

$$Q_a = C_d A_0 \sqrt{g \frac{\rho_w}{\rho_a} H^*} \sqrt{k \left(\frac{2}{k+1} \right)^{\frac{k+1}{k-1}}} \quad (2-6)$$

When the water column reaches the end of the pipe, the impact pressure of the water column can be calculated by the following method. Referring to Fig. 2.3, first a water hammer characteristic equation is applied between sections 1 and 2. Then the energy equation and continuity equation are applied between sections 2 and 3 where the latter is open to the air. The impact pressure head H_2 can be calculated by

$$H_2 = H_1 + \frac{a}{g} \left(U_1 + \frac{a}{B} - \sqrt{\left(\frac{a}{B} \right)^2 + 2U_1 \frac{a}{B} + \frac{2gH_1}{B}} \right) \quad (2-7)$$

where: a is the speed of the pressure wave when the water column reaches the orifice and B is a coefficient, defined as $B = (A/A_0)^2 + K - 1$. K is the minor loss coefficient of the

orifice which can be neglected since it is very small compared with A/A_o . U_1 and H_1 are, respectively, the velocity and pressure head at section 1-1 and are calculated from Eqs. (2-1) through (2-3).

When applying Equation (2-7), care must be taken in determining the appropriate value of pressure wave speed, since it is quite sensitive to the air content in the flow. For example, the wave speed in a pipeline containing water with 5% air content is only 20% of that without air (Wylie and Streeter, 1978). Since the air entrained in the water column during the filling process is difficult to determine, the wavespeed cannot be theoretically calculated. Therefore, a measured value of wave speed is needed to apply Equation (2-7). Consequently, this analytical model is not a predictive tool but rather, provides a means of exploring and explaining the behavior of this phenomenon.

2.2.2 Numerical solution approach

To simplify the analysis the governing equations are normalized by defining the following non-dimensional variables(Martin, 1976):

$$\lambda = \frac{x}{L} \quad \eta = \frac{V_a}{V_{a0}} \quad \phi = \frac{H^*}{H_0^*} \quad \psi = \frac{U}{\sqrt{g(1-x_0/L)H_b^*}} \quad \alpha = \frac{a}{\sqrt{g(1-x_0/L)H_b^*}}$$

$$\tau = \frac{t}{L\sqrt{\frac{(1-x_0/L)}{gH_b^*}}}$$

where the subscript "0" denotes initial values.

Eq. (2-1) becomes

$$\frac{d\eta}{d\tau} = -\psi \quad (2-8)$$

Eq. (2-2) becomes

$$\frac{d\psi}{d\tau} = -\frac{1}{\phi_b} \frac{\phi-1}{\lambda} - \frac{C_0}{2} (1-\lambda_0) \psi |\psi| - \frac{1}{2\lambda} (1-\lambda_0) \psi^2 \quad (2-9)$$

Eq. (2-3) becomes

$$\frac{d\phi}{d\tau} = -\kappa \frac{\phi}{\eta} \frac{d\eta}{d\tau} - \kappa \frac{\phi}{\eta} \frac{C_1 Y}{(1-\lambda_0)^{0.5}} \sqrt{2 \left(\frac{\phi}{\phi_b} - 1 \right) \left(\frac{\phi_b}{\phi} \right)^{1/k}} \quad (2-10)$$

when $H^*/H^*b < 1.89$ and

$$\frac{d\phi}{d\tau} = -\kappa \frac{\phi}{\eta} \frac{d\eta}{d\tau} - \kappa \frac{\phi}{\eta} \frac{C_1 \bar{y}_c}{(1-\lambda_0)^{0.5}} \sqrt{\left(\frac{\phi}{\phi_b} \right)^{1-1/k}} \quad (2-11)$$

when $H^*/H^*b > 1.89$.

Here

$$C_0 = fL/D$$

$$C_1 = C_d A_0 / A \sqrt{\rho_w / \rho_a}$$

$$\phi_b = H^* / H^*_0$$

$$\bar{y}_c = \sqrt{k \left(\frac{2}{k+1} \right)^{\frac{k+1}{k-1}}}$$

Eq. (2-7) is normalized as

$$\varphi_2 = \varphi_1 + \phi_b \alpha (1-\lambda_0) \left(\psi_1 + \frac{\alpha}{B} - \sqrt{\left(\frac{\alpha}{B} \right)^2 + 2 \frac{\alpha \psi_1}{B} + \frac{2}{B} \left(\frac{\varphi_1}{\phi_b} - 1 \right)} \right) \quad (2-12)$$

The resulting non-dimensional equations are nonlinear ordinary differential equations; they were solved numerically using a fourth-order Runge-Kutta technique (Ayyub and McCuen, 1996).

The boundary and initial conditions are (1) the driving pressure head (at the left hand side of the water column), taken as the head tank pressure (constant throughout the simulation); (2) the initial pressure head downstream of the water column, which is assumed to be atmospheric; and (3) the initial velocity of the water column, which is taken as zero to be consistent with the experimental tests conducted (although the analytical model is not limited to this situation).

A sensitivity analysis was conducted to determine the optimal time step increment. For most test scenarios, the numerical scheme was stable whenever the non-dimensional time step increment was less than 0.01. The exception was when the initial water column was long ($\lambda_0 = 0.8$) and the orifice size large ($d/D > 0.2$); in that case, a dimensionless time step less than 0.002 was required for stability. Since the computational effort required for a very small time step was negligible, it was decided to adopt a dimensionless time step increment of 0.001 for all runs. This represents a dimensional time step increment ranging from 6.975×10^{-4} to 9.85×10^{-4} seconds over the range of test conditions modeled, with the larger increments being associated with $\lambda_0 = 0.048$.

The simulation proceeds until the water column reaches 99.9% of the pipe length. At that point in time, if the orifice size is not zero, the air release is assumed to be complete. The impact pressure is then calculated using Equation (2-12) and the

resulting value is then compared with the maximum pressure magnitude calculated during the transient simulation; the larger of the two is taken as the maximum pressure for that case.

2.3 Sensitivity Analysis

From the theoretical equations describing the rapid filling of pipelines containing trapped air, it is seen that following parameters play important roles in affecting the pressure oscillation behavior. They are the friction factor, f , the orifice discharge coefficient, C_d , and the polytropic factor, k . These factors will be briefly discussed in this section.

2.3.1 Effects of the friction factor

It has already been observed that using the steady flow friction factor for unsteady flow under-estimates the pressure wave attenuation at the moderate and high frequencies (Chaudhry et al, 1985, 1990). Although substantial progress has been made on understanding the periodical pulsating of turbulent flows (Shuy and Aplet 1983; Fok, 1987; Suo and Wylie 1989; Vardy 1992), at this time there is no satisfactory practical model for predicting the friction effects in unsteady turbulent flows.

Fok (1987), Shuy and Aplet (1983) conducted an intensive literature review on this matter. Their studies shows that the difference between using the steady flow friction factor and the unsteady flow friction factor is not likely to be significant to pipeline designs where the most important criterion is the maximum pressure. However, the differences are greater for the minimum head, which means that using different friction models results in substantial differences in the prediction of the sub-

atmospheric pressure and of separation in a pipeline. In other words, if there is no column separation, the friction factors from different models will not produce significantly different results.

2.3.2 Effects of the orifice

The effects of the orifice on pressure oscillations are obvious. It is known that the orifice discharge coefficient plays a dominant role in determining the air release rate during the filling process. Strictly speaking, the discharge coefficient is affected by many factors, including the pipe size, the orifice size, the flow rate through the orifice, the specific weight of the fluid, the viscosity of the fluid, the ratio of differential to upstream pressure, and the specific heat of the gas. Other factors that affect the discharge coefficient include the surface roughness, dents in the edge of the orifice, and the eccentricities in locating the orifice in the pipe. In fact, because the discharge coefficient value oscillates with time as that of pressure, it is very difficult to make reliable measurements of a gas flow with an orifice meter when appreciable pulsations from any source whatsoever are present at the point of measurement (Brower, 1993). No way has been found to determine or predict correlation factors to compensate for such errors (Jones and Bajura 1989; Pascal 1983). Therefore in this paper, based on the geometric properties of the orifice, the discharge coefficient for a steady air flow through a flat flange edge orifice (American Gas Association, 1978) was tested and it was found that $C_d = 0.65$ gave the closest agreement to the experimental results. Figs. 2.4a and 2.4.b show the effects of C_d on the maximum air pressure using the proposed rigid water column model.

2.3.3 Effects of the polytropical component k

The dynamic condition existing in the air pocket during the transient motion is a very complex heat transfer problem. Graze (1968) proposed a rational heat transfer procedure to replace the conventional approaches, so that the temperatures inside of the air volume and outside of the pipe or the air chamber are considered. The comparisons between the experimental and mathematical results in our studies, as well as that by Graze(1968) proved that the conventional polytropic with the index, $k = 1.4$ predicts the magnitude of pressure accurately enough for engineering purposes. Fig. 2.5 shows the results of using different k values. It can be seen that $k = 1.4$ gives the closest results to the experimental values.

2.4 Experimental Program

Because there is currently no experimental data available describing flow transients in a rapidly filling pipe containing trapped air and experiencing air leakage, an experimental study was conducted at the T. Blench Hydraulic Laboratory, at the University of Alberta. Fig. 2.6 depicts the experimental apparatus used in this investigation. Here, a simple domestic water supply pressure tank (120 cm high and 42 cm in diameter) was used at the upstream end of the system to ensure an approximately constant value of the upstream head during the pipe filling process. Inflow to the pressure tank was from a standard municipal water supply line; a pressure regulator at the inlet to the tank facilitated a range of driving heads. The 10 m long pipe was made of galvanized steel and had an inside diameter of 35 mm. It consisted of three sections, separated by three quarter-turn ball valves located 48, 500 and 800 cm downstream of

the tank, respectively. These valves provided three different initial air volume and water column length scenarios. The downstream end of the pipe was either sealed to form a dead end, or outfitted with a cap containing a centered, sharp-edged, orifice to study the effects of air release on pressure transients in the system. Alternate pipe materials were not tested because of safety concerns, given the extremely high pressures observed during the tests.

Three high-frequency-response (1000 Hz) strain-gauge pressure transducers (PACE, Model KPI5) were installed along the pipe at distances of 284, 636, and 990 cm downstream of the tank, respectively. The transducers were calibrated using a fluid-pressure scale up to 7000 kPa. The calibration determined a linear voltage-pressure relation with an error of $\pm 0.5\%$. Each of these transducers was connected to a carrier demodulator (Validyne, Model CD15) which was, in turn, connected to a data acquisition board (National Instruments, AT-MIO-16XE-50) driven by a personal computer. A data acquisition program (written in LabView 4.0) was set to initiate data collection automatically when the pressure rose above a specified value. The pressure history and the maximum and minimum pressures at each of the three transducers were first displayed on the computer screen and then saved to a file for later analysis.

To facilitate calibration of the analytical model later on, the friction factor f of the pipe and the minor loss coefficient for the ball valves were indirectly measured under steady flow conditions. It was first determined that the minor loss coefficient for the ball valves ranged from 0.087 and 0.093 and that these minor losses amounted to slightly less than 10% of the total losses for the complete system (i.e., 10 m of pipe

including the three ball valves). The friction factor, f , determined based on total losses, ranged between 0.032 and 0.035. This is slightly higher than the value of 0.029 one obtains for these flow conditions, based on a roughness height of 0.15 mm for new galvanized steel (Massey, 1968). The tolerance is about 10%, which is acceptable since the Moody diagram is based on the experimental data that likely is accurate to within no more than 5% (Potter and Wiggert, 1997). The difference can be attributed to the fact that the pipe used was slightly roughened by mineral deposits, and to the inclusion of the minor losses in the computation of the measured friction factor. The latter was a practical convenience, since the minor losses were not considered explicitly in the analytical model.

Rapid filling of the pipe was achieved by manually turning the quarter-turn ball valve. Using a high-speed digital camera recording at 500 frames per second (RedLake Imaging, MotionScope, PCI 500), it was determined that the valve opening time (from fully closed to fully opened) ranged between 0.06 and 0.08 seconds. As is shown later, this period is less than half of the duration of the pressure oscillation cycle.

The speed of the waterhammer impact pressure wave is a necessary input when calculating the impact pressure in the analytical model. This was estimated by measuring the time difference of the pressure spike between the upstream and downstream transducers.

2.5 Experimental Results

Four upstream heads of 343 kPa (50 psi), 275 kPa (40 psi), 206 kPa (30 psi), and 137 kPa (20 psi); three different initial water column lengths of 0.48 m, 5 m, and 8

m; and 12 orifice sizes ranging from 0 to 19.8 mm were tested; resulting in a total of 144 test cases. To determine the consistency of results, each of the 144 tests was repeated at least five times. It was found that the difference between the highest and the lowest values of the peak pressure for a given test case was less than 10% for d/D values less than 0.086 and for d/D values greater than 0.257. For d/D values between 0.114 and 0.257, this difference could be up to 51%.

2.5.1 Pressure oscillation patterns within the air pocket during rapid filling

The recorded pressure oscillations for all runs were examined and it was found that three types of behavior could be defined, each representing a different pressure oscillation pattern depending on the relative size of the leakage orifice. For the situations of no air release or small orifice sizes, a long period pressure oscillation pattern was observed as the air was released, and no significant waterhammer impact pressure occurred. When the orifice size was large, no long period air pocket pressure oscillation occurred; instead only waterhammer impact pressure was observed. For the intermediate orifice sizes, the pressure oscillation pattern consisted of both long period and short period pressure oscillation patterns.

These three types of pressure oscillation patterns can be classified, according to the relative importance of the air cushioning effect on the waterhammer pressure, as: Type 1 behavior, in which the air cushioning effect is dominant and the waterhammer impact pressure is negligible; Type 2 behavior, in which the air cushioning effect is reduced and the waterhammer pressure begins to become significant and; Type 3 behavior in which waterhammer effect is dominant.

To illustrate each of these patterns of behavior, Figs. 2.7a to 2.7d present the pressure histories (gauge pressure) for an initial head of 206 kPa (30 psi) and an initial, non-dimensional, water column length, λ_0 of 0.5. Because the data acquisition software was programmed to begin collecting data when pressure rose above a specific value (60kPa), the pressure history did not start as zero. Each figure is discussed below.

Type 1 Behavior: Negligible waterhammer effect

As shown in Fig. 2.7a, for closed flows or when the orifice size was sufficiently small, the air pocket persisted for a long period, acting as a “shock absorber”, and the pressure in the air pocket oscillated with decaying peak magnitudes. It is significant to note, however, that the maximum pressure experienced may still be several times the upstream driving pressure, and sufficient to exceed the structural design capacity of drainage pipe systems. The pressure oscillation has a long period, in this case in the order of 1 second, which is approximately two orders of magnitude larger than that of the water hammer period. During the experiments, the sound of water column oscillation along the pipe and the sound of air release could be faintly heard. The upper limit of the orifice size ratio, d/D , for Type 1 behavior was less than 0.086 for all tests conducted.

Type 2 Behavior: Mitigated waterhammer effect

Fig. 2.7b shows two pressure oscillation histories for the same test scenario, for which the d/D ratio was increased beyond 0.086. Here, the pressure oscillation pattern can be divided into two distinct stages. During the earlier stage of filling, while the air pocket persisted and the volume of air released was insignificant, a long period pressure

oscillation pattern similar to Type 1 behavior with at least one cycle was observed. It was found that the duration of this long period pressure oscillation stage decreased as the orifice size and the initial water column length were increased. Later, once a substantial portion of the air had been released, the water column slammed into the pipe end and induced a waterhammer impact pressure. The period of the pressure oscillations was quite short after impact, compared to the period for the air pocket pressure oscillation. It was also found that this waterhammer pressure could be either higher or lower than the peak pressure observed during the long period pressure oscillation stage. During these experiments, a loud and vibratory air release sound at the orifice was first heard, followed by the sound of the impacting water column. The upper limit of the orifice size ratio, d/D , for Type 2 behavior was 0.171 to 0.257 for the range of conditions tested.

It was found that the patterns of the long period pressure oscillations were quite consistent between runs of the same test, as compared to the short period oscillation stage, as illustrated by the two test runs shown in Fig. 2.7b. In contrast, the short period water hammer pressure oscillation pattern was found to be highly variable between runs for the same test scenario. For example, as mentioned above, the difference between the highest and the lowest peak pressure for a given test scenario could be up to 51%. This variability is likely due to the sensitivity of the peak pressure to air entrainment in the water.

As illustrated in the pressure history of Test 2 shown in Fig. 2.7b, the pressures went slightly below atmospheric (less than 1kPa) after a huge positive pressure spike.

Throughout the experiments, very few cases had such a negative pressure, which is believed to be the effect of negative pressure wave. Since the frequency of the occurrence of such negative pressure observed in the experiments was very low, the negative pressure was not investigated in this study.

Type 3 Behavior: Waterhammer dominated

Beyond a critical value of the orifice size ratio d/D (0.171 to 0.257 for the range of conditions tested), the air release was so rapid that the air pocket no longer acted as a shock absorber in the system. For these experiments the sound during the air release was sharp and short, and was immediately followed by the loud sound of water impact on the pipe end. Fig. 2.7c illustrates a typical pressure history where it is seen that there is no long period pressure oscillation stage. Without reversal motion, the water column quickly reaches the pipe end and generates a large waterhammer impact pressure (14 times that of the upstream head for this case).

When the orifice size was further increased (d/D larger than 0.257 for the range of conditions tested), the air was released so quickly that it provided negligible resistance to the water column behind, as shown in the inset on Fig. 2.7d. Consequently, the water column quickly slammed into the orifice and generated a waterhammer impact pressure. During these experiments, no air release sound was heard, just the sound of the water column impacting on the pipe end.

Table 2-1 summarizes the general features of the pressure oscillation pattern for different orifice sizes.

2.5.2 Magnitude of peak pressures as a function of the orifice ratio and water column length

Fig. 2.8 presents all of the measured maximum peak pressures observed during rapid pipe filling, as a function of orifice size and grouped by the type of behavior (based on examination of the entire pressure oscillation pattern). In the figure, the horizontal axis is the relative orifice size, d/D , and the vertical axis is the absolute pressure head normalized by the upstream head. For Type 1 behavior, because of the cushioning influence of the air pocket, the maximum pressure remains relatively consistent (from about 1.5 to 3 times the upstream head). For Type 2 behavior the maximum pressure rises rapidly since the mitigating effect of the air pocket decreases as air release rate increases. In this zone, the data scatter is large, likely because the impact pressure is sensitive to air entrainment. The highest maximum pressures were 15 times the upstream head. For a given initial water column length (or air volume), the observed peak maximum pressure values were similar in magnitude and occurred at a fairly consistent orifice size (d/D of approximately 0.171 to 0.254 for the range of conditions tested); however there was a slight tendency for this critical hole size to decrease as the initial volume of air decreased. For Type 3 behavior, the maximum pressures are due to waterhammer impact only. These were observed to decrease with increasing orifice size (as seen in Fig. 2.8) because, as the orifice size increases, the change in water velocity decreases, decreasing the impact pressure.

Fig. 2.9a illustrates the effects of the initial water column length, λ_0 , on the observed maximum pressure for each type of behavior. Here the upstream pressure was

the highest value tested: 343 kPa ($H^*/H_b^* = 4.57$). For both Type 1 and Type 2 behavior, the maximum pressure was observed to increase with λ_0 (i.e., to decrease as the initial air pocket volume decreased because of the diminishing air cushioning effect) and for the range of conditions tested, the maximum pressure was approximately 3 times the value of the upstream head. For Type 3 behavior, it was found that the experimental data for $\lambda_0 = 0.8$ and $\lambda_0 = 0.5$ were asymptotic to a single recession curve for a given upstream head. The asymptotic feature of the impact pressure indicated that for a large λ_0 (i.e., λ_0 greater than 0.5 for the tested conditions), the maximum pressure was only dependent on the orifice size and the upstream head, not the initial water column length.

2.5.3 Magnitude of peak pressures as a function of the driving pressure

Together, Figures 2.9a ($H^*/H_b^* = 4.57$) and 2.9b ($H^*/H_b^* = 2.43$) illustrate the effect of varied driving pressure on peak pressures. Based on these two figures, and those for the two intermediate driving pressures (not shown) the following observations were drawn. For Type 1 behavior, there was a consistent trend, with higher driving pressures associated with higher peak pressures. Peak pressures ranged from about 1.2 to 3 times the upstream head, with the larger values associated with the smaller initial air volumes and higher upstream pressures. For Type 2 behavior, the data scatter was large and there was no systematic relationship between the upstream pressure and the peak pressures observed for a given value of λ_0 . For Type 3 behavior, the maximum pressure magnitude seems to be independent of upstream pressure, which is consistent with the conclusions of Albertson and Andrews (1971).

2.5.4 The speed of the waterhammer pressure wave

The dependence of wavespeed on air entrainment is a well-documented effect (e.g., Pearsall, 1965). Here, it was found that the wave speed varied considerably, from 200 m/s to 1400m/s, varying with the relative orifice size and the initial water column length. It was observed that the wave speed approached a constant value for a given initial water column length when the relative orifice size, d/D , was larger than a specific value ($d/D > 0.257$ in the tested range). It was also found that the wave speed for a short initial water column length was much lower than that for a longer initial water column length. Additional experiments were conducted incorporating a short section of transparent pipe (over a limited range of pressures, because of safety concerns) and it was observed that a shorter initial water column length was more likely to trap air pockets; therefore, more air could be entrained, likely explaining the reduced wave speed in these cases.

2.6 Analytical Model Verification

The experimental observation, that the long period pressure oscillation pattern has a period two orders of magnitude higher than that of the water hammer cycle speed, justifies the applicability of the rigid water column approach used in the proposed analytical model. In order to verify this model, comparisons of calculated and observed pressure oscillation patterns and peak pressures were conducted. The speeds of the pressure waves measured in the experiments were used as input parameters in the calculations, as was the friction factor. The minor losses due to the ball valves were

considered implicitly, since the friction factor determined for the pipe included the effects of minor losses.

2.6.1 Comparison of the calculated and measured pressures

Fig. 2.10 shows a comparison of computed and observed pressure oscillation patterns for the three type of behavior. As shown in Fig. 2.10a, the model can approximately reproduce the actual pressure oscillation pattern of Type 1 behavior, especially for the first cycle of the oscillation. However, starting from the second cycle, the computed pressure oscillation frequencies and peak attenuation are less than that observed in the experiments. One explanation might be that the steady flow friction factor used in the calculations underestimated the actual unsteady flow friction factor and, consequently the model did not sufficiently attenuate the peak pressure (Wylie and Streeter, 1978). Another explanation might be the fact that the computational model assumes that the air pocket remains intact, whereas in the additional experiments conducted with a short section of transparent pipe, the air pocket was observed to roll up and split into several smaller pockets.

Fig. 2.10b shows a comparison between measured and computed values for Type 2 behavior. Here it is seen that the computed period of pressure oscillation was much shorter than was observed in the experiments. This might be attributed to a limitation in the numerical model, which assumes that the air-water interface is vertical and once the water column reaches the end of the pipe, the air will be totally released. Therefore, the model can only simulate part of the long period oscillation pattern (i.e., the stage before the water column reaches the orifice.)

For Type 3 behavior (shown in Fig. 2.10c), the pressure oscillation took place only after the water column had reached the orifice. Therefore, as expected, the model can only simulate the amplitude and the approximate timing of the maximum air release pressure before the water column reaches the orifice. The rest of the peaks in the experimental pressure oscillation shown in Fig. 2.10c were caused by the release of the residual air pockets.

Fig. 2.11 shows the comparison between the computed and observed peak pressures for each type of behavior. It was found that for 94% of the tests of Type 1 behavior, the difference between the computed and observed peak values was less than 10%. For 90% of the tests of Type 2 behavior, this error was less 10% for the initial peak and for the air release pressure peak, 85% of the tests had an error less than 15%. For Type 3 behavior, 92% of the tests had a peak error less than 15%.

To further analyze the accuracy of the model results, a simple statistical analysis was conducted by defining a relative error as:

$$\varepsilon = \frac{|P_{\text{experiment}} - P_{\text{calculation}}|}{P_{\text{calculation}}} \quad (2-13)$$

Table 2-2 presents the results of this analysis, providing minimum, maximum and mean relative errors along with the standard deviation for each pressure behavior situation. As the table indicates, the average error ranges from 5 to 11%.

The above comparison demonstrates that, if the friction factor and the speed of pressure wave are known, the current model is able to quantify the amplitude of the impact pressure and the long period air pocket oscillation pattern, especially the first

cycle, for a rapid filling flow in a pipe with an air release at the pipe end. More importantly, the model successfully identified the type of behavior for all air release cases.

2.6.2 Martin's (1976) model

The proposed analytical model extends beyond that presented by Martin (1976), in that it also considers high rates of air release and the changing water column length during pipe filling. A comparison between Martin's (1976) model and the experimental data showed good agreement only for those cases where both the initial air pocket volume and the orifice size were small (d/D less than about 0.08). The error increases as the initial water column length decreases and Martin's constant water column length approximation results in a higher maximum pressure than that observed experimentally.

2.7 Conclusion and Discussion

The observations from our physical experiments confirm that air trapped in a rapidly filling pipe can induce high-pressure surges, especially when air leakage occurs. The pressure peaks observed from the experiments are certainly high enough to blow off manhole covers and explain sewer ruptures. In the Gallagher Hill Park situation, for instance, air leakage was negligible ($d/D \approx 0.002$), so a conservative estimate of the peak pressure (3 times the upstream head) would be 400 to 500 kPa (60 to 75 psi). This is at least one order of magnitude greater than the structural loads that typical urban sewer systems are designed for.

The experiments revealed that there are three types of pressure oscillation patterns in a rapidly filling horizontal pipe, depending on the relative size of the leakage orifice. When no air is released or orifice sizes are small, the cushioning effects of the air pocket prevents the water column from impacting on the pipe end and generating high water hammer pressures. However, the maximum pressure experienced may still be several times the upstream driving pressure. In this case, the pressure oscillation pattern has a long period, and the peak pressure remains relatively constant for a given initial air volume and upstream filling head. When the orifice size is very large, the air cushioning effect vanishes and the water column can easily impact on the pipe end, inducing a waterhammer impact pressure. In this case, the maximum pressure decreases with increasing orifice size, since for the larger orifice sizes, water escapes and mitigates the waterhammer effect. For intermediate orifice sizes, the pressure oscillation pattern consists of both long period oscillations (while the air pocket persists) followed by short period pressure oscillations (once water hammer dominates). In this case, the maximum observed pressures increase rapidly with increasing orifice size, since the cushioning effect of the air pocket decreases as the air release rate increases. The highest maximum pressures (up to 15 times that of the upstream head) were observed at the upper limit of this intermediate region, which occurs at a fairly consistent orifice size.

The analytical model presented here integrates the computation of air pocket pressure and air release pressure in a rapidly filling horizontal pipe. If the friction factor and the wave speed are known, the model is satisfactory in determining the amplitude

of the peak pressure for the entire orifice range and is able to approximately simulate the pressure oscillation pattern of Type 1 behavior, the case of a negligible waterhammer impact effect. Although the model is unable to simulate the pressure oscillation pattern when the air release is substantial, it can predict the type of pressure oscillation behavior and the peak pressure.

In terms of future research, both experimental and analytical studies are required for scenarios closer to real sewer system configurations, such as the rapid filling of a sewer trunk–drift tube-dropshaft system, rapid filling in a horizontal pipe of varied cross-sectional area, and the air release from a vertical pipe which serves as a drop shaft or a manhole.

2.8 Reference

Ayyub, B.M. and McCuen, R.H. (1996). *Numerical Methods for Engineers*, Prentice Hall, NJ, 362 pp.

Albertson, M.L., and Andrews, J.S. (1971). "Transients caused by air release." In *"Control of Flow in Closed Conduits."* (J.P.Tullis, ed.), pp.315-340. Colorado State University, Fort Collins, Colorado.

American Gas Association (1978). *Orifice Metering of Natural Gas, American National Standard*, ANSI/API 2530.

Binder, R.C. (1950). *Fluid Mechanics*, Prentice-Hall Inc., NJ.

Brower, Jr. et al. (1993). "On the compressible flow through an orifice." ASME, *Journal of Fluids Engineering*, 660/Vol.115.

- Burton, L.H., and Nelson, D.F. (1971). "Surge and air entrainment in pipelines." *In "Control of Flow in Closed Conduits."* (J.P.Tullis, ed.), pp.257-294. Colorado State University, Fort Collins, Colorado.
- Cabrera, E., Abreu, A., Perez, R., and Vela, A. (1992). "Influence of liquid length variation in hydraulic transients." *Journal of Hydraulic Engineering*, ASCE, Vol.118, No.12, pp.1639-1650.
- Cardle, J.A and Song, C.C.S. and Yuan, M. (1989). "Measurements of mixed transient flows." *Journal of Hydraulic Engineering*, ASCE, Vol.115, No.2, pp.169-181.
- Chaudhry, M.H. (1985). "Limitations of hydraulic—transient computations." *21st IAHR Congress*, Melbourne, Australia, 19-23 August, pp.132-136.
- City of Edmonton (1995). *A Report on the July 4, 1995 Storm Event*. Drainage Branch of Transportation Department, City of Edmonton, Alberta, Canada.
- EHG (1996). "Hydraulic transient evaluation of the City of Edmonton sewerage system, Phase I." *Research Report*, Environmental Hydraulics Group Inc., Ontario, 1996.
- Fok, T.K. (1987). *A Contribution to the Analysis of Energy Losses in Transient Pipe Flow, A thesis submitted for the Degree of Doctor of Philosophy*, University of Ottawa.
- Graze, H.R. (1968). "A rational thermodynamic equations for air chamber design." *Third Australasian Conference on Hydraulics and Fluid Mechanics*, Sydney, Australia, pp.57-61.

- Hamam, M.A. and McCorquodale, J.A. (1982). "Transient conditions in the transition from gravity to surcharged sewer flow." *Canadian Journal of Civil Engineering*, Vol.9, No.2, pp.189-196.
- Holley, E.R. (1969). "Surging in laboratory pipeline with steady inflow." *Journal of Hydraulic Engineering*, ASCE, Vol.95, No. 3, pp.961-979.
- Jones, E.H. and Bajura, R.A. (1989). "A numerical analysis of pulsating laminar flow through a pipe orifice." *Journal of Fluids Engineering*, Vol.113, pp.199-204.
- Jönsson, L. (1985). "Maximum transient pressures in a conduit with check valve and air entrainment." *Proc. Int. Conf. on Hydr. of Pumping Stations*, Manchester, England, pp.55-69.
- Martin, C.S.(1976). "Entrapped air in pipelines." *Proc., 2nd Int. Conf. on Pressure Surges*, B.H.R.A., Sept., F2, 15-28.
- Massey B.S. (1968). *Mechanics of Fluids*, Van Nostrand Company Ltd., London, England.
- Pascal, H. (1983). "Compressibility effect in two-phase flow and its application to flow metering with orifice plate and convergent-divergent nozzle." *Journal of Fluids Engineering*, ASME, 1983, pp.394-399.
- Pearsall I.S. "The velocity of water hammer waves." *Symposium on Surges in Pipelines*, Proceedings 1965-66, London, England, Vol 180, pp. 12-20.
- Potter, M.C. and Wiggert, D.C. (1997), *Mechanics of Fluids*, Second Edition, Prentice Hall, NJ.

- Shuy, E.B. and Aplet, C.J. (1983). "Friction effects in unsteady pipe flow." 4th *International Conference on Pressure Surges*, BHRA, pp.147-164.
- Suo, L. and Wylie, E.B. (1989). "Impulse response method for frequency-dependent pipeline transients." *Journal of Fluids Engineering*, Vol.111, 478-483.
- Vardy, A. (1992). "Approximating unsteady friction at high Reynolds numbers." *Proceedings of the International Conference on Unsteady Flow Fluid Transient*, Durham, UK.
- Wylie, E. and Streeter, V. (1976). *Fluid Transients*, McGraw-Hill International Book Company.
- Volkart, P.U. (1982). "Self-aerated flow in steep partially filled pipes." *ASCE Journal of Hydraulic Engineering*, Vol.108, No.9, pp.1029-1046.
- Wylie, E.B. and Streeter, V.L. (1978), *Fluid Transients*, McGraw-Hill, New York.

Table 2-1 Pressure pattern for different orifice sizes

Behavior	Orifice size(d/D)	Feature
Type 1	<0.086	Air cushioning effect is significant and water hammer pressure is negligible. Pressure pattern is regular, with a long period.
Type 2	0.086 ~ 0.2	Air cushioning effect is intermediate and water hammer effect is mitigated. Pressure pattern is initially regular with a long period before impact, and irregular with a short period after impact.
Type 3	>0.2	Air cushioning effect vanishes and water hammer pressure dominates.

Table 2 -2Comparison between measured and calculated peak pressure values

Pressure Type	ϵ_{min}	ϵ_{mean}	ϵ_{max}	Standard Deviation
Type 1	0.000105	0.054	0.30	0.048
Type 2 (initial peak)	0	0.10	0.28	0.091
Type 2 (impact peak)	0	0.11	0.32	0.093
Type 3	0	0.068	0.24	0.051

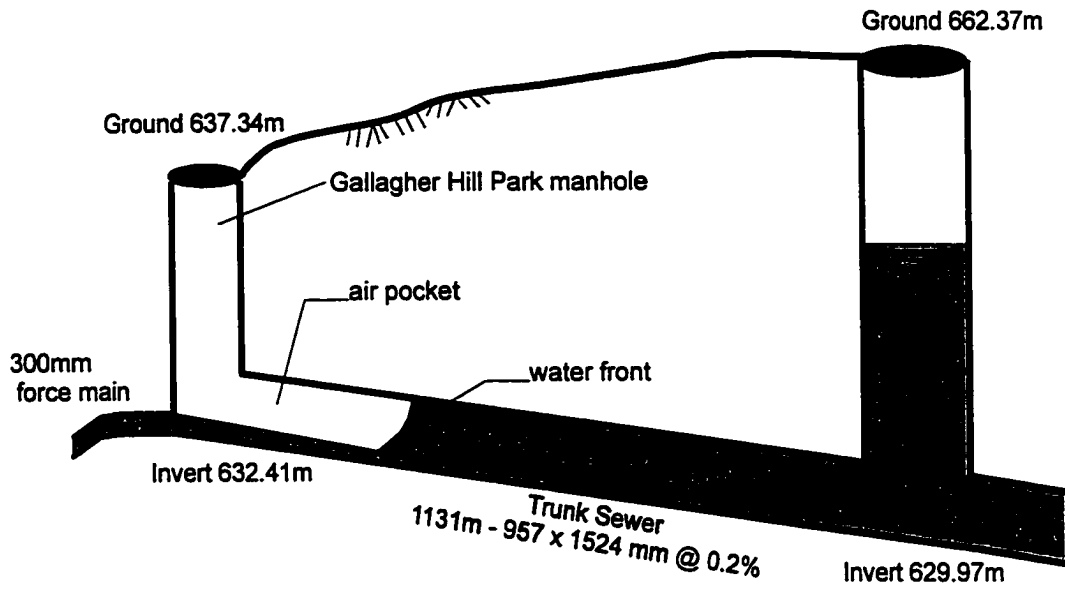


Figure 2.1. The trunk profile at Gallagher Hill Park (adapted from EHG, 1996).

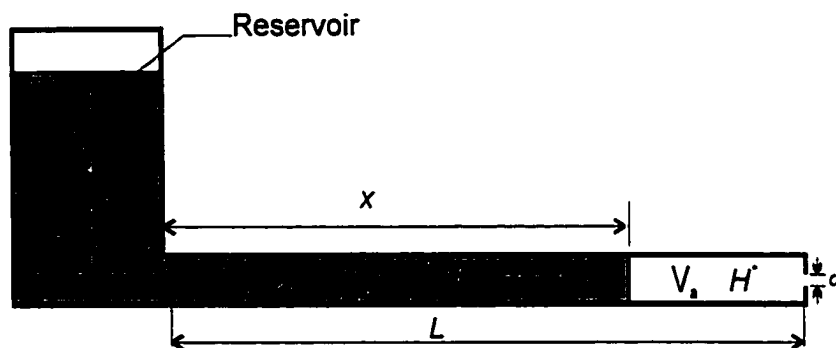


Figure 2.2. Defining sketch for the theoretical analysis.

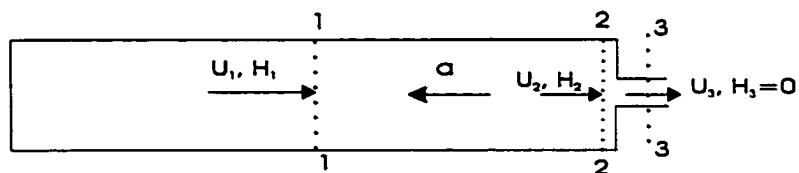
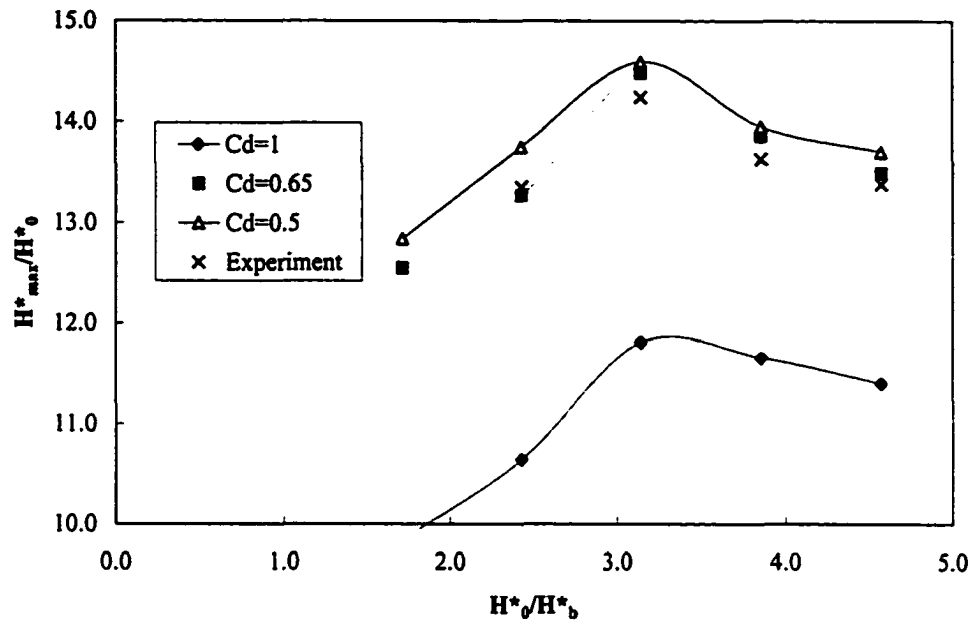
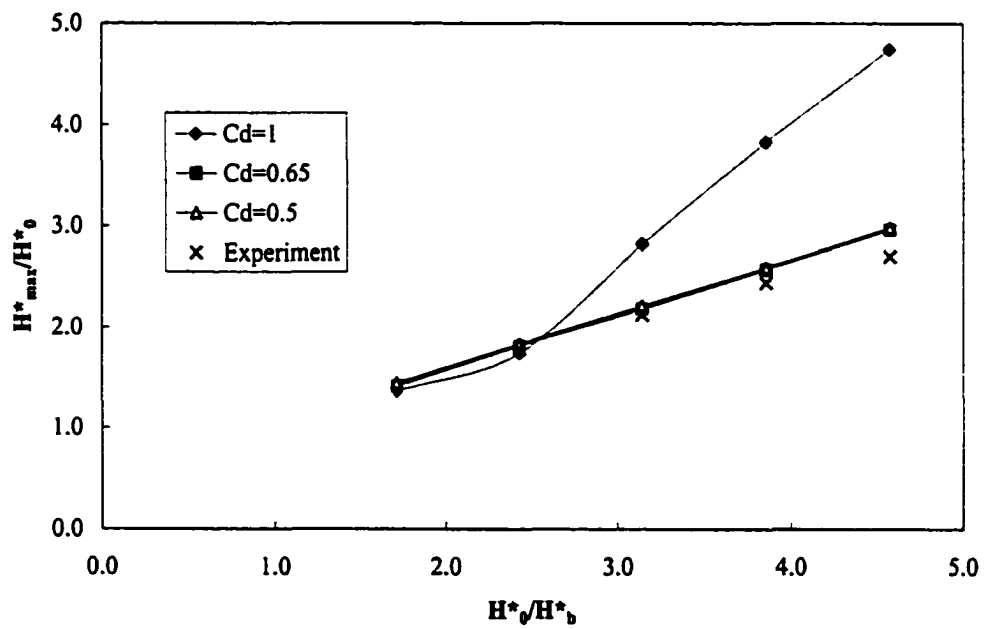


Fig. 2.3 Defining sketch for the impact pressure calculation



(a) $d/D = 0.2, \lambda_0 = 0.8$



(b) $d/D = 0.057, \lambda_0 = 0.8$

Fig. 2.4 Effect of discharge coefficient of the orifice

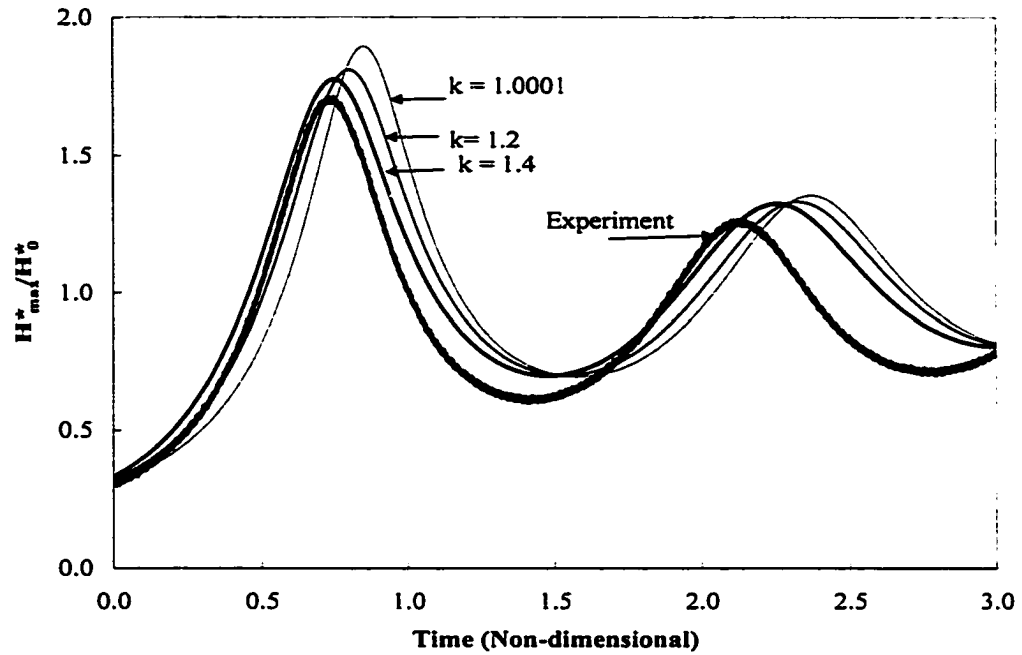


Fig. 2.5 Effects of polytropical component k ($H_0=275$ kPa, $x_0=5$ m)

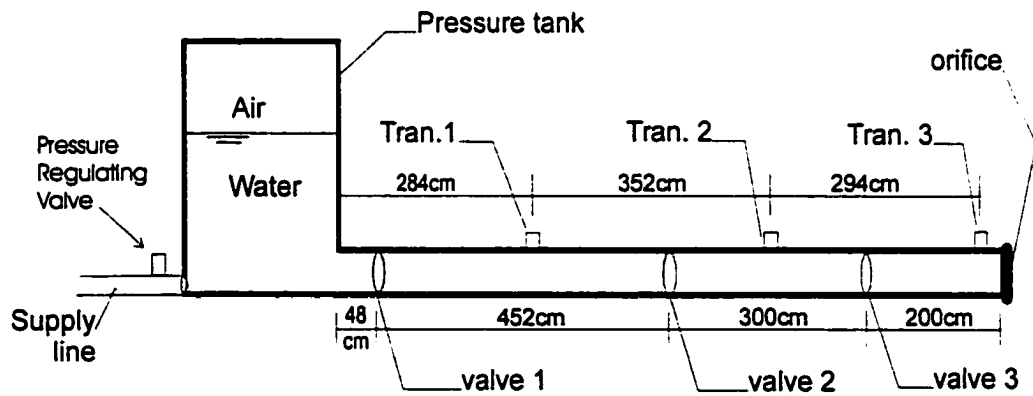


Figure 2.6. Diagram of the experimental apparatus.

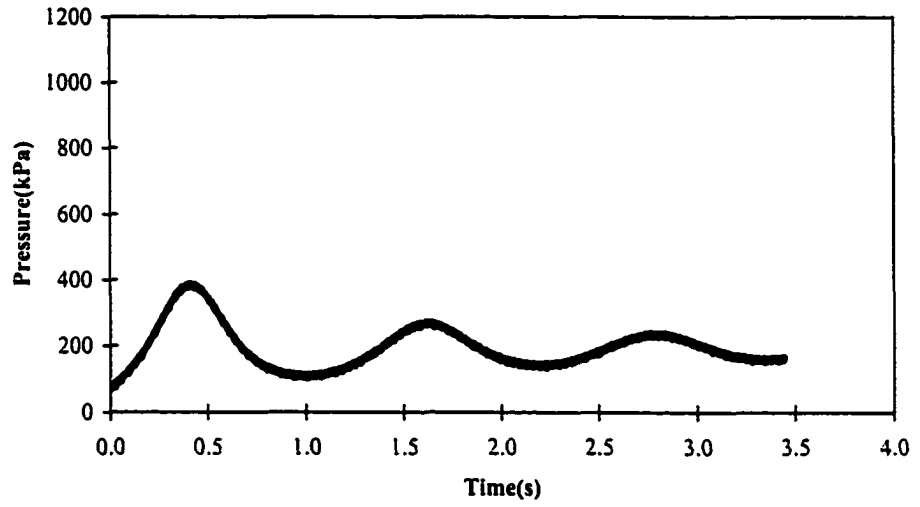


Fig. 2.7a Type 1, Negligible waterhammer effect, d/D :

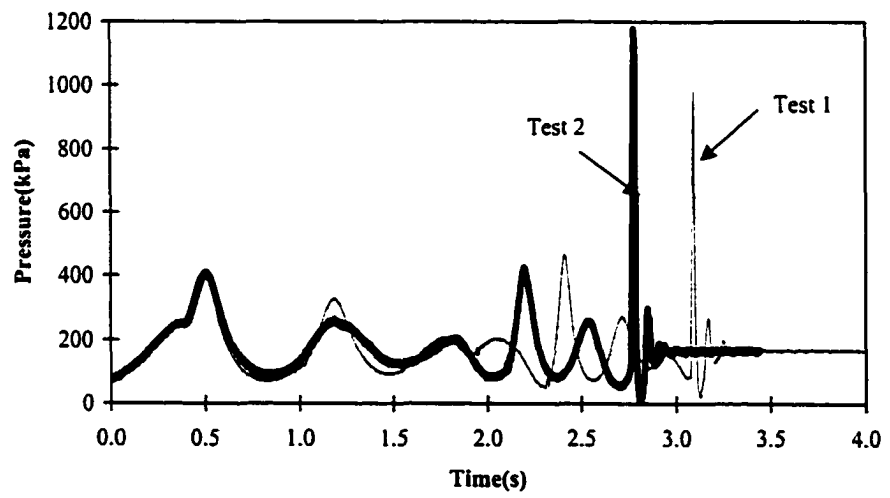


Fig. 2.7b Type 2, Mitigated waterhammer effect, $d/D = 0.114$

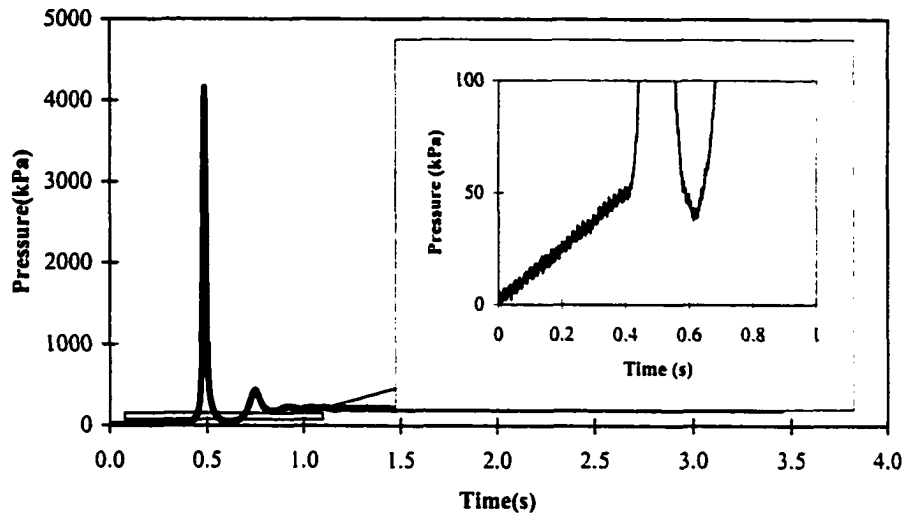


Fig. 2.7c Type 3, waterhammer dominated, $d/D = 0.2$

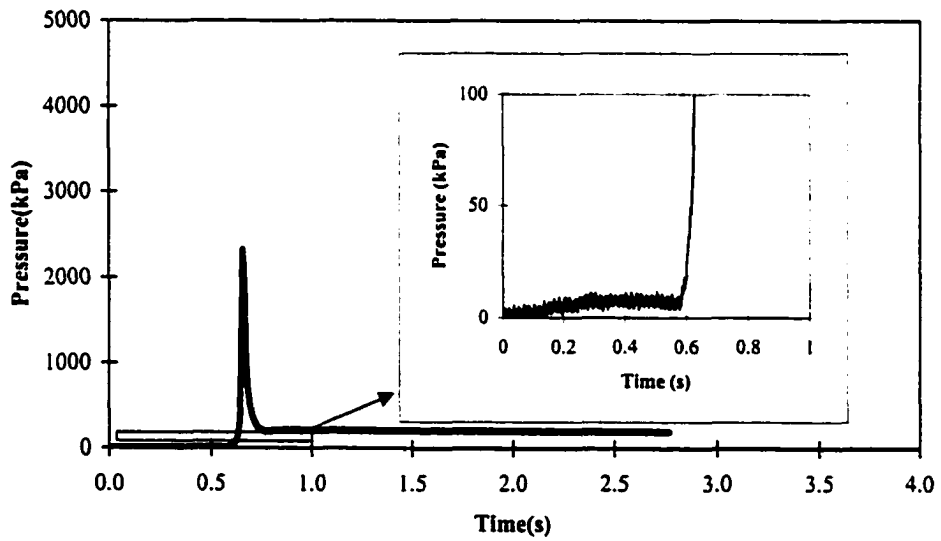


Fig. 2.7d Type 3, waterhammer dominated, $d/D = 0.34$

Fig. 2.7 Pressure Oscillation Patterns ($H_0^*/H_b^* = 3.14$, $\lambda_0 = 0.5$)

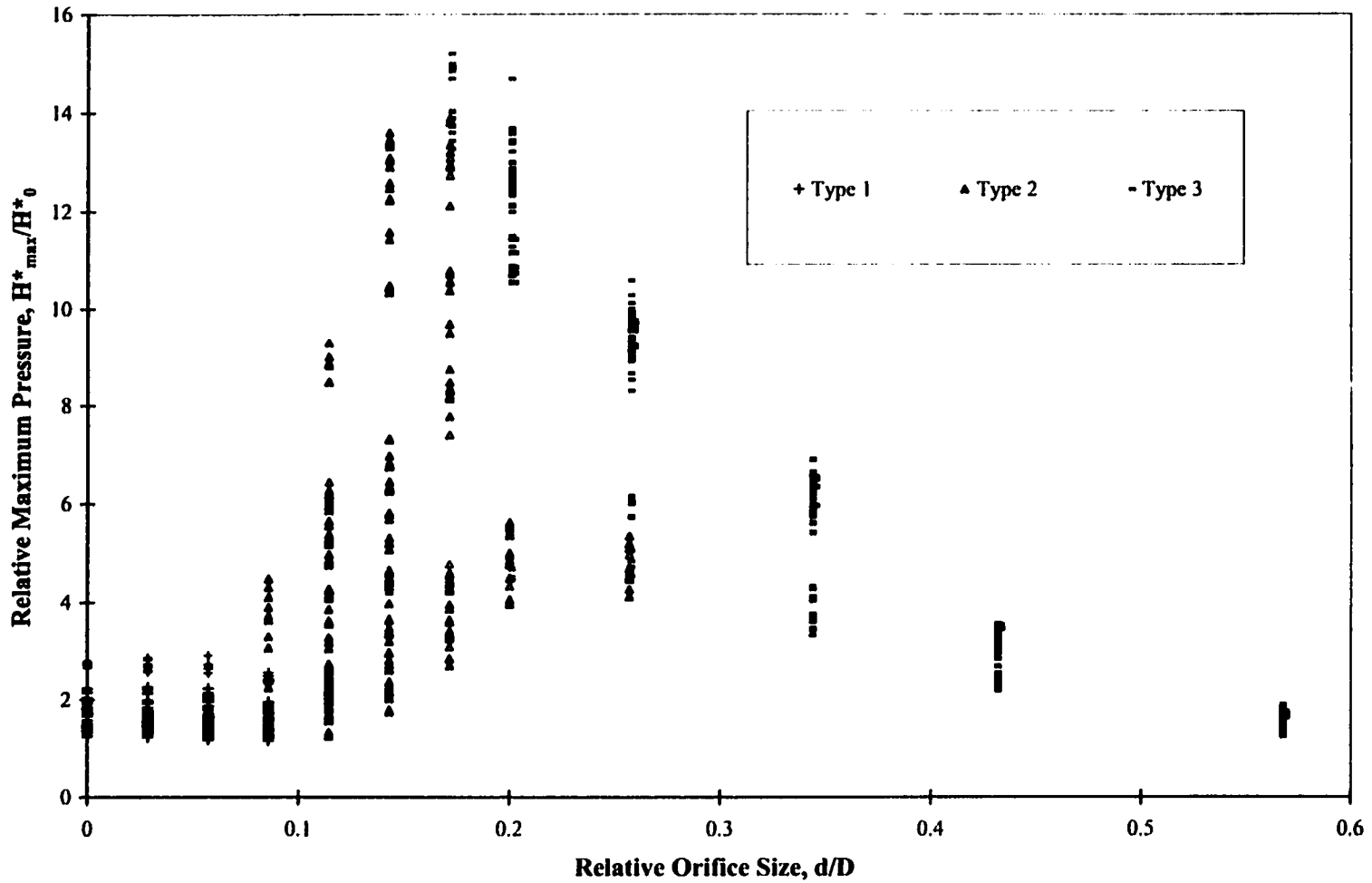


Fig. 2. 8 Relation between maximum pressure and relative orifice size for different types of behavior

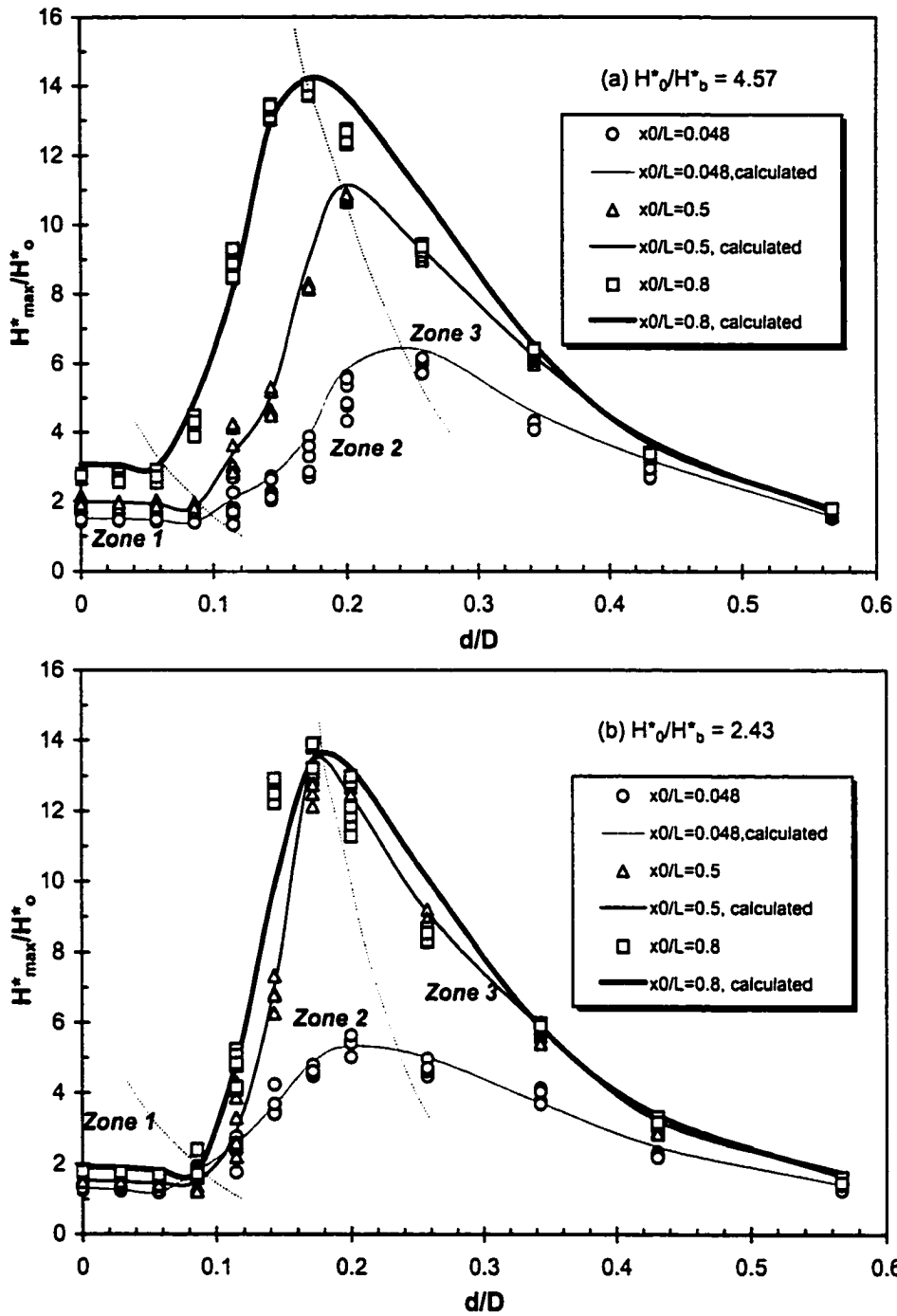
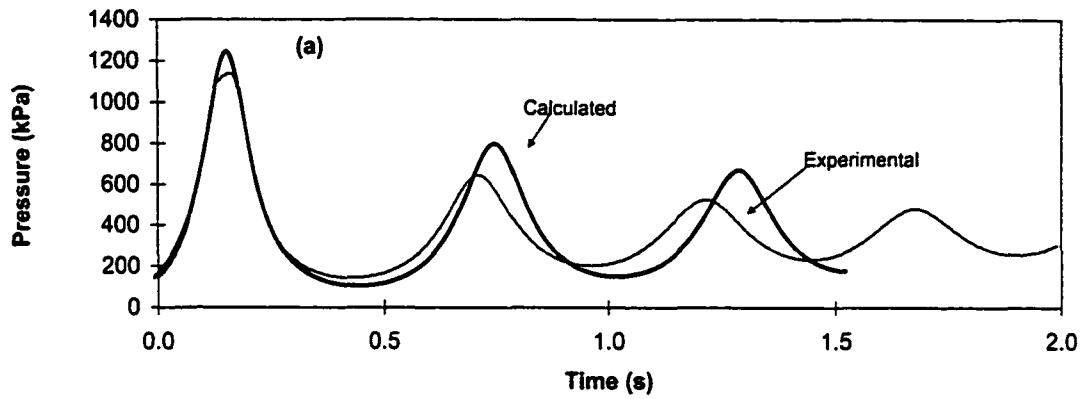
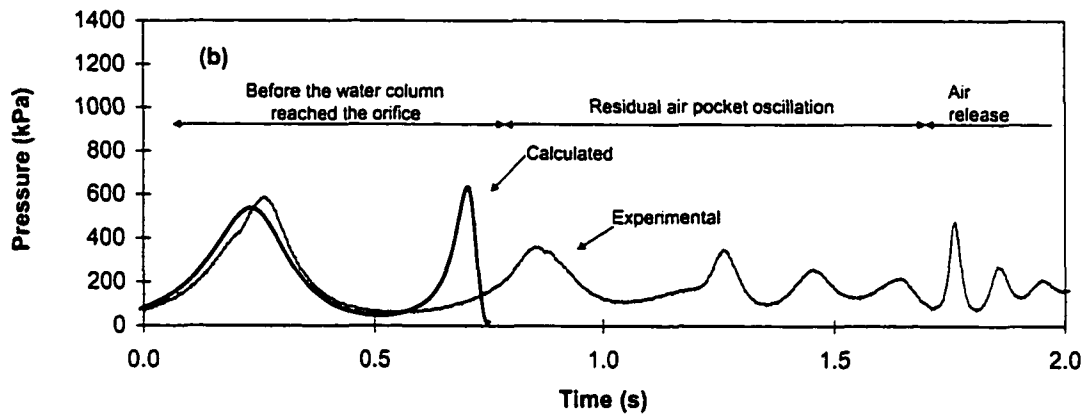


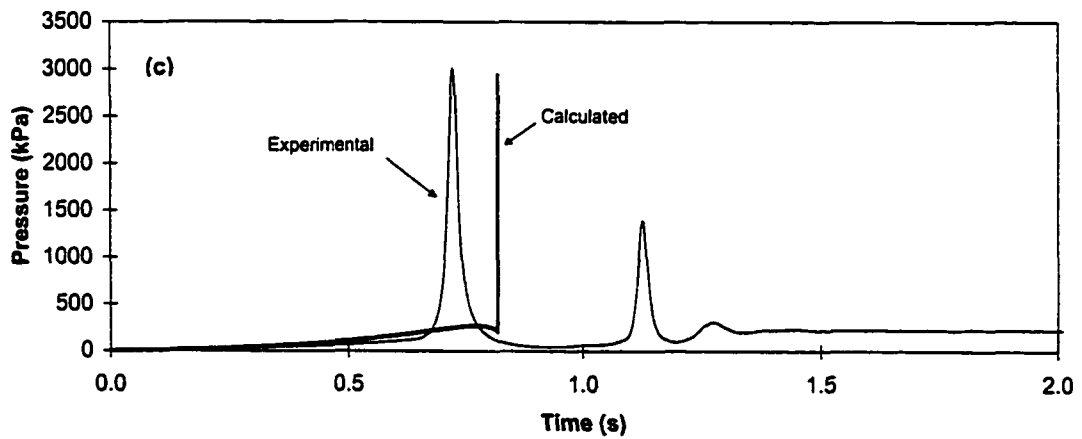
Fig. 2.9 The relation between maximum pressure and relative orifice size



$$(H_0^*/H_b^* = 4.57, \lambda_0 = 0.8, d/D = 0.028)$$



$$(H_0^*/H_b^* = 3.86, \lambda_0 = 0.5, d/D = 0.114)$$



$$(H_0^*/H_b^* = 4.57, \lambda_0 = 0.5, d/D = 0.171)$$

Fig. 2.10 A comparison between calculated and experimental pressure oscillations

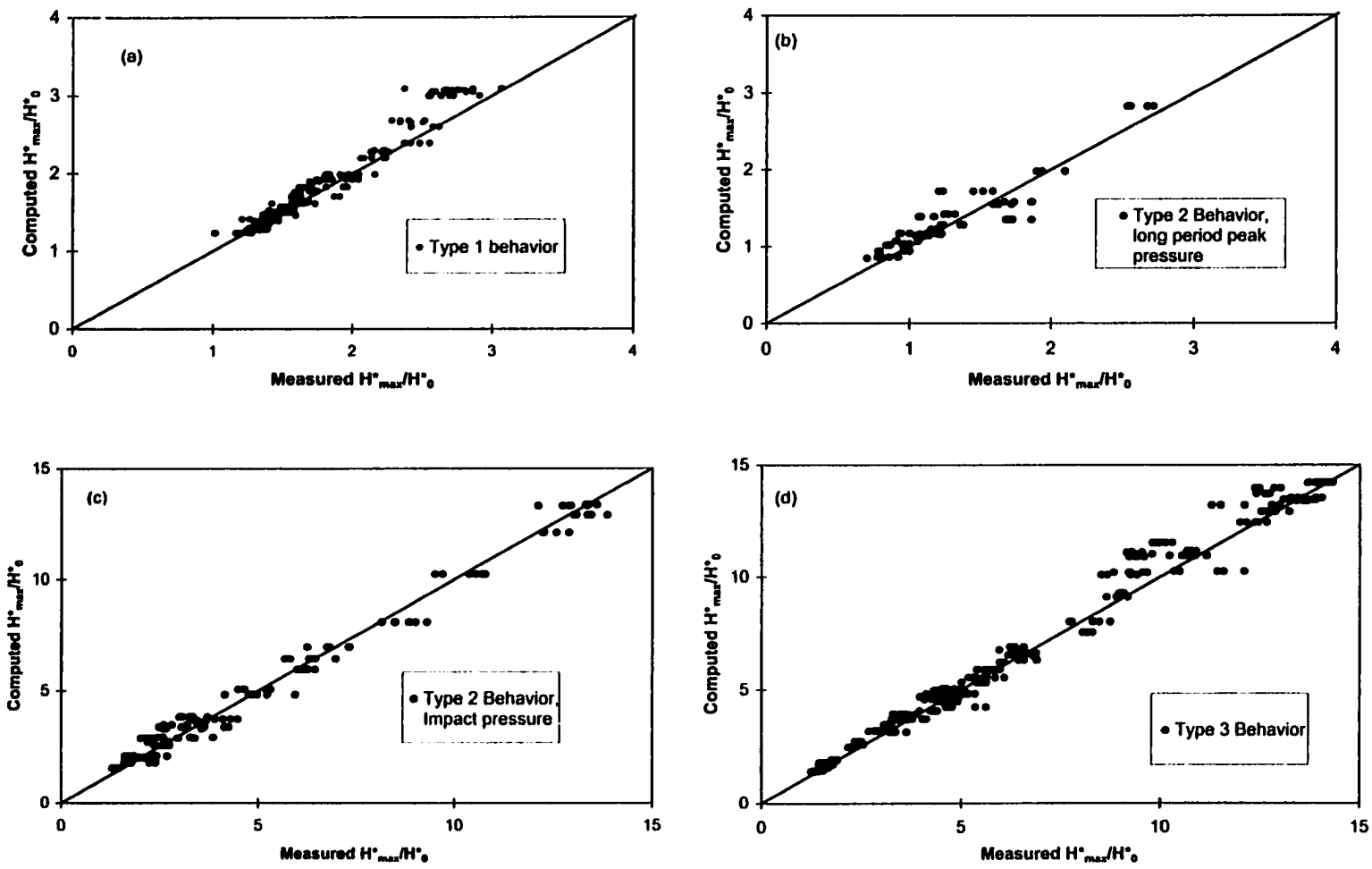


Fig. 2.11 A comparison between computed and measured maximum pressures

3.0 OBSERVATION OF THE AIR-WATER INTERACTION IN A RAPIDLY FILLING HORIZONTAL PIPE²

3.1 Introduction

One of the key issues in the design of urban drainage systems is the structural integrity of these systems under hydraulic overloading. Because these systems are typically designed for low return period events (1:5 to 1:10 years), it is expected that their hydraulic capacity would frequently be exceeded. When this happens, flow transitions from open channel to pressurized flow occurs, and the associated surges created in the system often trap air pockets which can induce severe pressure transients that can damage the sewers (Cardle *et al.* 1989, Guo and Song 1990, Li and McCorquodale 1999).

As a first step in investigating the effects of trapped air on pressure transients in a sewer trunk, the authors have conducted experimental and analytical studies of flow transients in a rapidly filling horizontal pipe under various air leakage conditions (Chapter 2). An analytical model was developed to predict the pressure variations in such systems, assuming the water column to be separated from the air phase by a vertical interface. In verifying this model with the our experimental data, we found that the model was able to predict the general nature of the filling process and the magnitude of peak pressures; however, it was limited in its ability to simulate the complete pressure oscillation pattern for cases where the air leakage was

² A version of this chapter is currently under review with American Society of Civil Engineers(ASCE), *Journal of Hydraulic Engineering* (submitted on May 11, 2000)

moderate. In addition the wave speed, which depends strongly on the air entrainment within the water column, is a required input to this analytical model when the air leakage is significant, limiting the predictive capabilities of the analytical model. Because it is possible that these deficiencies might be attributed to the model's simplified assumptions, we conducted further experimental investigations to explore the actual air-water interface shape, the mechanism of air entrainment, as well as the speed of the pressure wave in a rapidly filling pipe containing trapped air. The results of these investigations are presented here.

3.2 Experimental Apparatus and Operations

Fig. 3.1 depicts the experimental apparatus used in this investigation which was conducted at the T. Blench Hydraulic Laboratory at the University of Alberta. A simple domestic pressure tank 120 cm high and 42 cm in diameter was used at the upstream end of the system to achieve the high heads up to 400 kPa required to develop a range of experimental conditions. This tank also maintained an approximately constant head (± 5 cm) during the pipe filling process. The entire pipe was 10.36 m long and consisted of two parts that were attached together by a flange connection. The first 10m was made of galvanized steel and consisted of three sections, separated by three quarter-turn ball valves located 48 cm, 500 cm and 800 cm downstream of the tank, respectively. These valves provided three different initial air volumes and water column lengths. There were three transducers installed on the steel pipe branch to record the pressures. The second pipe segment was 36 cm long and was made of transparent Plexiglas. The downstream end of the Plexiglas pipe was either sealed to form a dead end or outfitted with a cap containing a

centered, sharp-edged orifice to study the effects of air release on the pressure transients in the system. Both the steel pipe and the Plexiglas pipe had an inside diameter of 35 mm. Because our previous experiments conducted using a steel pipe (see Chapter 2), resulted in a peak pressure up to 5000 kPa, which was beyond the allowable pressure for the 35mm Plexiglas pipe (1400kPa), these tests were conducted over a more limited range of pressure conditions. Also, no transducer was installed on the Plexiglas pipe for safety reasons. Instead, the pressure was measured 10cm upstream of the Plexiglas section, to provide an approximate representation of the pressure at the pipe end. A detailed description of the instrumentation used for pressure measurement is provided in Chapter 2.

For this investigation, a high-speed, high-resolution digital video camera (RedLake Imaging, MotionScope PCI 500) was used to monitor and record events in the entire transparent pipe section, as shown in Fig. 3.1. The recording rate (in frames per second) was selected to optimize the picture resolution, while at the same time ensuring the rate was high enough to capture these dynamic events. The event duration typically lasted about 1 to 15 seconds (depending on the extent of air release involved), and recording rates of 125 and 250 frames per second were found to be optimum (the resolution for both was 240x210 pixels).

Various methods were explored to ensure the quality of the images. The camera was adjusted to a slight vertical angle (within 3 ° of horizontal) to obtain the best picture quality. Two 1000 watt quartz halogen lights were positioned on either side of the camera to provide sufficient light. The inner and outer wall surfaces of the Plexiglass pipe were cleaned before each test. Nevertheless, the image quality still

varied among test groups due to some unexpected factors, such as: the vibration of the pipe during valve opening operations; the condensation of water droplets on the inside of the pipe; and, the reflection off of air bubbles within the water column. In this investigation, only those tests with good image quality were assigned a physical interpretation.

3.3 Results of Observations

Thirty test cases, involving two different upstream heads (275 kPa and 137 kPa), three initial water column lengths ($x_0 = 0.48\text{m}$, 5m, and 8m), and 5 orifice sizes (0, 2, 4, 7, 12mm) were tested. The recorded pressure histories in these experiments as well as those from our previous investigations in Chapter 2, revealed that there are three types of pressure oscillation patterns in a rapidly filling horizontal pipe, depending on the relative size of the leakage orifice. When no air is released, or when the orifice size is small, waterhammer effects are negligible because of the air pocket cushioning effect. When the orifice size is very large, this air cushioning effect vanishes and the water column can easily impact on the pipe end, inducing a waterhammer pressure surge. For intermediate orifice sizes, the cushioning effect of the air pocket decreases as the air release rate increases. It was found that these three types of pressure behaviors corresponded to three types of air-water phase relationships. In the following sections, the air-water interface shapes, and the synchronously recorded pressure oscillation patterns, for these three types of behavior are described.

3.3.1 Zero or minimal air release – waterhammer effects negligible

Figure 3.2 shows a series of photographs and the associated pressure variations (measured upstream of the Plexiglas pipe section), for the case of no air release. The arrows in all of the photographs indicate the direction of the air-water interface movement and the letters on the graph denote the corresponding photograph. The lines in the photographs indicate the approximate profiles of the air-water interface. Here, the upstream head, P_o , was 137 kPa, the initial water column length, x_o , was 5 m, and there was no orifice (i.e., $d = 0$ mm). In this figure, time represents the interval since valve opening. It is seen from the pressure history that right after the valve was opened, the air in front of the water column was compressed and the pressure within this air pocket increased, reaching the first peak at instant b . As the figure illustrates, the overall pressure oscillation pattern has a long period ($T \approx 1.54$ second; T will be used to indicate the period of one cycle, hereafter). The graph also shows that the pressure peaks attenuate over time due to the dampening effect of the pipe wall friction.

The photographs suggest that the water front was less air entrained and, rather than a vertical air-water interface, the water approached the pipe end along the bottom first (Fig. 3.2a). After reaching the pipe end, the water column rolled up (Fig. 3.2b) and the air, which was initially ahead of the water column, was then trapped on top of the water column. After that the pressure dropped, indicating the air pocket underwent expansion (Fig. 3.2c) until the pressure reached the first trough (Fig. 3.2d). After that, the air pocket gradually elongated (Figs. 3.2e and f).

Figure 3.3 shows a series of photographs and the associated pressure history for a minimal air leakage case ($d = 2\text{mm}$) which has the same upstream pressure head ($P_0 = 137\text{kPa}$) as the previous case but a smaller initial air pocket size ($x_0 = 8\text{m}$). The photographs indicate that, although there was some air leakage from the orifice in the pipe end, most of the air remained trapped in the pipe. The interface profiles, the degree of air entrainment in the water front, and the pressure oscillation pattern were similar to those for the no-air-leakage case discussed above, except that the oscillation period was slightly shorter ($T \approx 1$ second) since the initial air volume in this case was smaller.

Figure 3.4 shows another minimal air leakage case which had the same orifice size and initial water column length as the case shown in Fig. 3.3, but a higher upstream head ($P_0 = 275$ kPa). The white cloud in Fig. 3.4a indicates the degree of air entrainment in the water column. A comparison between Figs. 3.3a and 3.4a indicates that, for a given initial water column length and orifice size, the higher the upstream pressure, the steeper the interface profile and the greater the air entrainment, as the water column approaches the pipe end. Figs. 3.4c and 3.4d indicate that the air entrainment in the water column (which appears white in the water) was reduced after the water column reached the pipe end. It was not clear whether the entrained air was released through the orifice or was incorporated into the trapped air pocket. The pressure history graph shows that the pressure oscillation period of this case was shorter ($T \approx 0.612$ second) and the peak pressure was higher ($P \approx 800$ kPa) than that for the case of the lower upstream head presented in Fig. 3.3 (where $T \approx 1$ second, $P \approx 300$ kPa). A comparison between these three pressure oscillation patterns (Figs. 3.2

to 3.4) indicates that the oscillation period and the peak pressure are dependent on the initial air volume and the upstream pressure head. The smaller the initial air volume and the higher the upstream head, the shorter the oscillation period and the higher the peak pressure.

3.3.2 Large air release – waterhammer effect dominated

This situation occurs when the orifice in the pipe end is large enough to allow for significant air release ahead of the propagating water front, so that there is a negligible air cushioning effect. Fig. 3.5 shows a series of photographs and the associated pressure variations (measured upstream of the Plexiglas pipe section), for the case of a large air release. Here, P_0 was 275 kPa, x_0 was 5 m, and d was 7 mm. The pressure history for this case differs from that of the minimal air release cases presented earlier in that the pressure rise is abrupt, the pressure attenuation is rapid, and the peak pressure is quite large ($P \approx 3500$ kPa as compared to 800 kPa in the small air release case shown in Fig. 3.4), thus illustrating the significance of the air cushioning effect for the case of minimal air release, discussed above.

Figs. 3.5a to c indicate that the water column was highly air-entrained before as it approached the pipe end. Unlike the minimal air release situation, there was no air pocket trapped on top of the flow and almost all of the air was released from the orifice by the time that the water column reached the pipe end (except for the entrained air). Since no air pocket was trapped, there was virtually no air cushioning effect and the water column slammed into the pipe end and induced a waterhammer pressure (point d in pressure history). During this particular test, it was observed that the entire experimental apparatus moved slightly downstream and a loud water

slamming sound was heard, both clear indications of the high impact pressure. Fig. 3.5d indicates that the water column was less white after the waterhammer peak pressure occurred; however, it is interesting to note from Fig. 3.5e that after the first pressure peak, the water column became white again. This might be attributed to the arrival of entrained air from the upstream water column, or could be due to the re-expansion of entrained air as the pressure suddenly dropped. From Figs. 3.5f to h, it is seen that this entrained air coalesced into increasingly larger bubbles. Once these bubbles were released, the water column again impacted the pipe end and subsequently induced the second, much smaller, pressure peak (point *h* in the pressure graph). After all of the air bubbles were expelled through the orifice, the flow was steady and the pressure was constant (after point *h* in the pressure graph).

Figure 3.6 shows a series of photographs and the associated pressure variations for another test conducted using the same pressure head and initial water column length as in the case just presented (Fig. 3.5; $d = 7$ mm), but with an even larger orifice size ($d = 12$ mm). In this case, as in that previous one, the peak pressure occurred after the water front impacted on the pipe end and the air was released (point *e* in the pressure graph). However, unlike the previous case, here the air content in the water column did not appear to increase after the first pressure peak (Fig. 3.6f); indicating that, for this orifice size, the water release was greater and carried much of the entrained air with it so that there was less air left behind to re-expand. Consequently, unlike the previous case, here there was no second peak.

3.3.3 Intermediate air release – mitigated water hammer effect

An intermediate situation occurs when the orifice size in the pipe end is not large enough to allow for a significant amount of air to release ahead of the propagating water front, and therefore a moderate cushioning effect occurs. Figure 3.7 shows a series photographs and the associated pressure variations for this intermediate air release case. In the figures, the arrows indicate the direction of movement of the air pocket, and the numbers represent the approximate velocities of the air pockets. Here, P_0 was 275 kPa, x_0 was 0.48 m, and d was 4 mm. The first four photographs encompass the first two pressure oscillation cycles, and as the figures illustrate, the peaks are associated with the reversal of the air-water interface, indicating at least some air cushioning effects.

After air ahead of the water front was released, the air bubbles on top of the water (Fig. 3.7e) started to coalesce into increasingly larger air bubbles and ultimately into what could be described as air pockets (Figs. 3.7f to m). Subsequent figures suggest that the larger air pocket is unstable, as it is characterized by a broken surface (Figs. 3.7j and p) and a prominent surface wave (Figs. 3.7m and n).

The variations in the speeds of the air pockets illustrate the random nature of the air pocket movement. Once an air pocket reached the orifice and was released, the water column slammed into the pipe end, generating an impact pressure. However, in this case, the magnitude of the pressure peak was mitigated by the cushioning effect of the residual air pockets. The randomness with which the air pockets moved, and then reached the pipe end caused the pressure oscillation to have a long period irregular pattern (from points *e* to *p* in the pressure graph). After the last air pocket

was released (the one near the pipe end shown in Fig. 3.7q), the impact pressure could not be cushioned because there were no residual air pockets within the flow. Therefore, the final stage of the pressure oscillation pattern had a short period and a sharp peak, as shown in the pressure graph at point *q*.

Fig. 3.7 suggests that, for intermediate air release situations, the entire pressure oscillation can be divided into three stages. The first stage is the release of the air in front of (or entrained in) the water column. At this stage, the air acts as a shock absorber and the waterhammer effect is negligible. The pressure pattern is regular and has a long period. The second stage is the evolution of trapped air pockets during which air bubble coalescence may occur. The hypersensitive behavior of the air pockets mitigates the water impact pressure; therefore, the pressure oscillation pattern is irregular and has a long period. The third stage occurs after the release of the last air pocket, in which the water impact pressure dominates, although the peak magnitude has been mitigated by the earlier air cushioning effect (as compared to the large air release case presented in the last section).

Figure 3.8 shows a series of photographs and the associated pressure variations for another intermediate air release case which had a longer initial water column length. Here, P_0 was 275 kPa, x_0 was 5 m, and d was 4 mm. The first pressure peak (point *c* in the pressure graph) occurred when the air pocket was compressed (Fig. 3.8c). Unlike the previous case, after the first peak, there was no visible air bubble coalescence; instead, a large air pocket went through compression and expansion and induced another long period oscillation cycle (From Figs. 3.8e to h). Once this air pocket reached the orifice and was released, the water column impacted

on the pipe end and induced a short and sharp pressure oscillation (the pressure history after point h in the pressure graph). A comparison of the pressure oscillation duration between Fig. 3.7 and Fig. 3.8 indicates that, for a given upstream head and orifice size, the shorter the initial water column length, the longer the long period pressure oscillation.

3.4 Implications for the Analytical Model

As discussed in the introduction, one reason for conducting this investigation was to explore the validity of some of the assumptions made in the analytical model described in Chapter 2. Specifically, the model assumes the water column contains a single, discrete, air pocket and that it is separated from the air phase by a vertical interface. Clearly neither of these is strictly true and the implications of these observations to our analytical model are discussed below.

3.4.1 Shape of the air-water interface

In this study, it was observed that the air-water interface in the rapidly filling pipe was relatively steep only when the orifice size was very large (i.e. when the air release was substantial). In all other cases, it was observed that the interface was non-vertical. Relating this to the behavior of the analytical model in Chapter 2, it was found that the model was acceptable for simulating the peak pressure for the entire air leakage range, but could only model the entire pressure oscillation pattern accurately for very small or very large air release cases. For intermediate air release situations, it was found that the analytical model calculated pressure histories that were shorter than the measured ones. This might be explained by the observation that, during filling, the non-vertical interface traps air on top of the water column and this trapped

air resides as air pockets within the flow after the water column reaches the pipe end. These air pockets cause the long period pressure oscillation to persist. In contrast, in the model, the vertical interface implies that whenever the water column reached the pipe end, the air was completely released and consequently the pressure oscillation ceased.

3.4.2 Effects of air entrainment

These investigations showed that differing degrees of air entrainment occurred within the water column, depending upon the nature of the air release. Two mechanisms of air entrainment were observed in the rapidly filling pipe: (1) air intrusion along the pipe wall where the velocity of the water is close to zero because of the wall friction (dominant when the orifice size was small and air release was negligible); and, (2) air entrainment due to the small and strong turbulent eddies in the water front (dominant when the orifice size was large, and air release was large).

The most significant influence of entrained air is in reducing the speed of the pressure wave. This has potentially significant implications to our analytical model, since the calculation of the impact pressure (associated with the large air release cases) requires as input the speed of pressure wave. Therefore, some predictive capability regarding the air content (and therefore the resulting pressure wave speed) would, in turn, improve the predictive capability of our analytical model.

Visual observations from this investigation indicated that the air content in the water column depended upon the orifice size, the upstream pressure head and the initial length of the water column, in that greater degrees of air entrainment appeared to be associated with larger orifice sizes and higher upstream heads. Unfortunately, it

was not possible to actually measure the air content of the flow in our experiments, because of the short duration of the flow transients and the limited length of the transparent section of pipe (which was necessary for safety reasons, given the high pressures). Therefore, we investigated the relationship between these parameters and the wave speed directly, and then related the wave speed and the air content using an established relation from the literature, as discussed below.

In our experiments, the speed of the pressure wave was determined by measuring the duration of propagation of the pressure peak along the pipe between pressure transducers (located as shown in Fig. 3.1). Since the wave speed was time dependent, a lumped wave speed value was obtained by averaging the wave speeds of the first three wave cycles for a given filling condition. Our previous study described in Chapter 2 indicated that this was a reasonable approximation for modeling purposes, since the impact pressures calculated by the analytical model using this averaged wave speed were very close to the measured values. Fig. 3.9 shows the variation of this averaged wave speed a , as a function of orifice size, d/D , upstream pressure head, ϕ , and initial water column length, λ_0 (which in essence represents the initial volume of air). This figure indicates that the effect of upstream head on wave speed is not as significant as that of the other two variables.

The wave speed is significantly affected by the initial water column length with the shorter water column being associated with lower wave speeds. For example, as Fig. 3.9 shows, the wave speed for $\lambda_0 = 0.048$ is only about half of that which occurred for values of λ_0 of 0.5 and 0.8. This can be explained by the higher air content in the flow for a short initial water column situation. It was observed that,

for $\lambda_0 = 0.048$, the air content in the flow was still substantial when the water column slammed into the pipe end, even for the large orifice sizes. In contrast, for the cases where $\lambda_0 = 0.5$ and 0.8 , it was observed that there was a critical relative orifice size, d/D , of about 0.2 , below which, most of air was still trapped in the flow when the water column slammed into the pipe end; and above which, the air was easily expelled out of the pipe and little air was trapped. Fig. 3.9 suggests that, for cases where the initial volume of air in the pipe is 50% or less, the wave speed increases with orifice size and approaches the speed of sound in water (1440 m/s) when d/D is greater than this critical value.

Since the observations indicated a “bubbly flow” pattern at the time when the water column reached the pipe end in large orifice size situations, we were able to estimate air content from the observed wave speed values using an air fraction-wave speed relation for bubbly flow by Pearsall (1965):

$$a_m = \left[\frac{K_w P_a}{(1 - \alpha_a) P_a + \alpha_a K_w} \cdot \frac{1}{\alpha_a \rho_a + (1 - \alpha_a) \rho_w} \right]^{1/2} \quad (3-1)$$

where

a_m = speed of air-water flow;

a_a = speed of sound in air alone (here $a_a = 325$ m/s);

a_w = speed of sound in water alone (here $a_w = 1440$ m/s);

K_w = bulk modulus of water;

ρ_a and ρ_w = the densities of air and water, respectively; and

P_a = absolute air pressure.

Eq. (3-1) was applied to calculate the air fraction based on the measured average wave speeds shown in Fig. 3.9. The resulting air fraction variation with orifice size, initial water column length, and upstream pressure head is shown in Fig. 3.10, which indicates that the air fraction decreases as the relative orifice size d/D increases. As this was consistent with our visual observations, it is concluded that the results of Figure 3.9 do have the potential to enhance the predictive capability of our analytical model.

3.5 Conclusions

The purpose of this visual study was to explore the validity of the assumptions made in our analytical model for the simulation of flow transients in a rapidly filling horizontal pipe containing trapped air. The actual air-water interface shape and the nature of the air entrainment, as well as their effects on the pressure oscillation patterns were explored.

The observations indicated that, if the pipe end is sealed or the orifice size is small, the water column contains a negligible amount of entrained air and approaches the pipe end along the bottom. The air trapped on top of the water acts as a shock absorber; therefore, the overall pressure oscillation pattern has a long period. The smaller the initial air volume and the higher the upstream head, the shorter the oscillation period and the higher the peak pressure.

The observations further indicated that, if the orifice is large, the water column is highly air entrained and the water front is steep. In this case, the air release is significant and there is no visible air pocket trapped on top of the flow by the time that the water column reaches the pipe end. Without the trapped air pocket, the air

cushioning effect vanishes and the water column can easily slam into the pipe end and induce a sharp and short period waterhammer pressure.

It was also observed that, if the orifice is not large enough to allow for a significant air release, the water front contains a moderate amount of air and is steeper than that observed in the small air release case. After the water reaches the pipe end, some air is still trapped within the flow as bubbles or pockets whose random behaviors cause the pressure oscillation to have a long period, irregular pattern. When the last air pocket is released, the sharp and short period water impact pressure dominated, although the peak magnitude was mitigated by the earlier air cushioning effect.

3.6 References

- Cardle, J.A., Song, C.C.S., and Yuan, M. (1989). "Measures of mixed transient flows." *Journal of Hydraulic Engineering*, ASCE, 115(2), 169-185.
- Guo, Q., and Song, C.C.S. (1990). "Surging in urban storm drainage systems." *Journal of Hydraulic Engineering*, ASCE, 116(12), 1523-1537.
- Kalinske, A.A. and Robertson, J.M. (1943). "Closed conduit flow." *Transaction of ASCE*.
- Li, J. and McCorquodale, A.(1999). "Modeling mixed flow in storm sewers." *Journal of Hydraulic Engineering*, ASCE, 125(11), 1170-1179.
- Martin, C.S., 1976, Entrapped air in pipelines, *Proceeding of the Second International Conference on Pressure Surges*, London, England,F2-15.
- Martin, C.S. and Padmanabhan, M.(1979). "Pressure pulse propagation in two-component slug flow." *Transaction of the ASME*, Vol. 101, 44-52.
- Pearsall I.S. (1965). "The velocity of water hammer waves." *Symposium on Surge in Pipelines, Proceedings 1965-66*, Vol 180, 13-20.

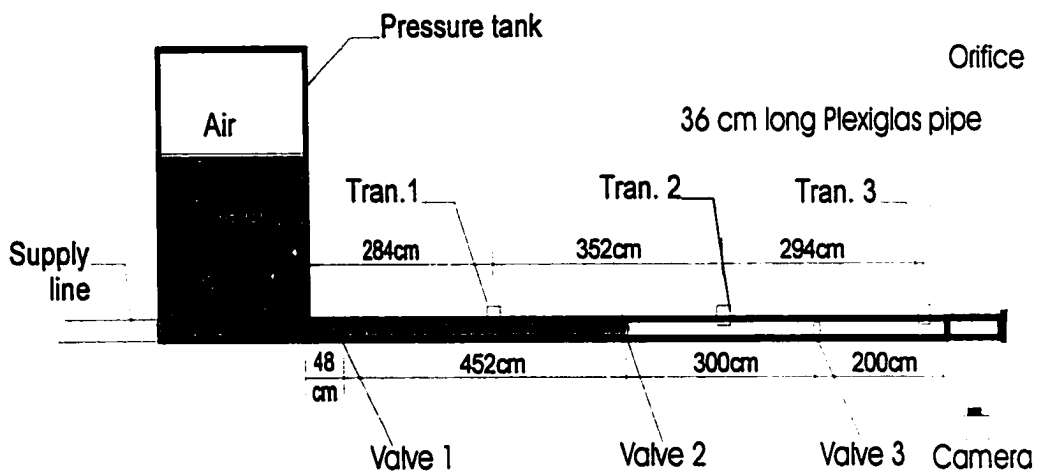


Fig. 3.1 Diagram of the experimental apparatus

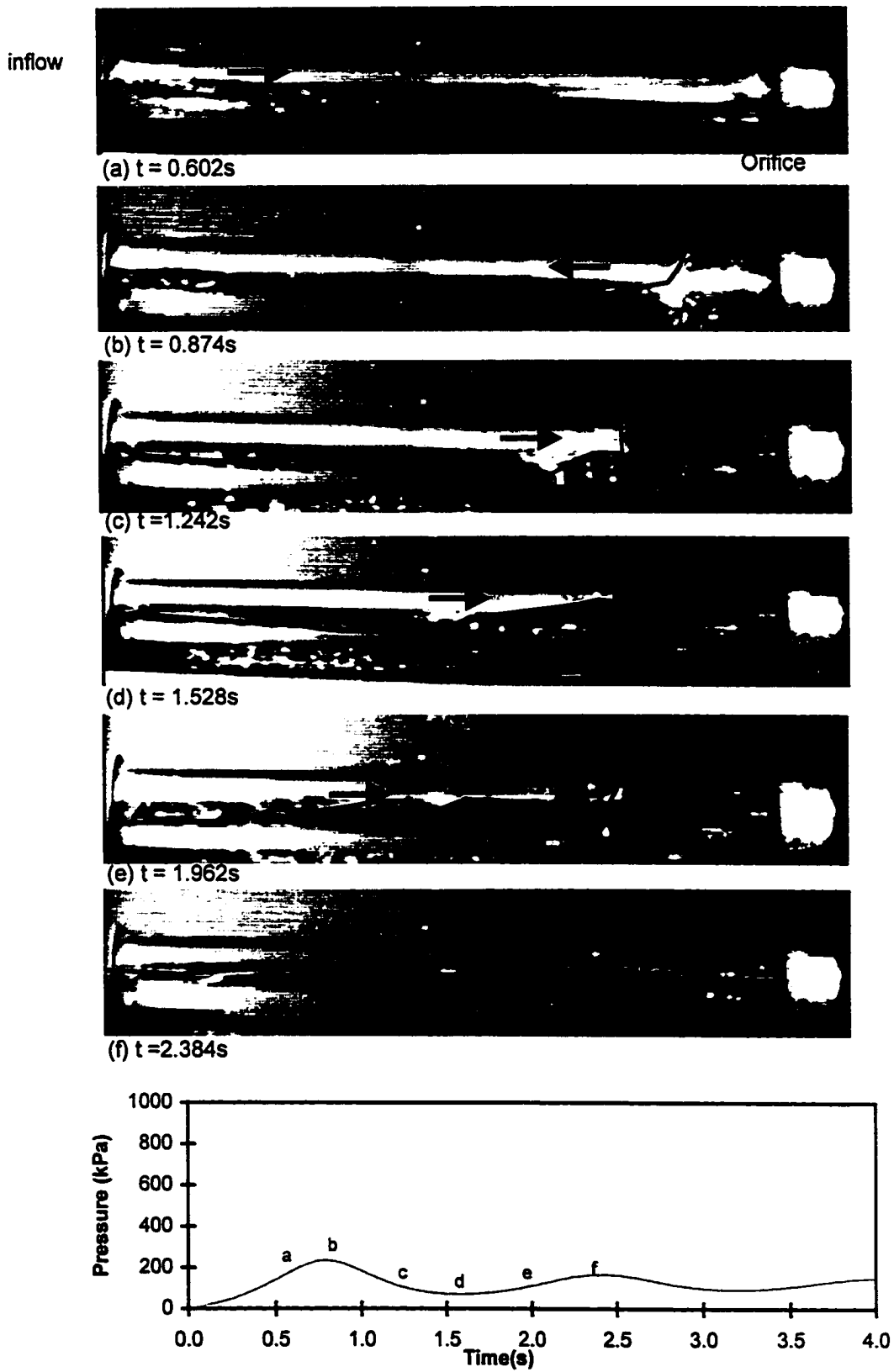


Figure 3. 2 No air release case, type 1 behavior ($P_0 = 137kPa$, $x_0 = 5m$, $d = 0mm$)

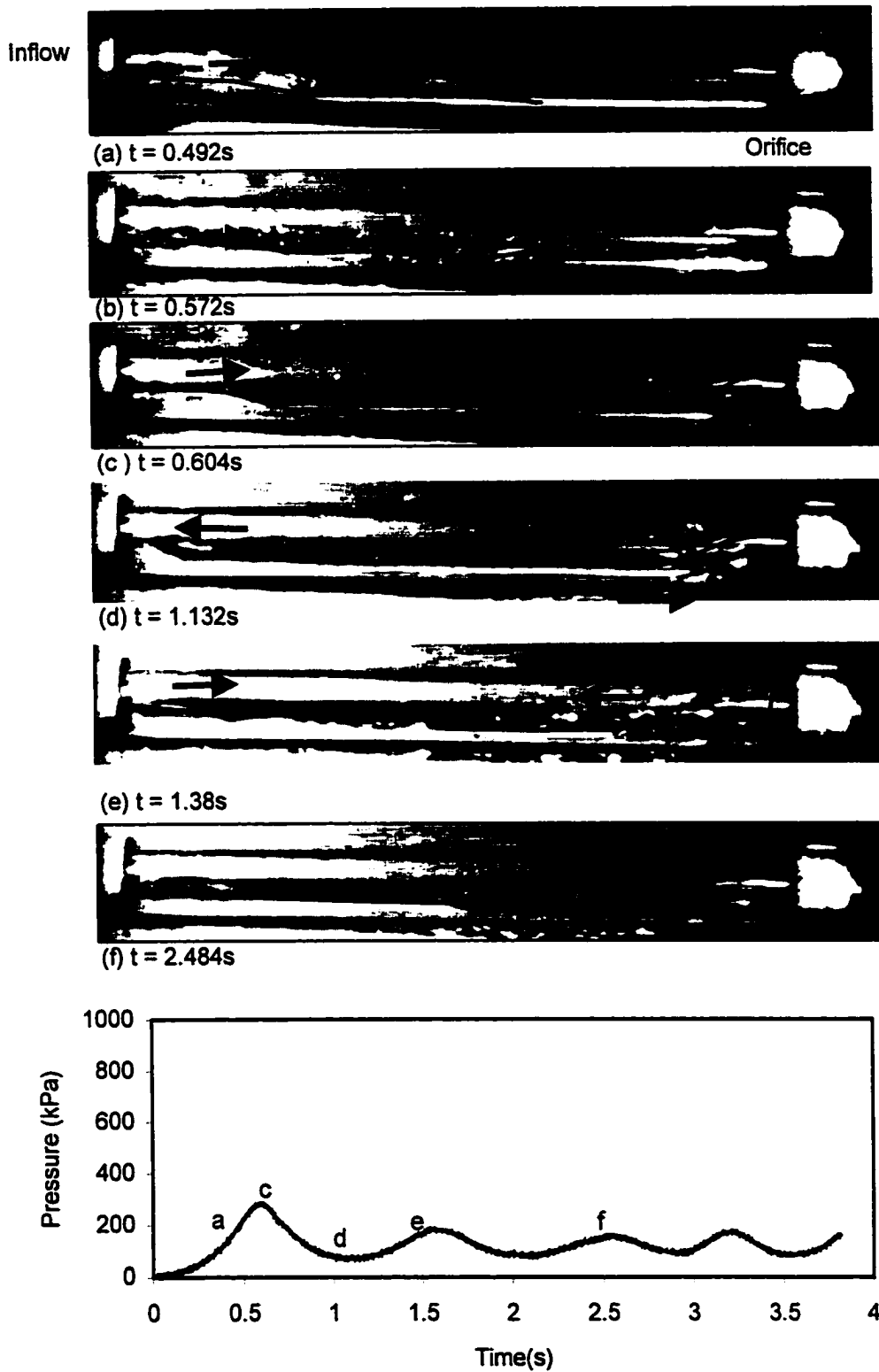


Figure 3.3 Small air release case, type 1 behavior($P_0 = 137$ kPa, $x_0 = 8$ m, $d = 2$ mm)

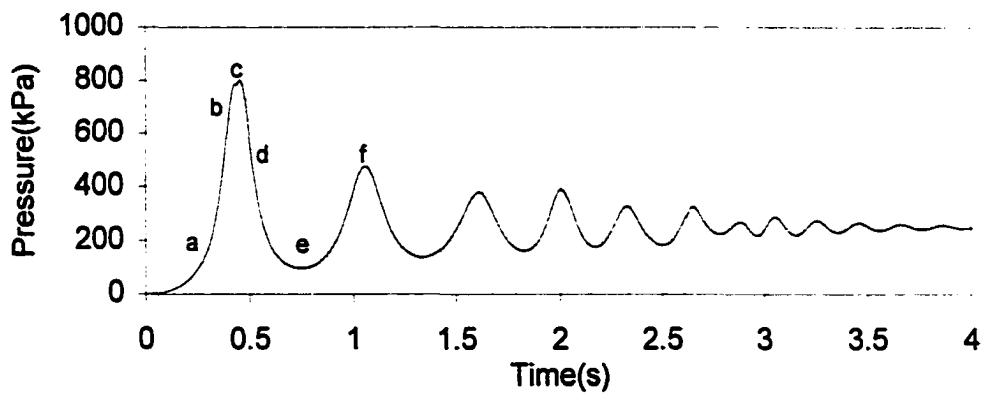
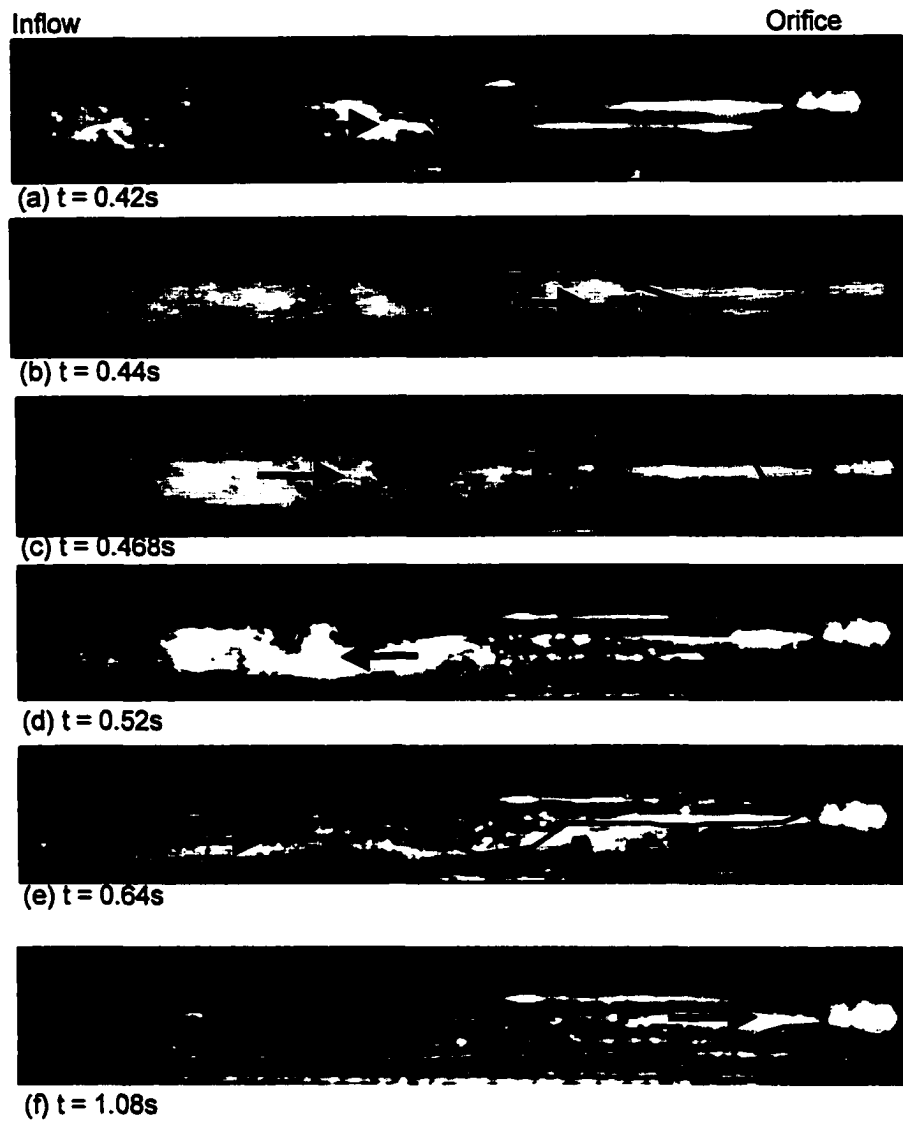


Figure 3.4 Small air release case, type 1 behavior ($P_0 = 275kPa$, $x_0 = 8m$, $d = 2mm$)

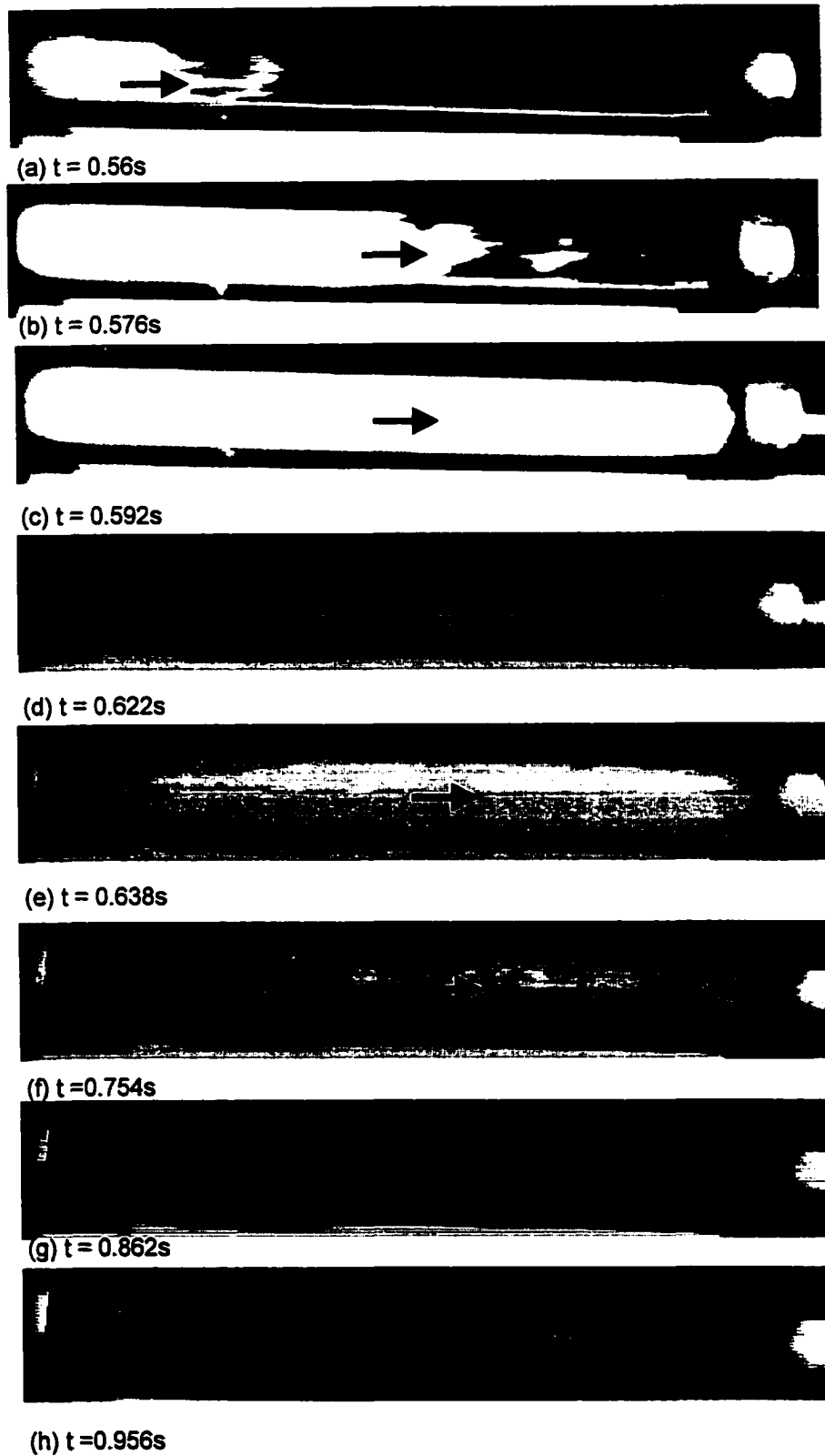


Figure 3. 5 Large air release, type 3 behavior
 $(P_0 = 275kPa, x_0 = 5m, d = 7mm)$

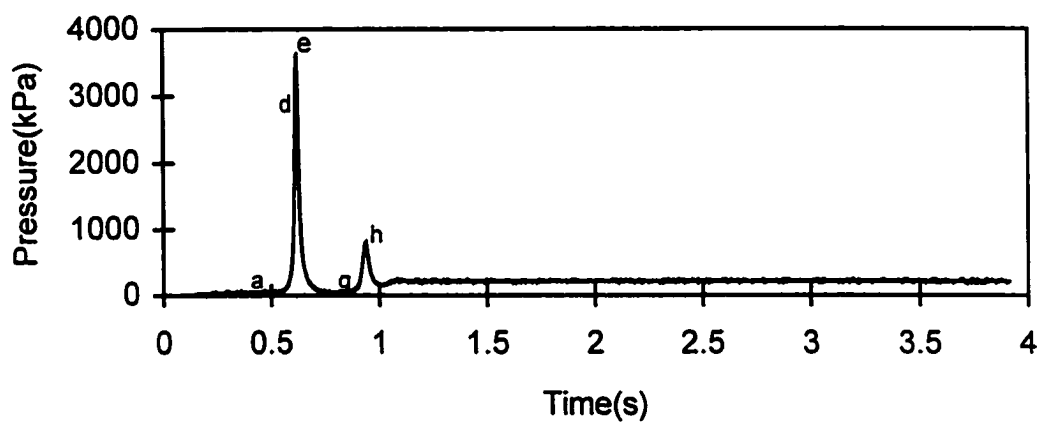


Figure 3. 5 Large air release, type 3 behavior
($P_0 = 275\text{kPa}$, $x_0 = 5\text{m}$, $d = 7\text{mm}$)-continued



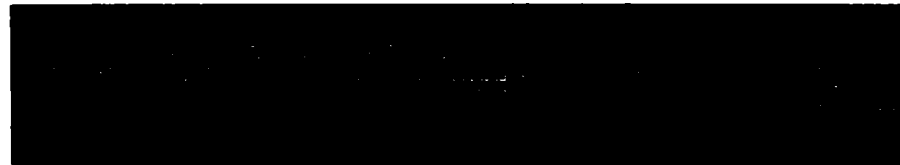
(a) $t = 0.574s$



(b) $t = 0.582s$



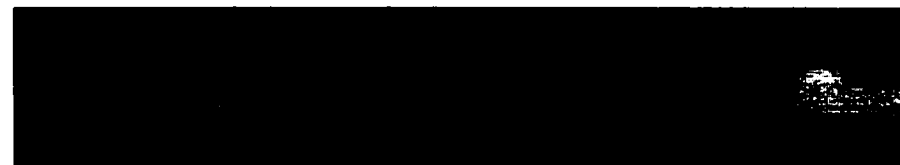
(c) $t = 0.590s$



(d) $t = 0.598s$



(e) $t = 0.614s$



(f) $t = 0.694s$

Fig. 3.6 Large air release, type 3 behavior ($P_0 = 275kPa$, $x_0 = 5m$, $d = 12mm$)

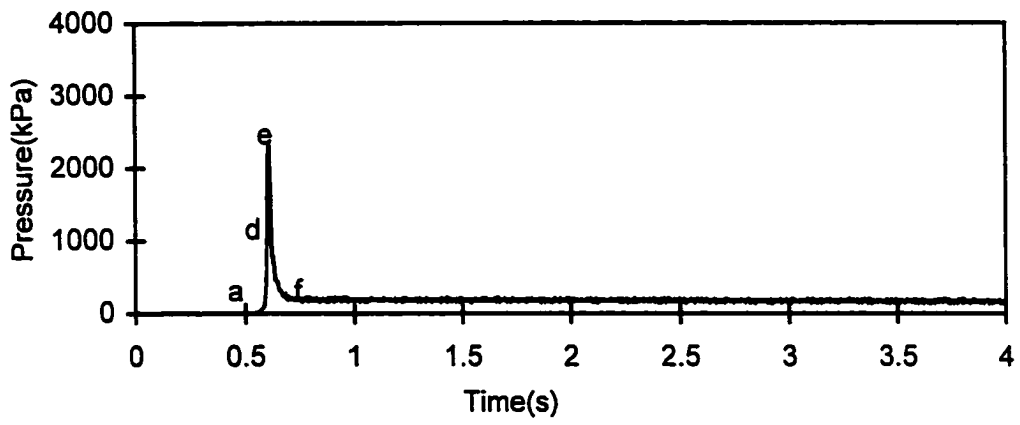


Fig. 3.6 Large air release, type 3 behavior
($P_0 = 275\text{kPa}$, $x_0 = 5\text{m}$, $d = 12\text{mm}$)-continued

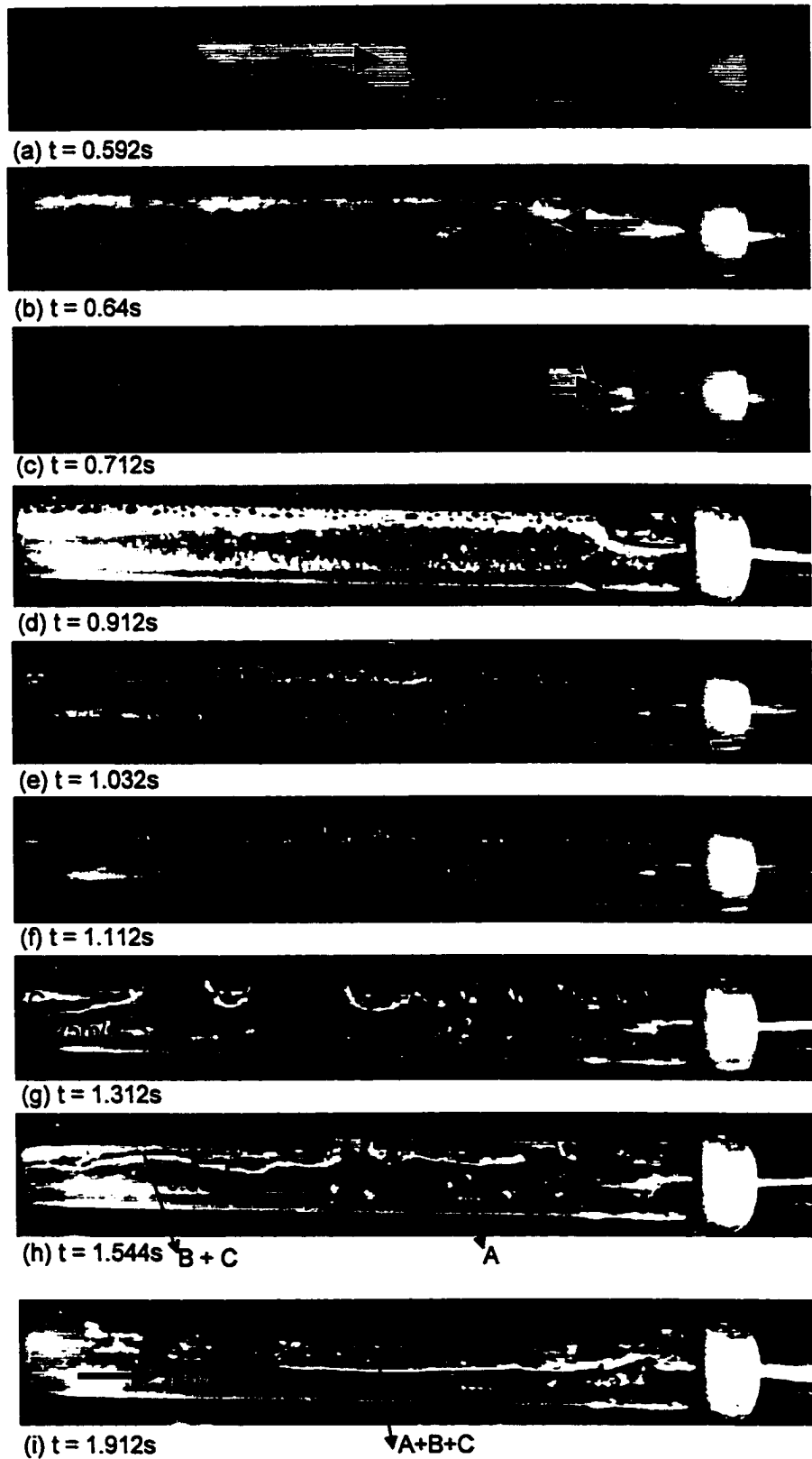


Fig.3. 7 Intermediate air release, type 2 behavior

($P_0 = 275 \text{ kPa}$, $x_0 = 0.48\text{m}$, $d = 4\text{mm}$)

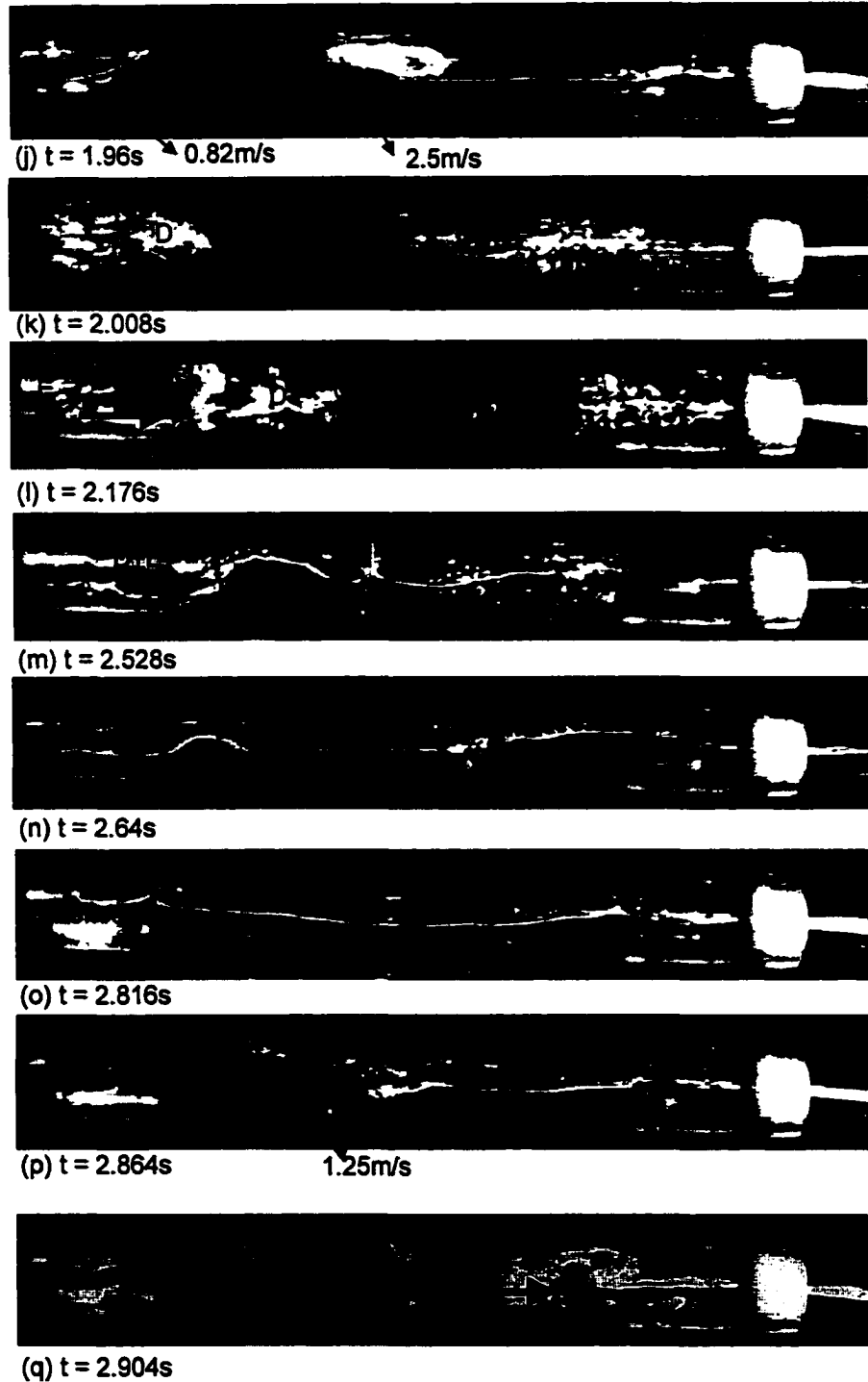


Fig.3. 7 Intermediate air release, type 2 behavior
 ($P_0 = 275$ kPa, $x_0 = 0.48$ m, $d = 4$ mm)-continued

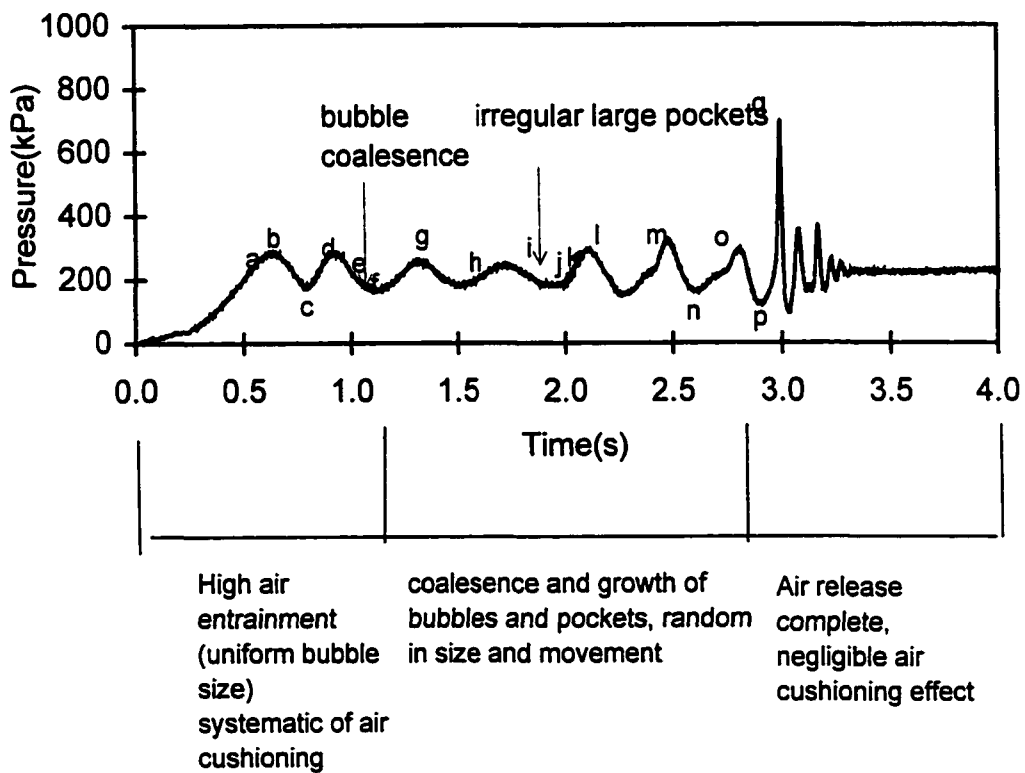
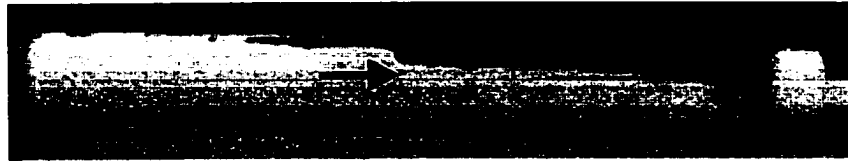


Fig. 3.7 Intermediate air release, type 2 behavior
 $(P_0 = 275 \text{ kPa}, x_0 = 0.48\text{m}, d = 4\text{mm})$ -continued



(a) $t = 0.432\text{s}$



(b) $t = 0.512\text{s}$



(c) $t = 0.6\text{s}$



(d) $t = 0.72\text{s}$



(e) $t = 1.224\text{s}$



(f) $t = 1.304\text{s}$



(g) $t = 1.36\text{s}$

Fig. 3.8 Intermediate air release, type 2 behavior

$(P_0 = 275\text{ kPa}, x_0 = 5\text{m}, d = 4\text{mm})$



(h) $t=1.52\text{s}$

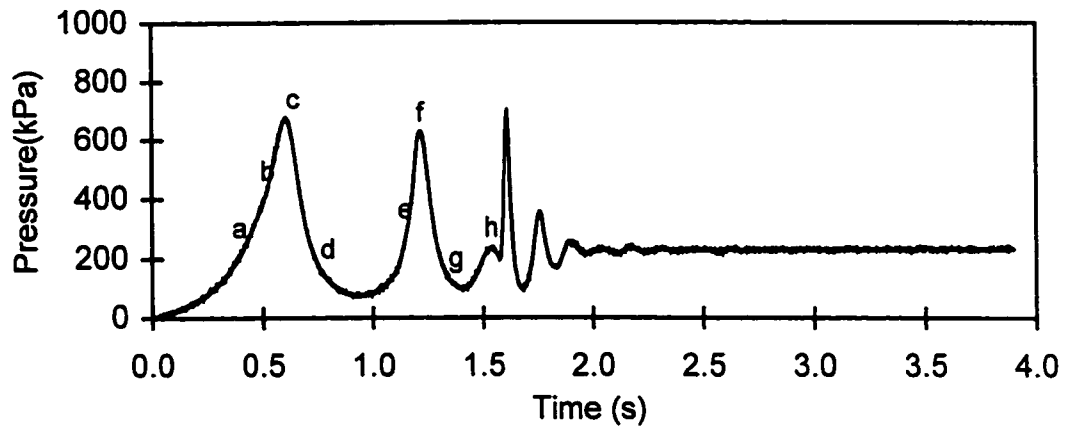
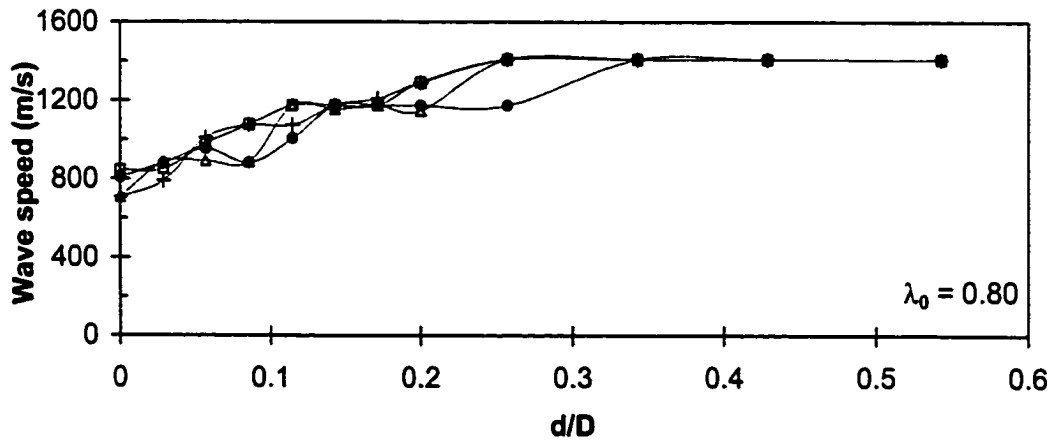
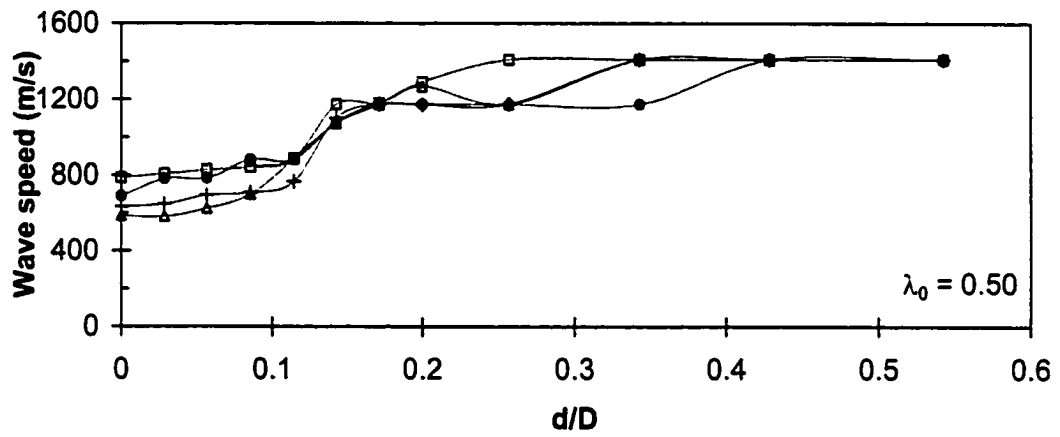
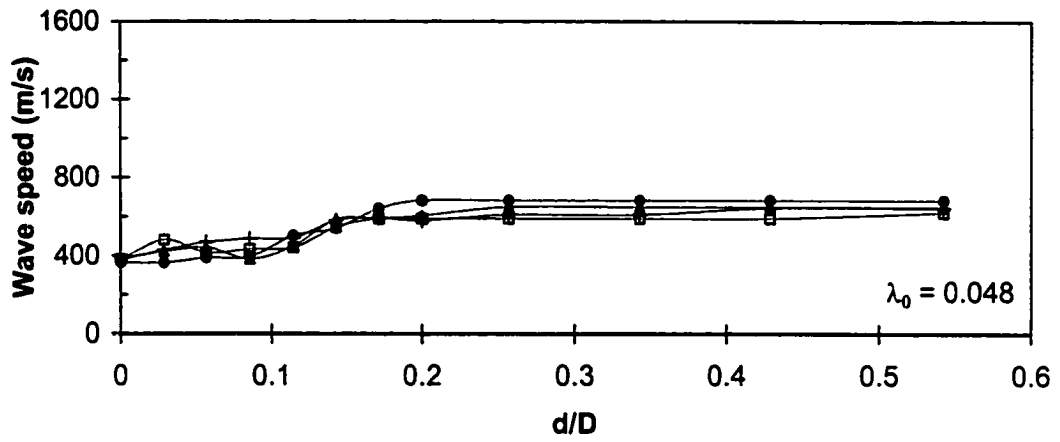


Fig. 3.8 Intermediate air release, type 2 behavior
($P_0 = 275 \text{ kPa}$, $x_0 = 5\text{m}$, $d = 4\text{mm}$) - continued



\square $\phi=4.57$
 $+$ $\phi=3.86$
 \triangle $\phi=3.14$
 \bullet $\phi=2.43$

Figure 3.9 The Measured Speed of Pressure Wave

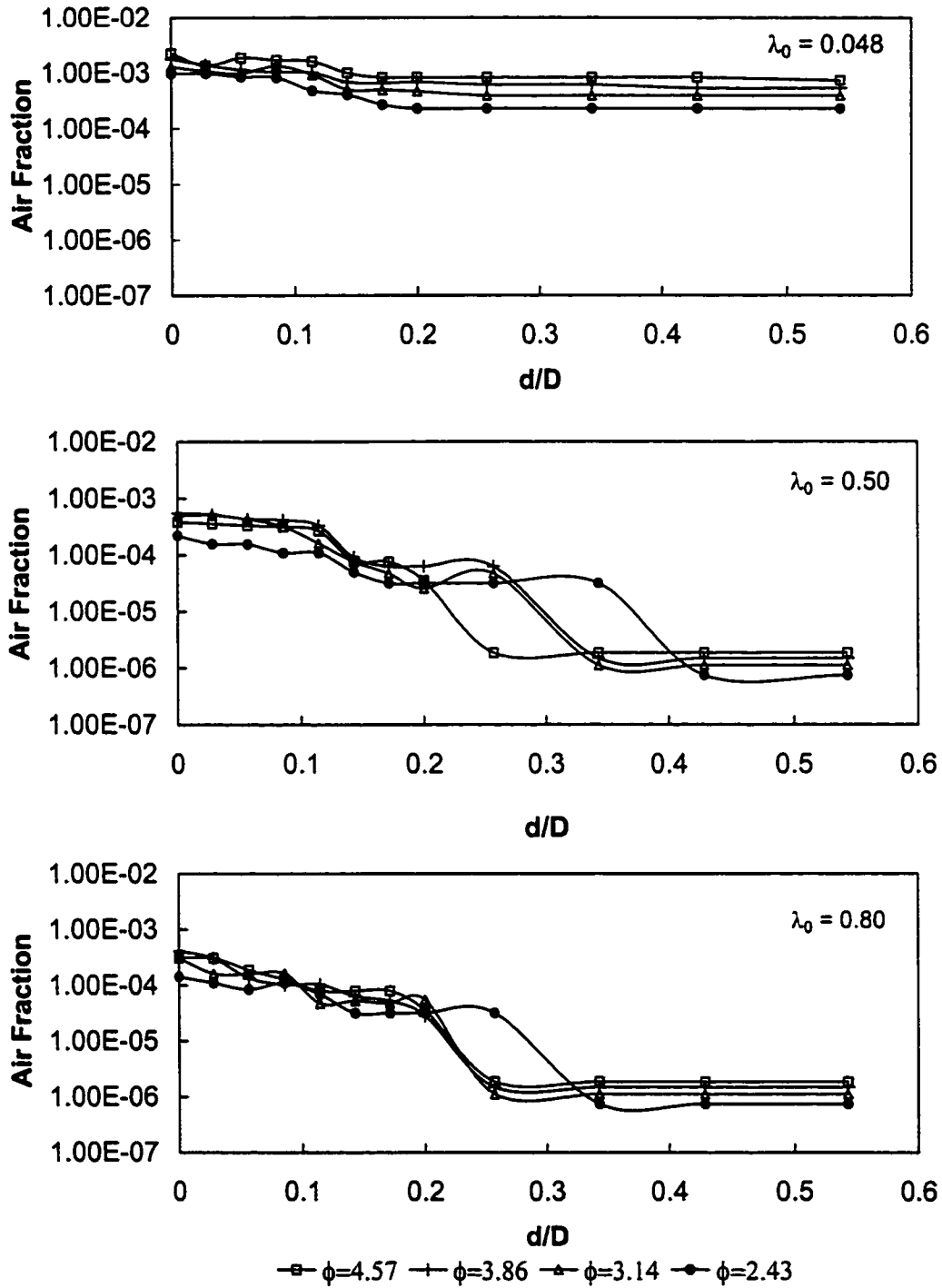


Figure 3.10 Air Fraction Relation with Orifice Size

4.0 EFFECT OF TRAPPED AIR DURING RAPID FILLING OF PARTIALLY FULL PIPES³

4.1 Introduction

Previous chapters describe the investigation of flow transients in a rapidly filling horizontal pipe containing trapped air. In those studies, the receiving pipe was assumed dry and was occupied by trapped air. As we know, in real sewer trunks, there is free surface flow upstream of a surcharge front during surcharge events. Therefore, it is practical and necessary to investigate the rapid filling of a receiving pipe which is partially full with the air pocket on top of the flow before the filling starts.

In this chapter, experiments conducted to investigate the rapid filling of a horizontal receiving pipe which has a tailwater are presented. The effects of the depth of the tailwater, the orifice size, and the driving head on the pressure transients were investigated. Here the pressure behavior is compared to that observed without tailwater (as discussed in Chapter 2) in order to assess whether that analytical model might be applied for cases where tailwater is present (i.e. whether the effects of tailwater might be modeled by simply accounting for the reduction in initial air pocket volume.) In addition, a *surge model* developed to simulate the effects of tailwater on the pressure oscillation pattern, is presented and evaluated.

³ The material in this chapter will be submitted to the American Society of Civil Engineers (ASCE), Journal of Infrastructure Systems.

4.2 Experimental Investigations

4.2.1 Experiment apparatus

Fig. 4.1 depicts the experimental apparatus used in this investigation, which was conducted at the T. Blench Hydraulics Laboratory at the University of Alberta. Here, a simple domestic water supply pressure tank (120 cm high and 42 cm in diameter) was used at the upstream end of the system to ensure an approximately constant value of the upstream driving head during the pipe filling process. Inflow to the pressure tank was from a standard municipal water supply line; a pressure regulator at the inlet to the tank facilitated a range of driving heads. As shown in Fig. 4.1, the entire pipe was 8.96 m long and consisted of two galvanized steel sections and one Plexiglas pipe section. The tailwater was developed by slowly filling the receiving pipe to a specified depth (measured using a ruler placed into the Plexiglas pipe section through a small drain hole.) Three quarter-turn ball valves provided three different initial water column lengths and corresponding air volumes. There were three transducers installed on the steel pipe to record the pressures. The far (right) end of the pipe was either sealed to form a dead end, or outfitted with a cap containing a centered, sharp-edged orifice to study the effects of air release on the pressure transients in the system. Both the steel pipe and the Plexiglas pipe had an inside diameter, D , of 35 mm.

The Labview 4.0 software program developed in Chapter 2 was used for automated collection of pressure data. The details of the calibration of transducers, the determination of pipe wall friction factor, valve losses, and speeds of the pressure waves are provided in Chapter 2.

4.2.2 Cases studied

To investigate the effects of varied upstream driving head, two reservoir heads of $H_0 = 275$ kPa and 137 kPa were implemented. Two different initial water column lengths of $x_0 = 5$ m and 8 m were tested. The tailwater was developed by slowly filling the receiving pipe and, when the water reached the pipe end, it induced a slight wave reflection. It was found that when the receiving pipe was long (i.e. the initial water column length was short, e.g. $x_0 = 0.48$ m), it took a long time for this reflection wave to die out, making it quite difficult to accurately control the tailwater depth. For this reason, the short water column length ($x_0 = 0.48$ m) was not pursued in this investigation. Five orifice sizes of $d = 0, 2, 4, 6,$ and 9 mm were tested to determine the effects of air release on pressure transients in this system. The depth of tailwater ranged from $y/D = 0$ to 0.8 in increments of 0.2 (where y is the tailwater depth and D the pipe diameter.)

4.3 Experimental Results

Fig. 4.2 presents all of the measured maximum peak pressures observed, as a function of orifice size and tailwater depth, grouped by initial water column length and driving head. In the figure titles, $\lambda_0 (x_0/L)$ is the relative initial water column length, H_0^* is the absolute driving pressure head, H_b^* is the absolute initial air pressure, which is assumed to be atmospheric, and d/D is the relative orifice size. The filled circular symbols represent the cases without tailwater ($y/D = 0$). It is seen from Fig. 4.2 that, similar to the no tailwater situations discussed in Chapter 2, the magnitude of peak pressure varies with d/D , indicating that the relative orifice size is the most important factor affecting the magnitude of the peak pressures.

4.3.1 No or small air release situations

For 'no or small air release' situations ($d/D < 0.114$ for the experiments), because of the cushioning influence of the air pocket, the maximum pressure remains relatively constant (from about 1.5 to 4 times the driving head). Within this range, the maximum peak pressure increased slightly with the tailwater depth except for $\lambda_0 = 0.56$ and $H^*_o/H^*_b = 3.86$ (Fig. 4.2 d) which shows larger pressure increases with tailwater depth, due to the reduction of initial air volume.

Figs. 4.3 and 4.4 illustrate the pressure oscillation patterns under different tailwater depths for $d/D = 0$ for $\lambda_0 = 0.56$ and 0.89 , respectively. It can be seen that, generally, under 'no air release' conditions, the pressure oscillation pattern is characteristic of the Type 1 behavior discussed in Chapter 2, in which the cushioning effects of the air pocket dominate the pressure oscillation pattern. Again, it is seen that the peak pressure increases slightly with y/D . The frequency of pressure oscillations also increases with the tailwater depth.

A comparison between (b) and (d) in Figs. 4.3 and 4.4 indicated that, for the 'no air release' situation, the variation in the magnitude of the peak pressure with the tailwater depth was more obvious for the situation of a short initial water column length (Fig. 4.3) than for a long initial water column length (Fig. 4.4).

4.3.2 Large air release situations

Fig. 4.2 shows that, for large air release cases ($d/D \geq 0.171$ for the experiments), the peak pressure magnitudes decrease as the tailwater depth increases. The reason is that, for large orifice ratios, the tailwater is more easily pushed forward (through the orifice) as the surge front approaches the pipe end; from the continuity equation

$$U_w = \frac{U_1 A_1 - U_c A_c}{A_1 - A_c} \quad (4-1)$$

(where U_1 , U_c , and U_w are the velocities of water column, tailwater, and surge front, respectively; A_1 and A_c are the pipe cross-sectional area and stagnant flow area, respectively), it is seen that an increased U_c will result a lower U_w and consequently a lower impact pressure, as we can see from the Allievi Equation (Wylie and Streeter, 1978)

$$\Delta H = -aU_w/g \quad (4-2)$$

(in which a is the speed of the pressure wave).

Figs. 4.5 and 4.6 illustrate the pressure oscillation patterns under a large air release condition ($d/D = 0.171$) for $\lambda_0 = 0.56$ and 0.89 , respectively. Generally, it can be seen that the magnitudes of peak pressures dropped as the tailwater depth increased although this is not always the case, particularly when the initial water column is short. Figs. 4.5 and 4.6 illustrate this, where for $\lambda_0 = 0.56$ (Fig. 4.5) the variation in the pressure pattern with the tailwater depth was much less systematic than seen in Fig. 4.6 for the long initial water column length ($\lambda_0 = 0.89$). This more random behavior might be explained by the fact that for the shorter water column length (Fig. 4.5), once the filling starts, the surge front will take a longer time to reach the orifice. This approaching front will disturb the free surface of the tailwater; and as a result, more air will be trapped by the surface wave. When the surge front containing the trapped air pocket reaches the orifice, the orifice will be choked and consequently the impact pressure on the pipe end waterhammer pressure will be cushioned by the trapped air pockets, as it is shown in Fig. 4.5c.

In contrast, for the longer initial water column length situation as shown in Fig. 4.6, the surge can reach the pipe end very quickly and the free surface instability of the tailwater has little time to develop. As a result, the pressure pattern does not change much as the tailwater depth increases.

4.3.3 Intermediate air release situations

A careful examination on Figs. 4.2.b, 4.2.c and the pressure oscillation patterns in Figs. 4.7 and 4.8, suggests that when $d/D = 0.114$, the magnitude of peak pressure first increases then decreases with the tailwater depth. As it was found in Chapter 2, under this orifice size, the pressure oscillation is Type 2 behavior (the mitigated waterhammer pressure). Because the air release capacity of this orifice size was not sufficient, air pockets were still trapped in the pipe when the water column reached the pipe end. As a result, the increase in tailwater depth first reduced the initial air volume therefore increased the pressure magnitude. When tailwater depth increased further ($y/D > 0.4$ as shown in Fig. 4.2), the orifice was likely submerged to some extent, which reduced its air release capacity; therefore, the impact pressure was mitigated due to the cushioning effects of the trapped air, as it is shown in Figs. 4.7c, 4.7d, 4.8c and 4.8d.

4.4 Theoretical Considerations

4.4.1 Governing equations

The governing equations for rapid filling in a receiving pipe with a tailwater are summarized as follows:

The air volume variation is

$$\frac{dV_a}{dt} = -A_1 U_1 \quad (4-3)$$

The momentum equation of the entire water column, including the momentum across the surge front, can be written as (Wiggert, 1972)

$$\frac{dU_1}{dt} = -g \frac{H - H_0}{x} - f \frac{U_1 |U_1|}{2D} - \frac{U_1^2}{2x} - \frac{(U_1 - U_w)(U_c - U_1)}{x} \quad (4-4)$$

where H_0 is the upstream driving head, H is the air pressure head, f is the Darcy-Weisbach friction factor, g is the gravitational acceleration ($9.81 \text{ m}^2/\text{s}$).

To calibrate the analytical model using the experimental results, a limitation was imposed on equation (4-4) by enforcing $U_c \equiv 0$ during the filling, which means the tailwater was considered as stagnant during the filling process. In fact, since the velocity of the free surface flow is usually much lower than that of the surge front during a surcharge or rapid filling event, this assumption could be acceptable if the filling or surcharging is so quick that the surface instability of the tailwater has little time to develop. If the velocity of the free surface tailwater flow is comparable to the surge speed, then U_c can no longer be regarded as zero. Although the effect of U_c on the pressure oscillation can be evaluated using the analytical model, such an effect will not be studied here because no experimental data is available to calibrate the calculation.

The variation of air mass with time is expressed as

$$\frac{dH^*}{dt} = -k \frac{H^*}{V_a} \frac{dV_a}{dt} - k \frac{H^*}{V_a} Q_a \quad (4-5)$$

where Q_a is the air discharge out of the trunk, which can be expressed by

$$Q_a = C_d A_0 Y \sqrt{2g \frac{\rho_w}{\rho_a} (H^* - H_b^*)} \quad (4-6)$$

where C_d is the discharge coefficient ($C_d = 0.65$, American Gas Association, 1978), and the pressure terms with asterisks denote the absolute value (hereafter), H_b^* is the absolute ambient pressure head in the air pocket, k is the polytropic exponent ($k = 1.4$ from Martin (1976), The sensitivity of parameter k and C_d have been discussed in Chapter 2.) Y is the factor of expansion, which can be written as (Martin 1976)

$$Y = \left[\frac{k}{k-1} \left(\frac{H_b^*}{H^*} \right)^{2/k} \frac{1 - (H_b^*/H^*)^{(k-1)/k}}{1 - H_b^*/H^*} \right]^{1/2} \quad (4-7)$$

If $Y = 1$, Eq. (8) is the conventional orifice discharge formula. A_0 is the orifice area.

If H^*/H_b^* is greater than 1.89, the orifice will be choked, and the air discharge can be calculated by

$$Q_a = C_d A_0 \sqrt{g \frac{\rho_w}{\rho_a} H^*} \sqrt{k \left(\frac{2}{k+1} \right)^{\frac{k+1}{k-1}}} \quad (4-8)$$

When the water column reaches the end of the pipe, the impact pressure of the water column can be calculated by the following equation (chapter 2)

$$H_j = H_i + \frac{a}{g} \left(U_i + \frac{a}{B} - \sqrt{\left(\frac{a}{B} \right)^2 + 2U_i \frac{a}{B} + \frac{2gH_i}{B}} \right) \quad (4-9)$$

where: a is the speed of the pressure wave when the water column reaches the orifice and B is a coefficient, defined as $B = (A_1/A_0)^2 + K - 1$. K is the minor loss coefficient of the orifice which can be neglected since it is very small compared with A_1/A_0 , where A_0 is the orifice cross-section area. U_i and H_i are, respectively, the velocity and pressure head at the end of water column and are calculated from Eq. (4-3) through (4-5).

As discussed in Chapter 2, it is difficult to calculate the speed of the pressure wave in a rapid filling pipe containing trapped air, therefore a measured value of wave

speed is needed to apply Equation (4-9). It was observed in our experiments that this value varied on a case by case basis, ranging from 200m/s to 1200m/s. The lowest value occurred for the shorter relative initial water column length of $\lambda_0 = 0.56$, and the highest value at $\lambda_0 = 0.89$. To test the sensitivity of peak pressures to the speed of pressure wave, instead of using the measured a value for each orifice size, approximate values of a based on the orifice range were used in the calculation. For $\lambda_0 = 0.56$, $a = 700\text{m/s}$ for $d/D \geq 0.114$ and $a = 200\text{m/s}$ for $d/D > 0.115$; for $\lambda_0 = 0.89$, $a = 1200\text{m/s}$ for $d/D \geq 0.114$ and $a = 700\text{m/s}$ for $d/D > 0.114$. Consequently, this analytical model is not a predictive tool but rather, provides a means of exploring and explaining the behavior of this phenomenon. Because the surge front is considered in Eq. (4-4), the analytical model is thus called a '*surge model*'.

Eqs. (4-3) through (4-9) are normalized by the same non-dimensional variables defined chapter 2. To save the space, the non-dimensional equations are not presented here. The non-dimensional equations were solved by a fourth-order Runge-Kutta method. An optimal dimensionless time step of 0.001 was chosen based on the sensitivity analysis discussed in chapter 2.

4.4.2 Comparison between calculation and experiment

Surge model – Figs. 4.9 through 4.13 shows the comparison of calculated and measured maximum pressure magnitudes under different driving heads, initial water column lengths, orifice diameters, and tailwater depths. In the figures, the circles represent the measured data, the solid lines represent the results of the surge model, and the dashed lines represent the results of the so-called *dry-front* model which will be discussed later. It is seen that for no and small tailwater depth cases ($y/D = 0$ in Fig. 4.9

and $y/D = 0.2$ in Fig. 4.10), the calculated values are close to the measured data. The discrepancy becomes prominent when y/D is larger than 0.4 for intermediate and large air release situations (Figs. 4.11 through 4.13), especially for the shorter initial water column length ($\lambda_0 = 0.56$). The reason is that, as discussed in section 4.3.2, for the shorter initial water column length situations, the tailwater surface was greatly disturbed by the propagating surge; also the orifice might have been choked. As a result, air pockets could have been more likely to be trapped as the orifice size and tailwater depth increased. Such a complicated air-water relationship in the receiving pipe made the pressure wave speed vary drastically and therefore the model is unable to reproduce a reasonable impact pressure. Moreover, at this stage, the model is unable to handle the disturbed tailwater and the choked orifice.

Dry-front model - As discussed in the introduction section, one thing we would like to look at is if our previous model (described in Chapter 2) for the rapid filling of the empty receiving pipe could be used. In other words could the tailwater effect be modeled by simply reducing the size of the air pocket in the specific initial conditions. To distinguish our previous model with the surge model, we will refer to our previous model as a *dry-front* model (hereafter). To apply the dry-front model for the tailwater situation, we just shift the air pocket location (from the top of the flow to the front of the flow) with the same initial air pocket volume V_{a0} (by increasing the initial water column length accordingly) as Fig. 4.14 illustrates.

The calculated results using the dry-front model are plotted as the dashed line in Figs. 4.9 through 4.13. It can be seen that, for $y/D = 0$ in Fig. 4.9, the surge model and the dry-front model have identical results since for $y/D = 0$ the governing equations of both

models are identical. A closer examination of Fig. 4.6 indicates that the dry-front model works fine for all 'no or small air release' cases (Type I behavior). Because, under small orifice size situations, the pressure oscillation is air-pocket dominant, and so the assumption of stagnant tailwater during the rapid filling is acceptable. For the larger orifice size situations, Fig. 4.6 indicates that the dry-front model produces comparable results to the measured data for the longer initial water column length of $\lambda_0 = 0.89$ except for $y/D = 0.8$, under which the air-flow relation becomes very complicated (probably due to submergence of the orifice, as discussed above). However, for shorter water column length situations such as $\lambda_0 = 0.56$, the discrepancy of the dry model becomes prominent under large orifice size conditions when $y/D > 0.4$, which is attributed to the effect of surge in destabilizing the tailwater surface.

Comparison between surge model and dry-front model - A comparison between the surge model and dry-front model configurations illustrated in Fig. 4.14 indicates that, if the tailwater is stagnant, the difference between the two models are the speeds of the surge fronts and the initial water column length, x_0 . Table 4-1 lists the relative error ε of the analysis, which is defined as

$$\varepsilon = \frac{|H_{\text{measurement}} - H_{\text{calculation}}|}{H_{\text{measurement}}} \quad (4-10)$$

From Table 4-1, it is seen that the maximum relative error for the dry-front model is about 3 times higher than that of the surge model.

4.5 Conclusions

In this chapter, we studied the pressure surge in a rapidly filling horizontal pipe which has a tailwater. The effects of initial flow depth, orifice size, initial water column

on pressure magnitude and oscillation pattern were investigated. The recorded pressure histories for all runs were examined and the three types of pressure oscillation behavior discussed in Chapter 2 were observed in tailwater cases. For small air release situations, the maximum pressure magnitudes increased with the tailwater depth because of the reduced initial air volume. For the large air release situations, the tailwater was pushed forward through the orifice as the tailwater depth increased therefore the surge front speed was reduced so was the impact pressure. Also under large air release situations, the free surface of the tailwater was disturbed during rapid filling (especially when the initial water column length was short), the disturbed free surface could have trapped air pockets and choked the orifice, therefore mitigated the impact pressure. For the intermediate air release situations, the maximum pressure magnitude first increased with the tailwater depth due to the reduced initial air volume then decreased with the tailwater depth due to choked orifice which cushioned the impact pressure. Our previous dry-front model was able to simulate the maximum pressure magnitudes for no or small air release situations. The surge model was able to simulate the maximum pressure magnitudes except for the situations where the orifice size was large and initial water column length was short.

4.6 References

- American Gas Association (1978). *Orifice Metering of Natural Gas, American National Standard*, ANSI/API 2530.
- Martin, C.S. (1976). "Entrapped air in pipelines." *Proceedings of the second international conference on pressure surges*, London, September 22-24, 1976, BHRA Fluid Engineering, Cranfield, Bedford, England.

Wiggert, D.C.(1972). "Transient flow in free-surface, pressurized systems," *ASCE Journal of Hydraulic Division*, 98(HY1),11-27.

Wylie, E. and Streeter, V. (1976). *Fluid Transients*, McGraw-Hill International Book Company.

Table 4-1 Error analysis for the theoretical model

Y/D	ϵ_{min}		ϵ_{max}		ϵ_{mean}	
	Dry-front	Surge	Dry-front	Surge	Dry-front	Surge
	Model	Model	Model	Model	Model	Model
0	0	0	0.34	0.34	0.06	0.06
0.2	0.01	0.01	0.29	0.29	0.08	0.05
0.4	0.01	0.02	0.81	0.30	0.15	0.13
0.6	0.02	0.01	2.11	0.96	0.17	0.14
0.8	0.01	0.04	2.48	0.48	0.56	0.17

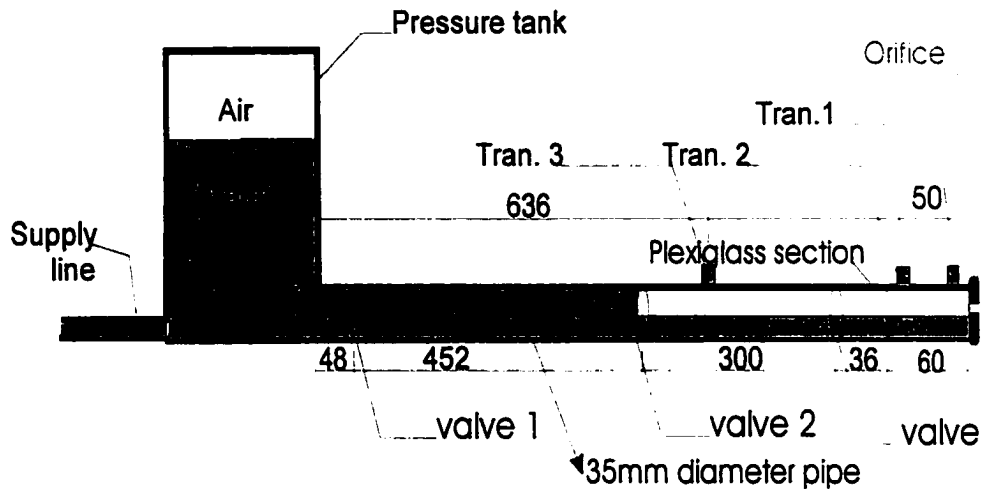


Fig. 4.1 Diagram of the experimental apparatus-Stagnant flow (unit of length: cm)

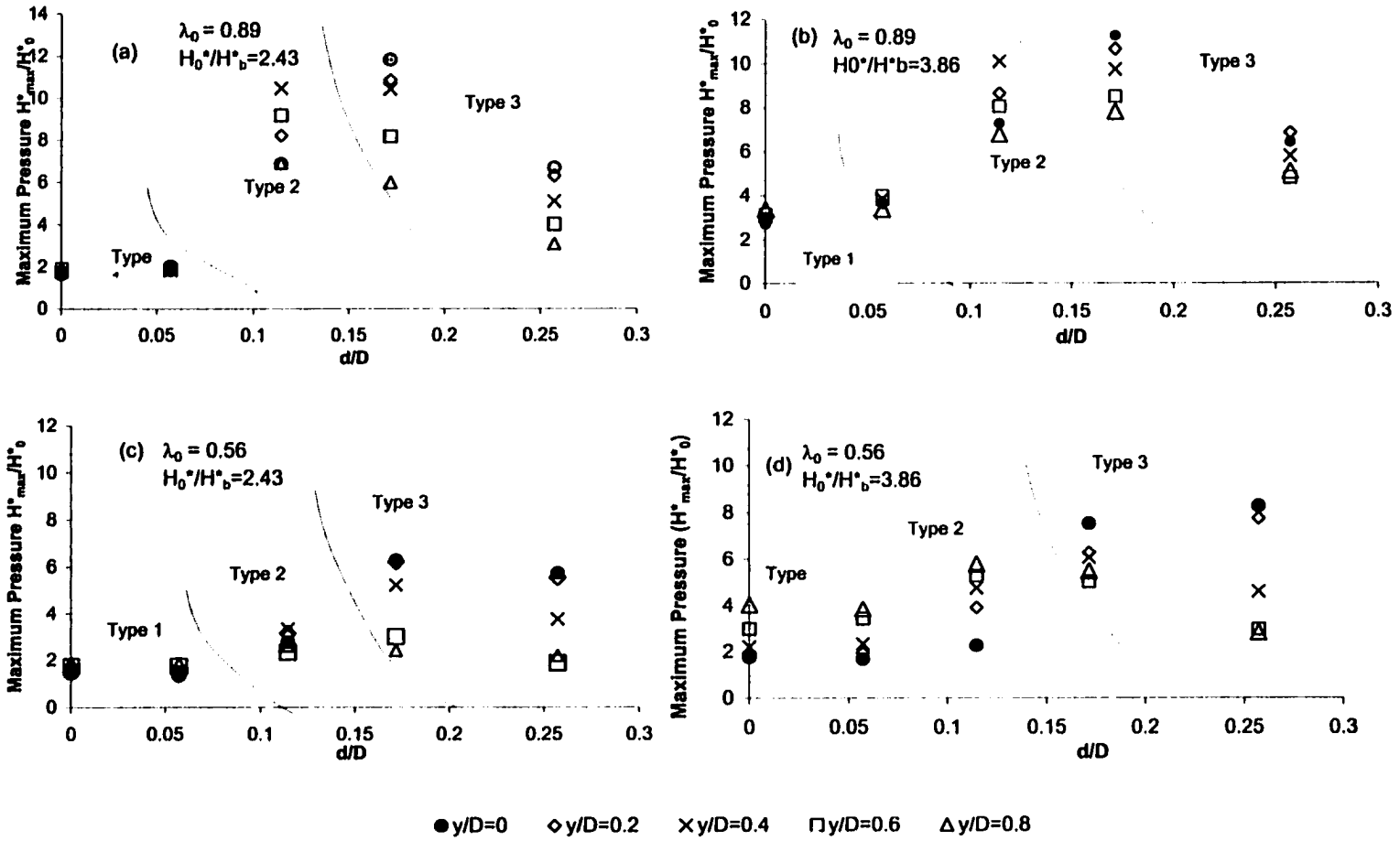


Figure 4.2 Maximum peak pressure relation with tailwater depth

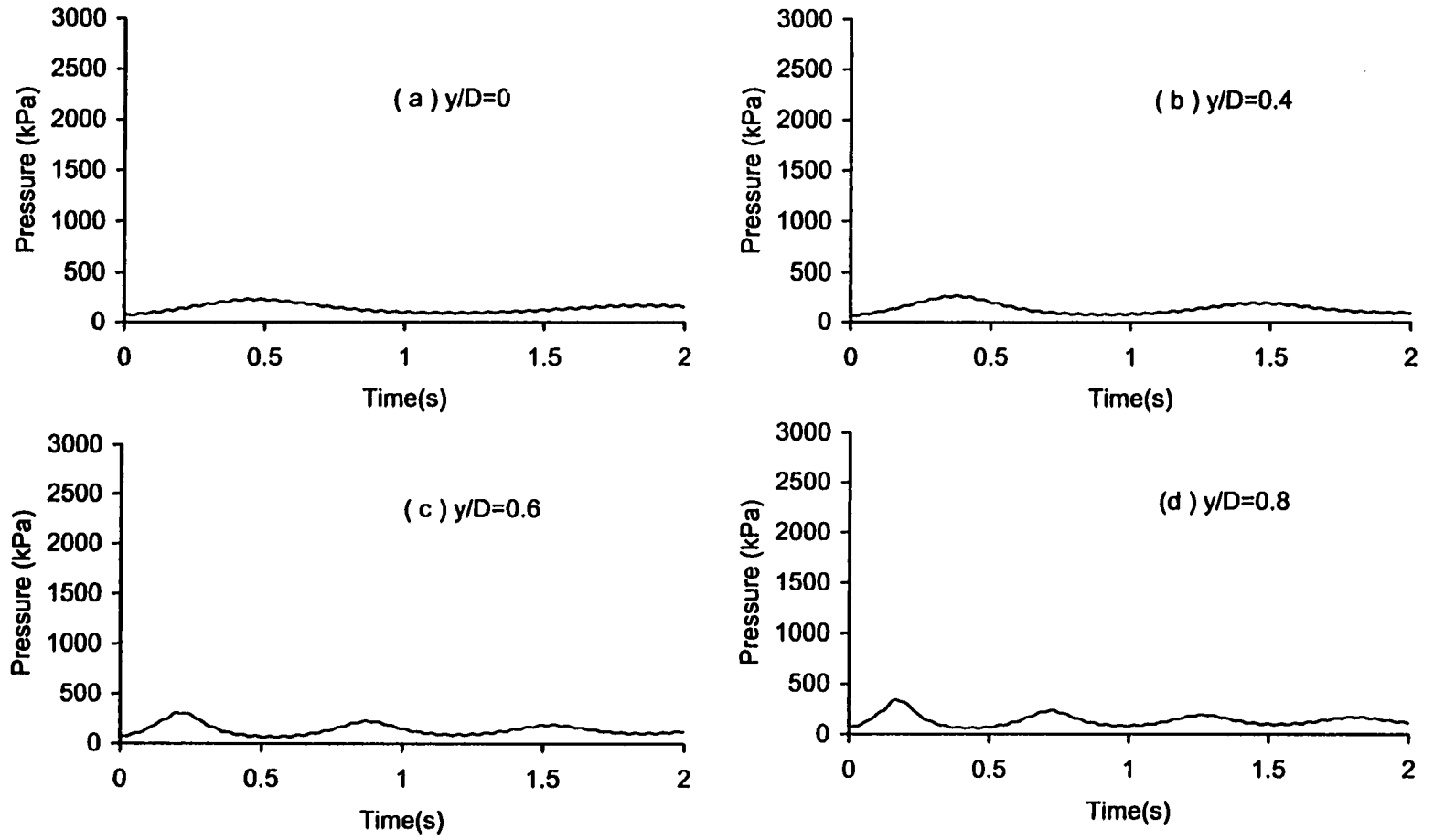


Fig. 4.3 Pressure Oscillation Pattern ($H^*_o/H^*_b = 2.43$, $\lambda_0 = 0.56$, $d/D = 0$)

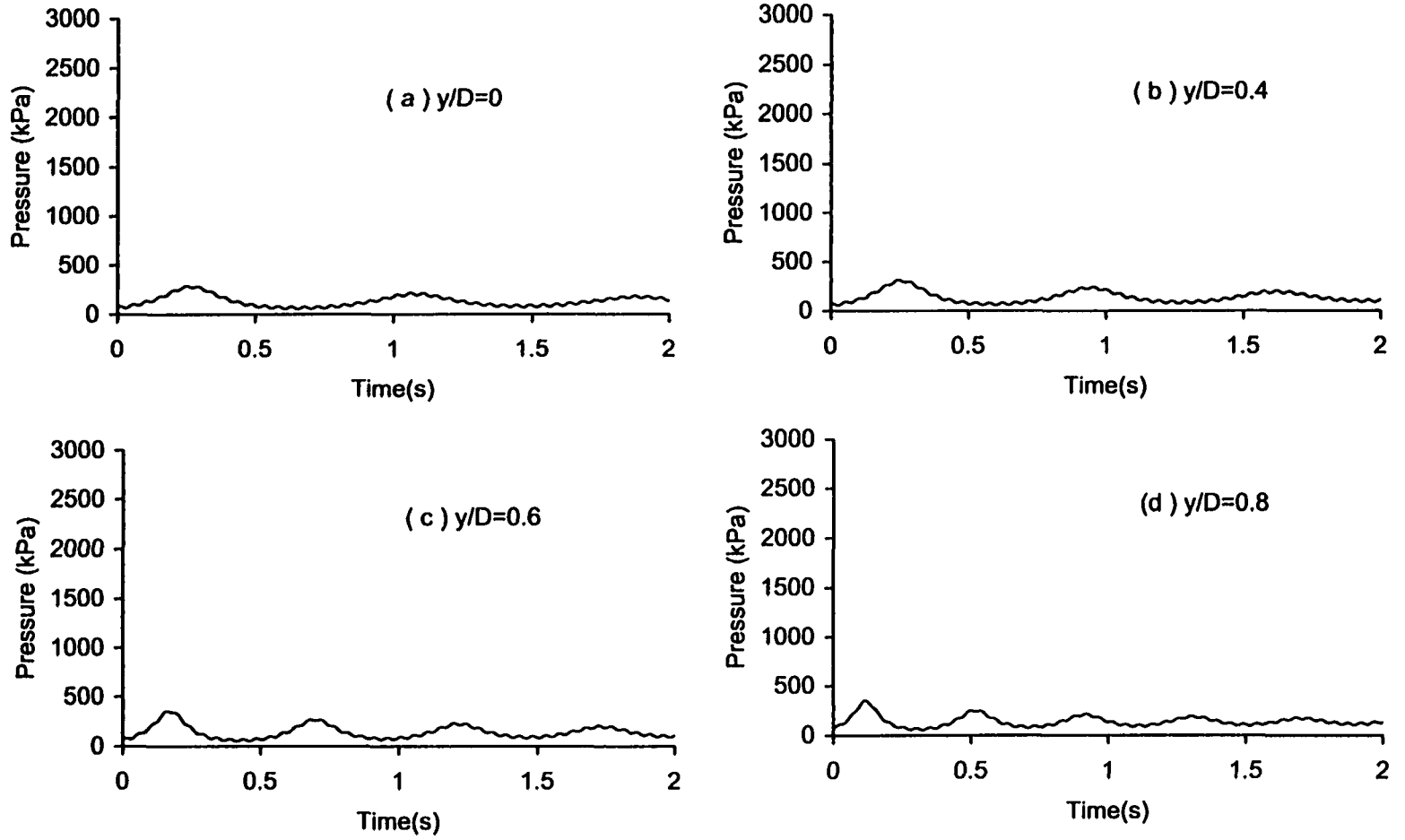


Fig. 4.4 Pressure Oscillation Pattern ($H^*_o/H^*_b = 2.43$, $\lambda_0 = 0.89$, $d/D = 0$)

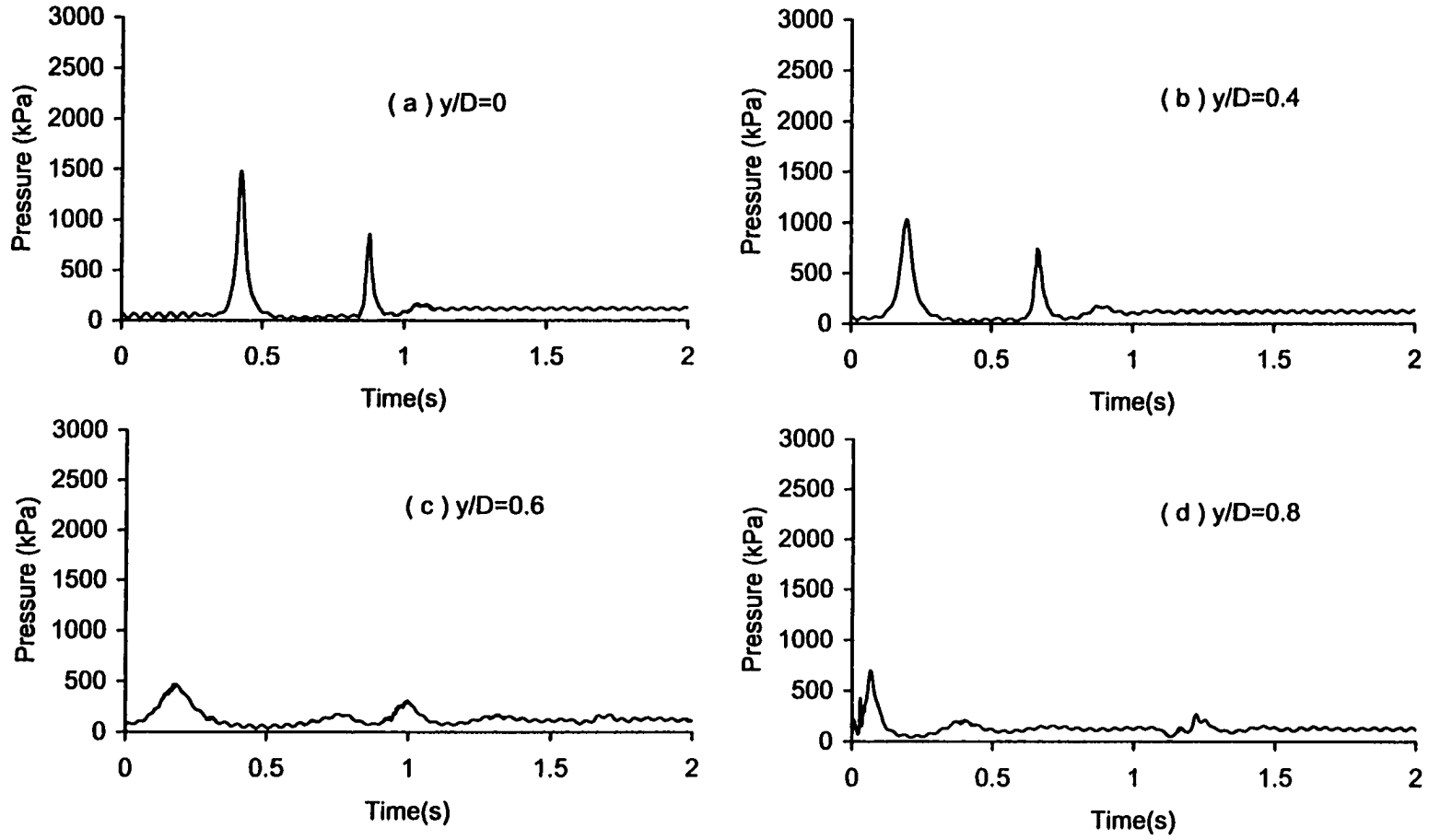


Fig. 4.5 Pressure Oscillation Pattern ($H^*_o/H^*_b = 2.43$, $\lambda_0 = 0.56$, $d/D = 0.171$)

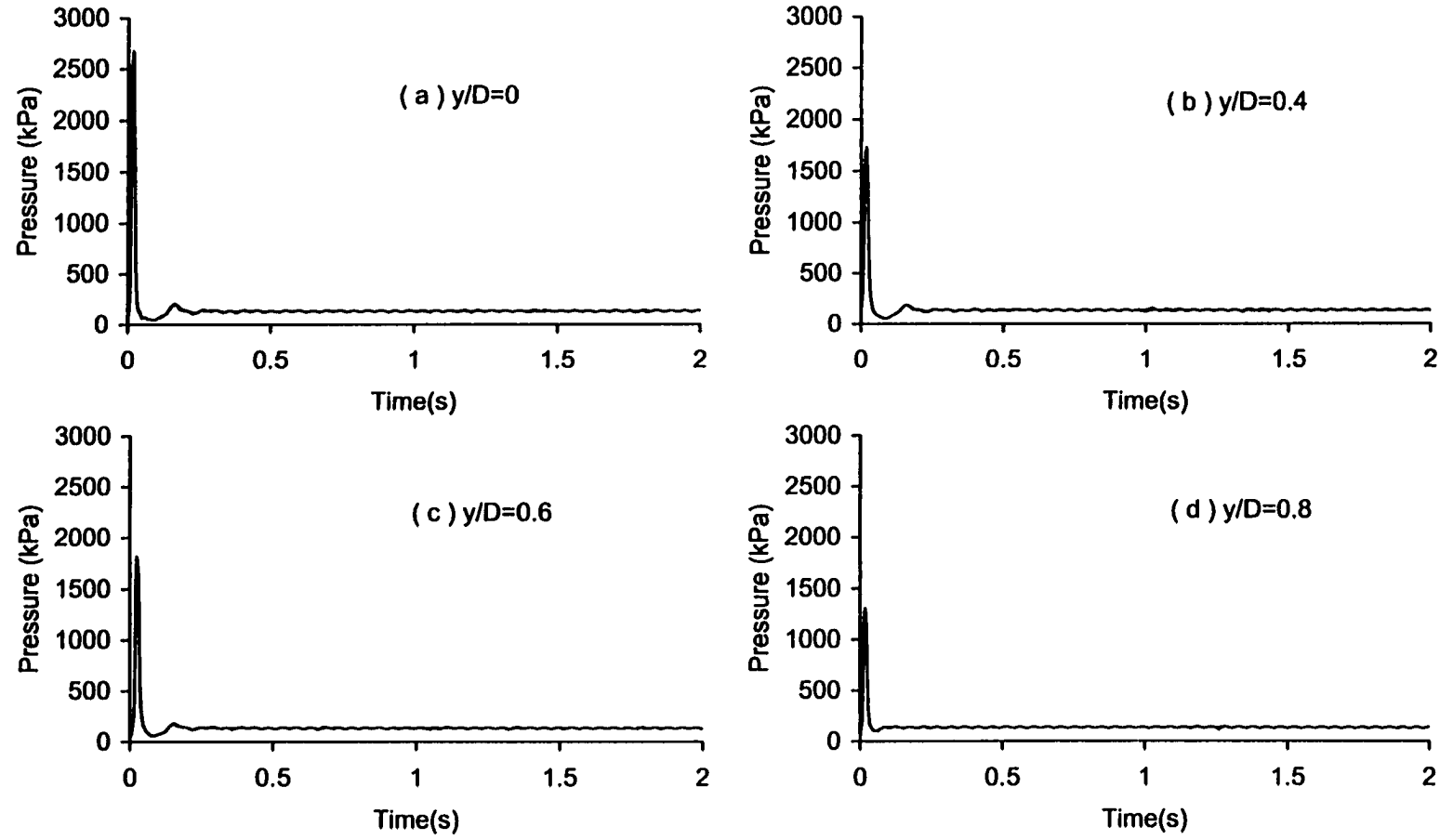


Fig. 4.6 Pressure Oscillation Pattern ($H^*_o/H^*_b = 2.43$, $\lambda_0 = 0.89$, $d/D = 0.171$)

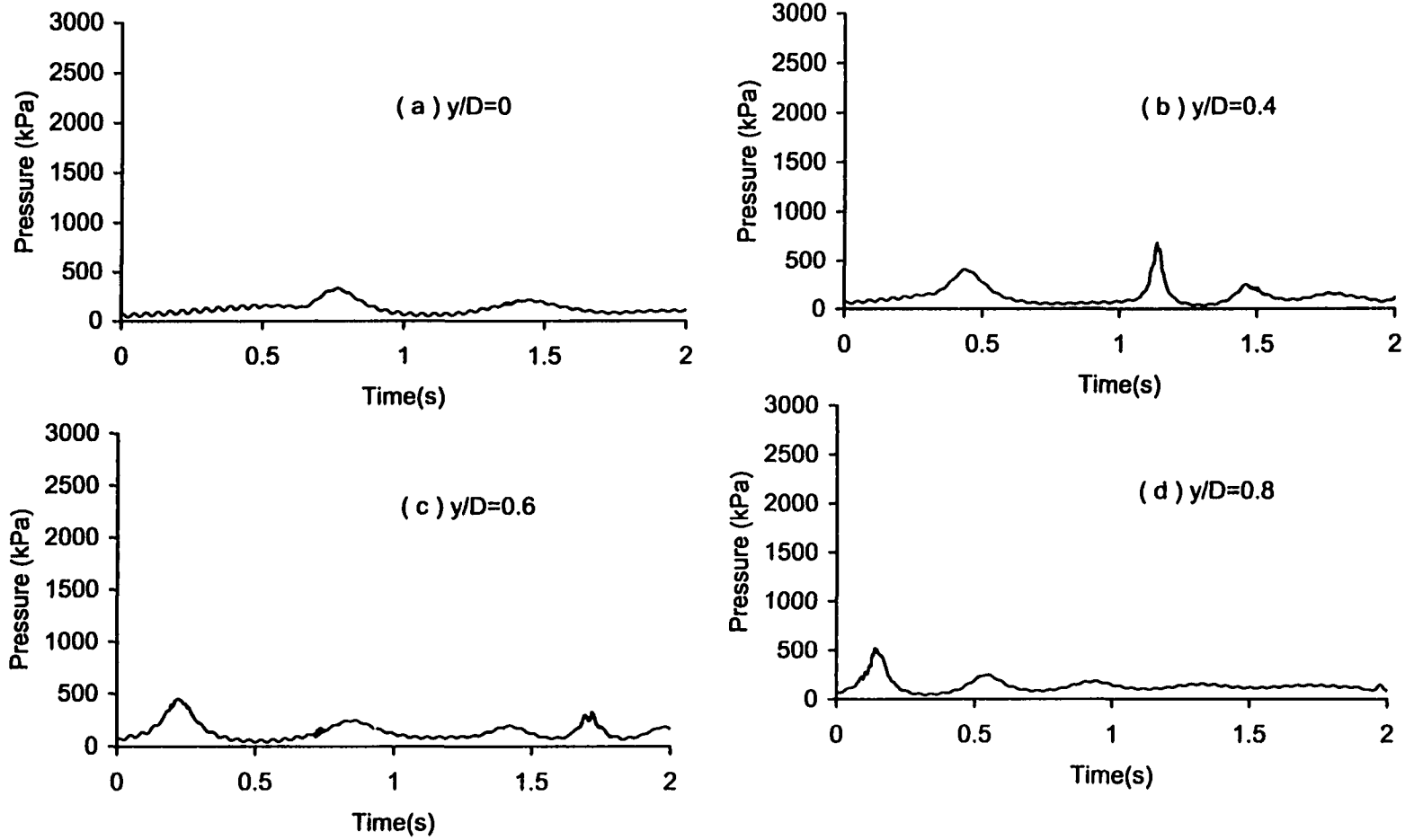


Fig. 4.7 Pressure Oscillation Pattern ($H^*_v/H^*_b = 2.43$, $\lambda_0 = 0.56$, $d/D = 0.114$)

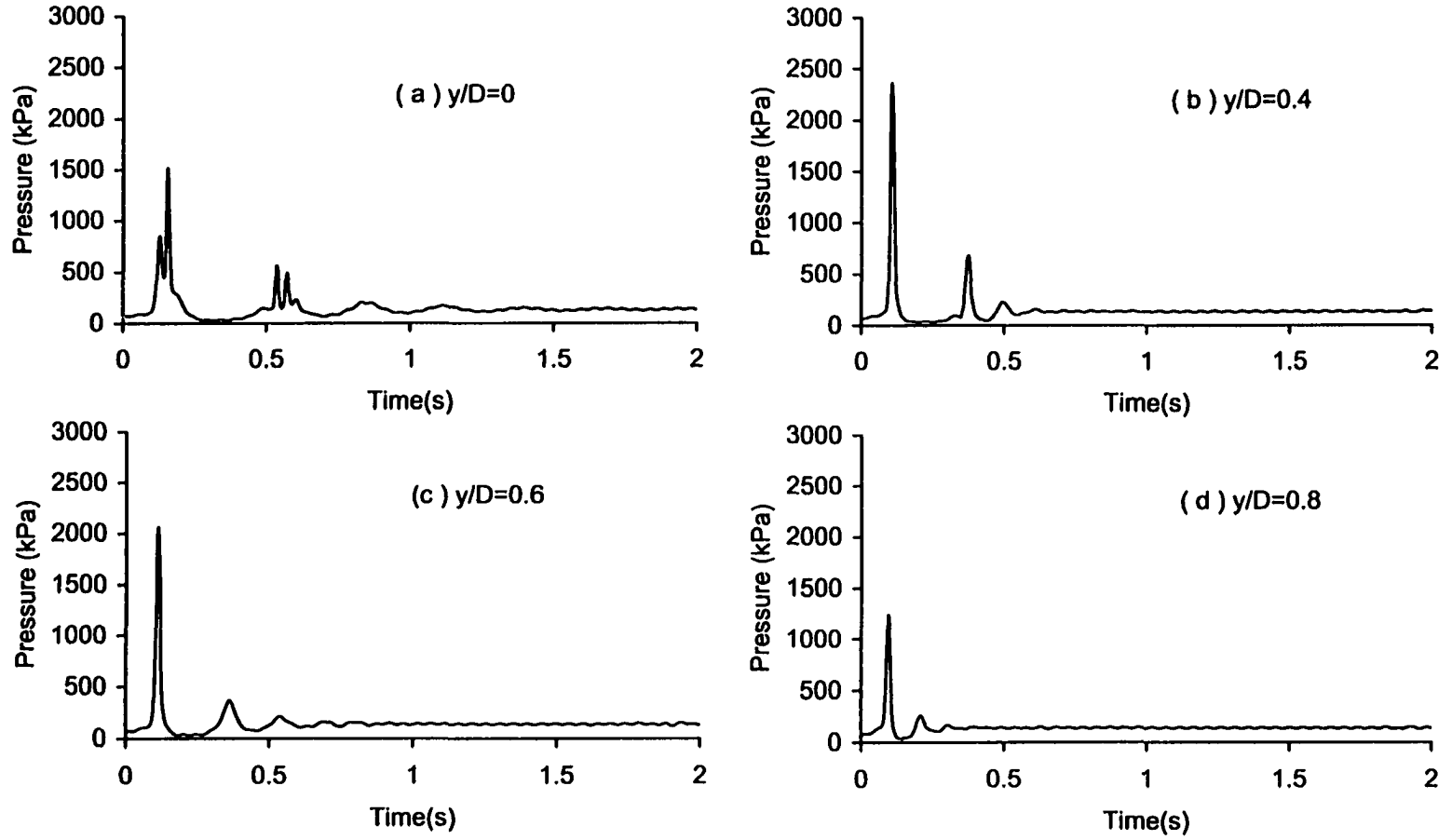


Fig. 4.8 Pressure Oscillation Pattern ($H^*_o/H^*_b = 2.43$, $\lambda_0 = 0.89$, $d/D = 0.114$)

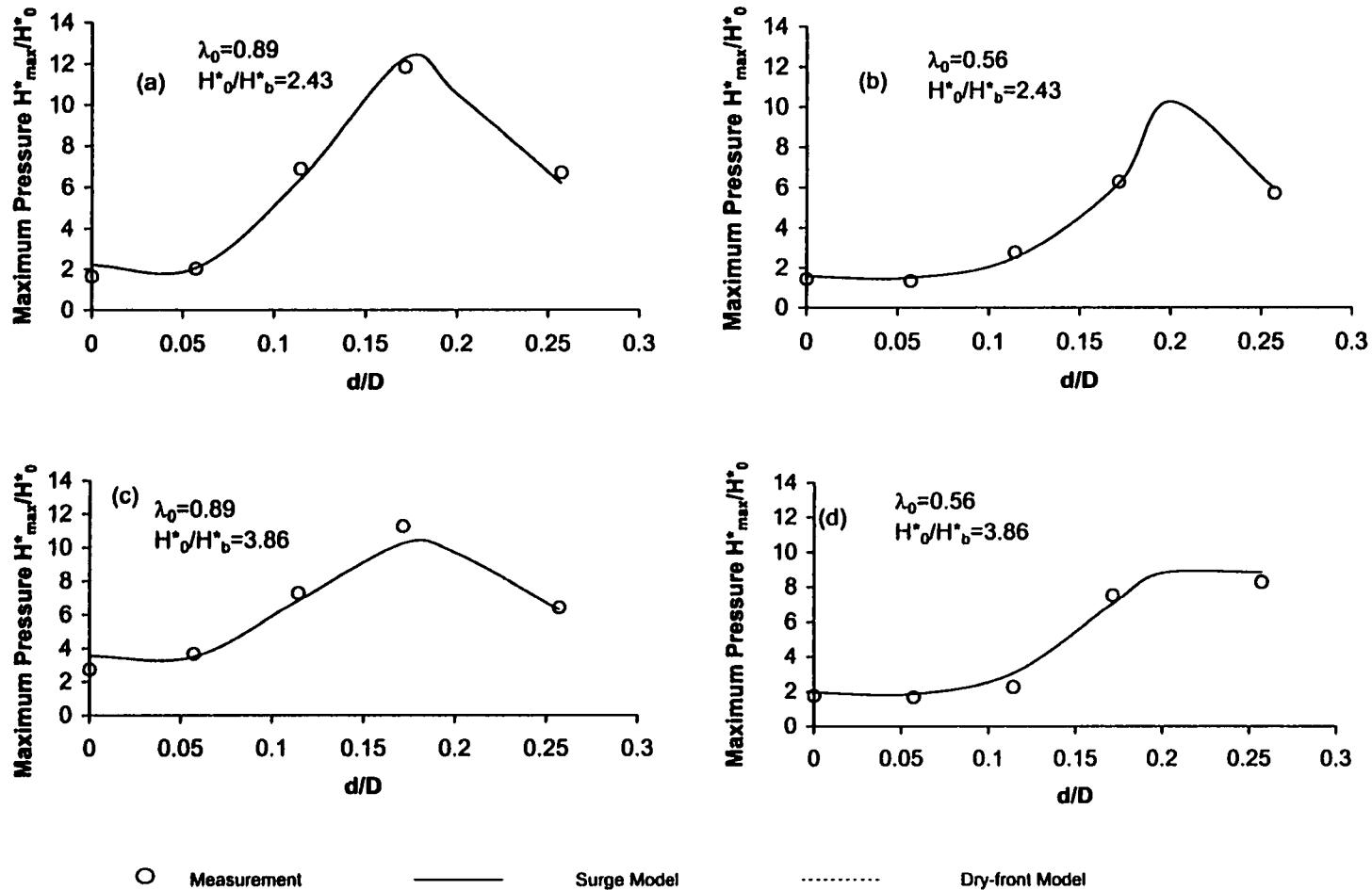


Figure 4.9 Comparison between calculated and measured maximum pressure magnitudes ($y/D=0$)

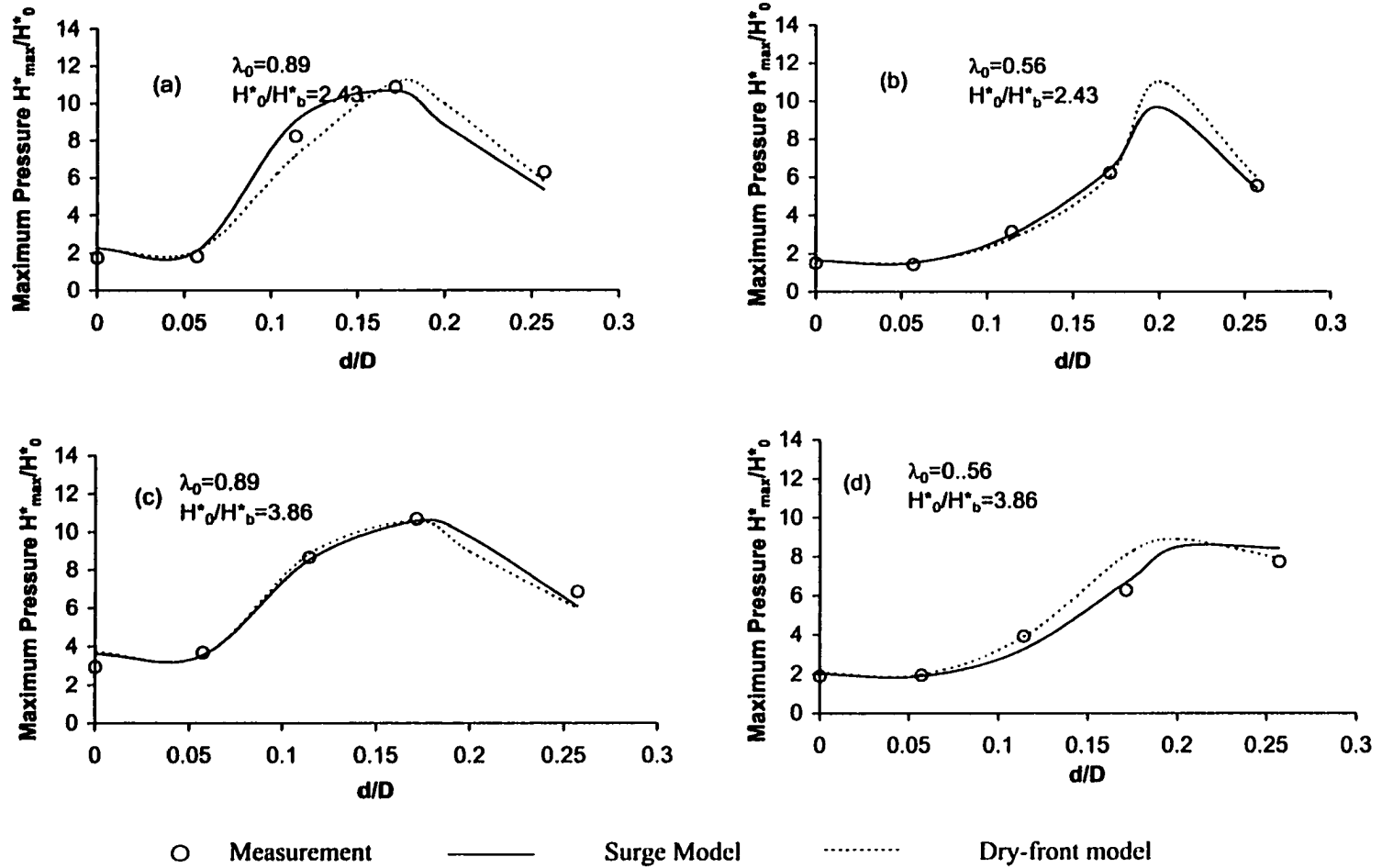


Figure 4.10 Comparison between calculated and measured maximum pressure magnitudes ($y/D = 0.2$)

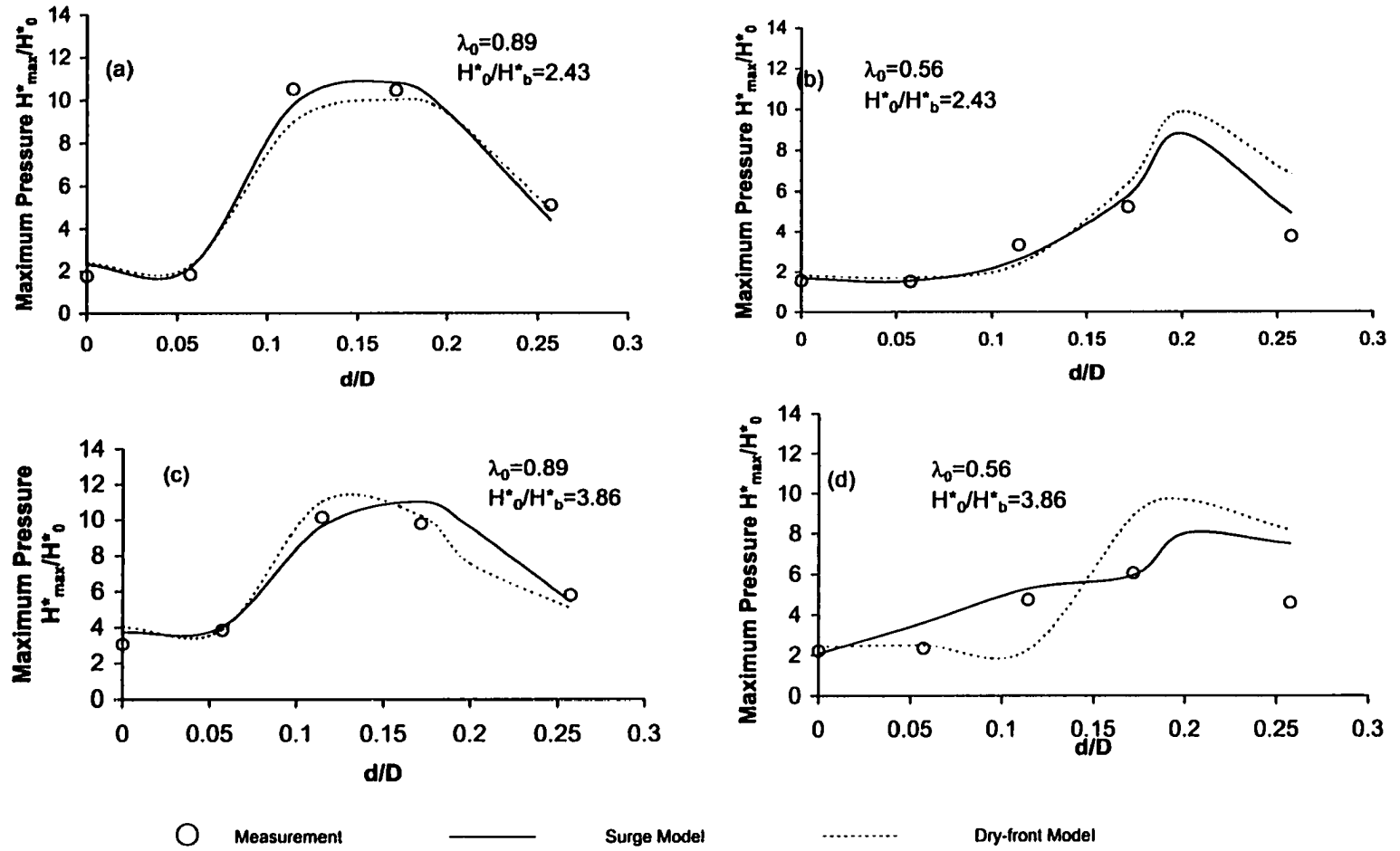


Figure 4.11 Comparison between calculated and measured maximum pressure magnitudes ($y/D = 0.4$)

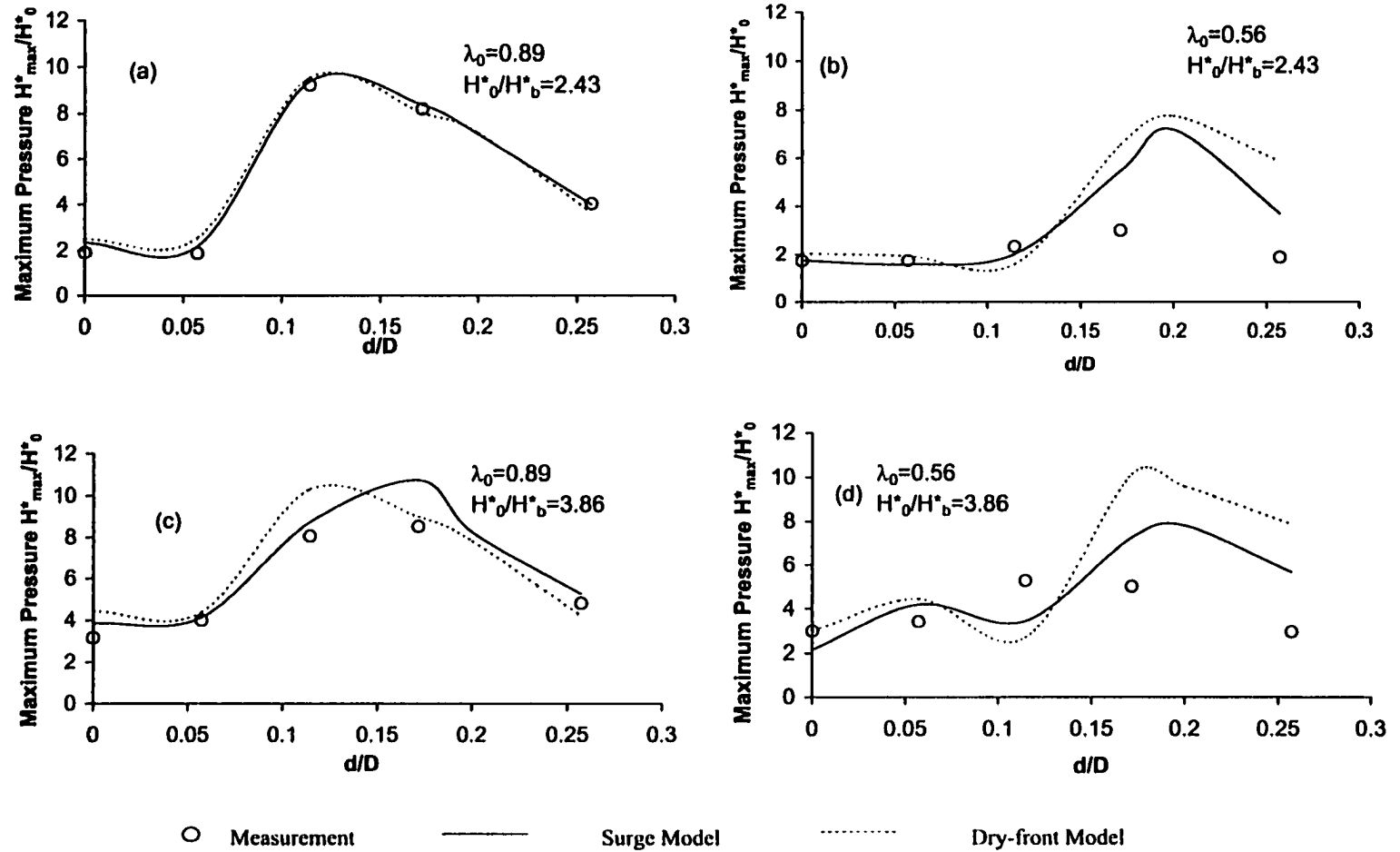


Figure 4.12 Comparison between calculated and measured maximum pressure magnitudes ($y/D = 0.6$)

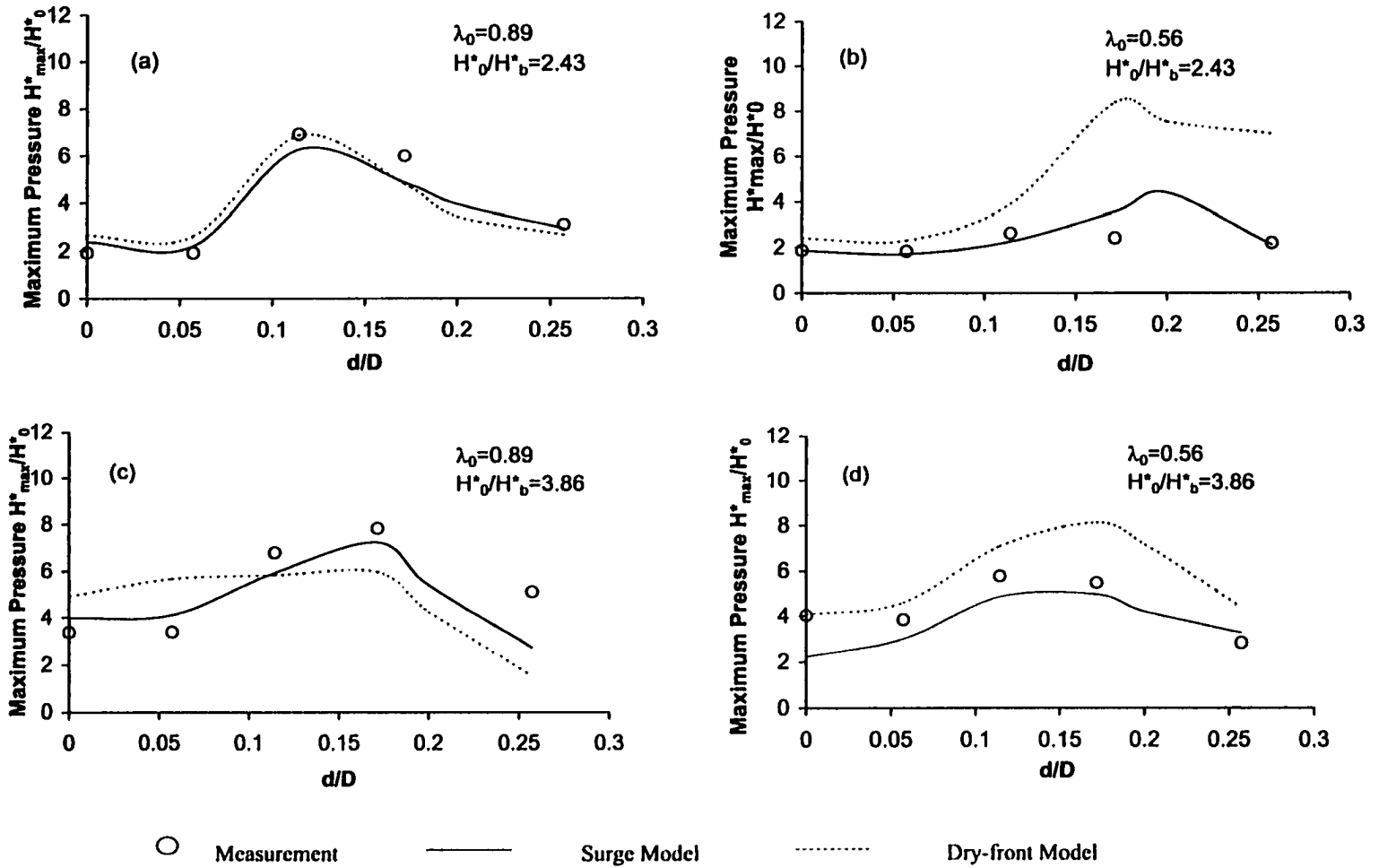


Figure 4.13 Comparison between calculated and measured maximum pressure magnitudes ($y/D = 0.8$)

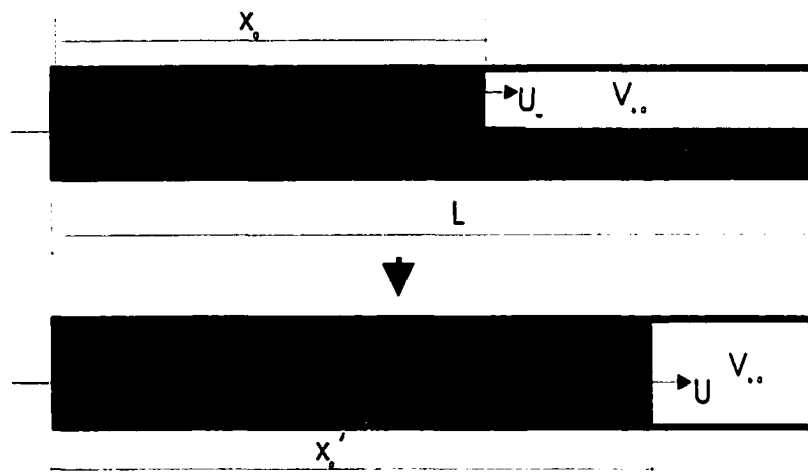


Fig. 4.14 Equivalent Dry-Front Model

5.0 PRESSURE SURGES IN A RAPIDLY FILLING HORIZONTAL PIPE WITH A DOWNSTREAM VERTICAL PIPE BRANCH⁴

5.1 Introduction

Urban sewer systems may be surcharged when the sewer is under-designed, when the storm flood exceeds the design return period, or when the sewer starts inline storage and pumping. The surcharging usually starts from the downstream and the flow quickly backs upstream, during which air ahead of the surge front may be trapped. When the trapped air is released through manholes or drop shafts, severe pressure oscillations may occur that may blow off manhole covers or cause pipe rupture (Hamman and McCorquodale, 1981; Zech, 1985; Cardel et al., 1989; Guo and Song, 1990; Li and McCorquodale, 1999).

In this chapter, the flow transients in a rapidly filling horizontal pipe with a vertical pipe branch at the downstream (called LP case, hereafter) is studied both experimentally and analytically. This configuration can be regarded as a simplified trunk-manhole system. This study serves two purposes: (1) to explore the effects of trapped air on pressure transients in a horizontal-vertical pipe system under different initial air volumes, orifice sizes, and operation heads; and (2) to compare these flow transients observed in the LP case with the earlier observation of the flow transients in horizontal pipes (called HP case hereafter).

⁴ A version of this chapter will be submitted for publication in Journal of Hydraulic Engineering, American Society of Civil Engineers (ASCE).

5.2 Theoretical Analysis

5.2.1 Configuration

The sketch of the theoretical model is shown in Fig. 5.1. At the upstream end (the left hand-side of the figure), there is a reservoir which provides a constant filling head H_0 . L_1 and L_s are the lengths, A_1 and A_s are the cross-section areas, and U_1 and U_s are the flow velocities in the horizontal and vertical pipe branches, respectively; x is the initial water column length.

5.2.2 Governing equations

The analytical model was developed based on the previous model for the rapid filling of a horizontal pipe (Chapter 2); therefore, the detailed theoretical derivation is neglected except the treatment of flow at the junction of the horizontal and vertical pipes.

It is assumed that when the water column reaches the junction, the continuity equation is satisfied at the junction; therefore,

$$U_1 A_1 = U_s A_s \quad (5-1)$$

Because the unsteady flow structures near the junction are very complicated (Yen, 1986; Yevjevich, 1964), the energy loss at the junction when the rapid filling flow passes through the junction is difficult to determine. Therefore, instead of establishing the energy relation for the flow at the junction, it is assumed that the pressure head in each branch adjacent to the junction will be the same (Yen, 1986).

$$H_{J1} = H_{Js} = H_J \quad (5-2)$$

in which H_{J1} and H_{Js} denote the pressure head of each branch at the junction, respectively.

Throughout this paper, subscript i denotes the branch number with $i = 1$ and s denoting the upstream horizontal and vertical pipe branches, respectively. The change of air volume in the i -th branch is

$$\frac{dV_{ai}}{dt} = -A_i U_i \quad (5-3)$$

in which V_{ai} is the air volume in front of the water column.

The momentum equation for the water column in the i -th pipe branch will be

$$\frac{dU_i}{dt} = -g \frac{H_i - H_{i-1}}{x_i} - f \frac{U_i |U_i|}{2D_i} - K_i \frac{U_i^2}{2x_i} - gS_i \quad (5-4)$$

in which, H is the air pressure head (when $i = s$, H_{i-1} will be H_J , the pressure head at the junction); K_i is the inlet energy loss of the i -th pipe; S_i is the slope of the i -th pipe ($S_1 = 0$ for horizontal pipe and $S_s = 1$ for the vertical pipe); f is the Darcy-Weisbach friction factor; and g is the gravitational acceleration (9.81 m/s^2).

It can be seen from equation (5-4) that the junction pressure, H_J , must be solved in order to simulate the pressure oscillation after the water column enters the vertical pipe. The junction pressure is obtained by differentiating equation (5-1) with respect to time and substituting equation (5-4) into the differentiated equation. The junction pressure can then be expressed as:

$$H_J = \frac{1}{\left(1 + \frac{L_1 A_s}{x_s A_1}\right)} \left(H_0 + \frac{L_1 A_s}{x_s A_1} H_s - \frac{fL_1}{2g} \left(\frac{U_1 |U_1|}{D_1} - \frac{L_1 A_s}{x_s A_1} \frac{U_s |U_s|}{D_s} \right) \right. \\ \left. - K_1 \frac{U_1^2}{2g} + K_s \frac{L_1 A_s}{x_s A_1} \frac{U_s^2}{2g} + L_1 \frac{A_s}{A_1} gS_s \right) \quad (5-5)$$

The governing equations for the air phase in each pipe branch are the same as presented in Chapter 2 (equations (2-3) to (2-6)). The pressure induced by the water column impacting on the vertical pipe end is equation (2-7).

5.2.3 Non-dimensional equations

Similar to the rapid filling of a horizontal pipe, the governing equations for the LP configuration are normalized by defining the following non-dimensional variables:

$$\lambda_i = \frac{x_i}{L_1}, \quad \eta_i = \frac{V_{ai}}{V_{a0}}, \quad \varphi_i = \frac{H_i^*}{H_0^*}, \quad \psi_i = \frac{U_i}{\sqrt{g(1-x_{i0}/L_1)H_b^*}}, \quad \alpha_i = \frac{a}{\sqrt{g(1-x_{i0}/L_1)H_b^*}}$$

$$\tau = \frac{t}{L_1 \sqrt{\frac{(1-x_{i0}/L_1)}{gH_b^*}}} \quad \alpha_i = \frac{A_i}{A_1} \quad V_{a0} = L_1 A_1 (1 - \lambda_{i0})$$

where $i = 1$ or s and the subscript “0” denotes initial values.

Eq. (5-3) becomes

$$\frac{d\eta_i}{d\tau} = -\alpha_i \psi_i \quad (5-6)$$

Equation (5-4) becomes

$$\frac{d\psi_i}{d\tau} = -\frac{1}{\varphi_b} \cdot \frac{\varphi_i - \varphi_{i-1}}{\lambda_i} - \frac{C_0}{2} \sqrt{\frac{1}{\alpha_i}} \psi_i |\psi_i| - \frac{K_i}{2\lambda_i} (1 - \lambda_0) \psi_i^2 - \frac{L_1}{H_b^*} S_i \quad (5-7)$$

In (5-4), $C_0 = fL/D(1-\lambda_0)$, a parameter representing the combined effects of friction, pipe size and initial water column.

Equation (5-5) becomes:

$$\varphi_j = \frac{1}{(1 + \alpha_s \frac{1}{\lambda_s})} \left\langle \begin{aligned} &1 - \varphi_b \frac{C_0}{2} (\psi_1 |\psi_1| - \sqrt{\alpha_s} \psi_s |\psi_s|) - \frac{\varphi_b}{2} K_1 (1 - \lambda_0) \psi_1^2 \\ &+ \frac{\varphi_b}{2} (1 - \lambda_0) \alpha_s \frac{1}{\lambda_s} K_s \psi_s |\psi_s| \\ &+ \frac{1}{\lambda_s} \varphi_s \alpha_s + \varphi_b \alpha_s \frac{L_1}{H_b^*} (S_s - S_1) \end{aligned} \right\rangle \quad (5-8)$$

The governing equations for the air phase are equations (2-8) through (2-11). Equation (5-6), (5-7), (5-8), (2-8), (2-9), and (2-10) constituted of the non-dimensional governing equations for the analysis of the LP case. These equations were solved using the same fourth-order Runge-Kutta Scheme described Chapter 2.

5.3 Experimental Investigation

As was observed in Chapter 2, generally, there are three types of pressure behavior in a rapidly filling horizontal pipe, depending on the size of air-release orifice. For no or small air release conditions, the air pocket pressure is dominant; for a large air release rate, the pressure is dominated by the water hammer pressure as a result of water slamming into the pipe end. For an intermediate orifice size, the pressure oscillation may be dominated either by the air pocket pressure or by the waterhammer pressure, depending on the mitigative effect of the residual air pockets in the flow. This experimental study will explore if the same pressure behavior exists in the LP case.

Fig. 5.2 depicts the experimental apparatus used in this investigation. The essential components were the same as those used in the previous investigations of a horizontal pipe (chapters 2, 3, and 4). However, to investigate the difference between the flow transients in the LP case and the HP case, a 35 cm (inner) diameter pipe was fitted

onto the downstream end of the existing 1000 cm horizontal pipe. This 60cm long pipe segment was either positioned vertically (to form an LP case) or positioned horizontally (to form a HP case). Therefore, the total pipe length for each case was the same. The end of the vertical pipe was either sealed, or outfitted with a cap containing a centered, sharp-edged orifice to study the effects of air release on pressure transients in the system. Two pressure transducers (PACE, Model kPV5) were positioned on the vertical pipe: one was located 5 cm below the top of the pipe and the other was located 5 cm above the top of the horizontal pipe. A third transducer was installed on the horizontal pipe branch at a location 636cm downstream of the pressure tank. Each transducer was connected to a digital demodulator which was in turn connected to a data acquisition board inside of a computer. The Labview 4.0 program, developed for the investigation and described in the previous chapters, was used to collect the pressure data. The details of the calibration of the transducers, the determination of pipe wall friction factor, and valve losses were provided in Chapter 2.

5.4 Experimental Results

One upstream pressure of 275 kPa, two initial water column lengths of 0.48m ($\lambda_0 = 0.048$) and 8m ($\lambda_0 = 0.8$), and 12 orifice sizes ranging from 0 to 19.8 mm were tested; resulting in a total of 24 test cases for the LP and the HP, respectively. To determine the consistency of the experimental results, each of the tests was repeated at least three times. It was found that the difference between the highest and the lowest values of the peak pressure for a given test case was less than 10% for relative orifice size, d/D , less than 0.086 and greater than 0.257. For the transitional range of d/D values between 0.114 and 0.257, this difference could be up to 32%. For illustration purposes,

the experimental peak pressure values shown throughout this paper are the averaged value for each test.

5.4.1 Pressure oscillation patterns within the air pocket during rapid filling

The recorded pressure oscillations for all runs were examined and it was found that the three types of pressure behavior defined in chapter 2 for a horizontal pipe also occurred in the LP case. To illustrate each of these patterns of behavior, Fig. 5.3 illustrates a few groups of pressure histories for the LP and HP cases.

As shown in Figs. 5.3a and b, for closed flows or when the orifice size was sufficiently small (Type 1 behavior), the pressure pattern for the LP case is quite similar to that for the HP case, with a long period and a decaying peak magnitude. However, the frequency of the oscillation in HP case is higher than that in the LP case. This can be explained by the fact that in the LP case, the gravity of the water column in the vertical pipe slows down the water column oscillation.

Fig. 5.3c shows examples of the oscillation patterns in the intermediate air release condition. Again we can see that both the LP case and the HP case have a similar pressure pattern (Type 2 behavior) of a long period air pocket pressure oscillation followed by a short period air release. Similar to the Type 1 behavior, the frequency of the long period pressure oscillation in the LP case is lower than that in the HP case, due to the gravity effects.

Fig. 5.3d shows examples of the oscillation patterns observed in the large air release situation, in which both the LP and the HP cases have a Type 3 behavior of waterhammer dominated pressure history. However here, unlike Type 1 and Type 2

behavior, the frequency of pressure oscillation in the HP case is slightly lower than that in the LP case, rather than higher.

5.4.2 Magnitude of peak pressures as a function of the orifice ratio and initial water column length

Fig. 5.4 present the measured maximum peak pressures observed during the rapid filling, as a function of orifice size. In the figures, the horizontal axis is the relative orifice size, d/D , and the vertical axis is the absolute pressure head normalized by the upstream driving head.

It is seen from Figs. 5.4a and b, for Type 1 behavior (the upper limit of the orifice size ratio, d/D , was less than 0.114 for all test conducted), the observed average peak pressures are very close for the LP case and the HP case, which indicates that the gravity has a minor effect on the maximum pressure magnitude under no or small air release conditions. However, as the orifice size increases, the difference between two cases becomes obvious. For the long initial water column length case ($\lambda_0 = 0.8$, shown in Fig. 5.4), the peak pressure in the LP case is lower than that in the HP case. However, as Fig. 5.5 shows, for the short initial water column length case ($\lambda_0 = 0.048$), the situation reversed. Since the waterhammer is dominant under large orifice situations, a possible explanation is that the variations of the speed of the pressure wave between the LP and HP cases were different. To explore this, consider Fig. 5.5 which shows the measured wavespeed as a function of d/D for various initial water column lengths. It can be seen that for $\lambda_0 = 0.8$, the speeds of the pressure wave in both the LP and the HP cases are very similar. However, for $\lambda_0 = 0.048$, the LP case had a higher wave speed when $d/D > 0.114$ and a lower wave speed for large orifice sizes. Because the air content is the key factor

affecting the speed of pressure wave, this behavior suggests that for a longer initial water column length ($\lambda_0 = 0.8$), the air is more easily released from a horizontal pipe than from a vertical pipe. However, for a short initial water column length ($\lambda_0 = 0.048$), the air seems to be more easily released from a vertical pipe than from a horizontal one. Supporting this, it can be seen from Fig. 5.3c that the pressure oscillation pattern for HP case is more irregular than that for the LP case, which indicates that the air release in the LP case is faster than that in the HP case.

5.5 Analytical Model Verification

In order to verify the analytical model, comparisons of calculated and observed pressure oscillation patterns and the average peak pressures were conducted. The speed of the pressure wave measured in the experiments was used as an input parameter for a particular case in the calculations. The friction factor of 0.035 measured in the previous experiments of the horizontal pipe (discussed in Chapter 2) was used.

Fig. 5.6 shows a comparison of computed and observed pressure oscillation patterns for the three type of behavior. As shown in Fig. 5.6a, the model can approximately reproduce the actual pressure oscillation of Type 1 behavior, especially for the first cycle. Fig. 5.6b shows a comparison between measured and computed values for Type 2 behavior. It is seen that the computed period of pressure oscillation was much shorter than was observed in the experiments. This might be attributed to the limitation in the numerical model discussed in Chapter 2, specially that the model assumes that once the water column reaches the pipe end, the air will be totally released. For Type 3 behavior shown on Fig. 5.6c, the model can only simulate the amplitude and the

approximate timing of the maximum air release pressure before the water column reaches the pipe end.

Figs. 5.7a and b show the comparison between the computed and observed average peak pressures for $\lambda_0 = 0.8$ and $\lambda_0 = 0.048$. It can be seen that generally the model produced results comparable to that of the experiments. For $\lambda_0 = 0.8$, the maximum relative error, which was defined as $(P_{\text{experiment}} - P_{\text{calculation}})/P_{\text{calculation}}$, occurs in small orifice zone (Type 1 and Type 2 behavior, as shown in Fig. 5.7a) and was about 24%. For $\lambda_0 = 0.048$, the maximum relative error, occurs near the upper bound of the transition zone (Type 2 behavior, as shown in Fig. 5.7b) and was about 22%. There are many factors affected the accuracy of the model, such as the rigid water column assumption, the simplification of junction flow behavior and the accurate speed of the pressure wave which, as discussed in Chapter 2, is difficult to measure. Nevertheless, if the friction factor and the speed of pressure wave are known, the current model is able to quantify the maximum amplitude of the pressure oscillation with reasonable accuracy in the LP case.

From Eq. (5-7), it is known that the gravity effect is controlled by two parameters: $\lambda_{s,\text{max}} = L_s/L_1$ and L_1/H_b^* where L_1 is the length of the horizontal pipe, and the L_s the length of the vertical pipe. Because in our experiments both L_s and L_1 are short, longer and larger pipe cases need to be studied in order to evaluate the effect of gravity in prototype situations. The verified analytical model was used to explore the long and large pipe cases. Fig. 5.8 and Table 5.1 shows the calculated maximum peak pressure in a horizontal pipe (1 m in diameter and 200 m in length) with a vertical pipe of different heights (1m in diameter). It is seen that the when the relative height of the vertical pipe

(L_2/L_1) is less than 0.1, the maximum pressure difference between the HP and LP cases will be less than 10%, under which the gravity effect can be neglected. This conclusion however, is not valid for the waterhammer pressure, since the experimental results indicated that the gravity effect should be considered when significant air is released, no matter how short the vertical pipe is.

5.6 Conclusions and Suggestions

The mitigative effect of a vertical pipe on pressure transients induced by trapped air pockets in a rapid filling LP system was investigated. The recorded pressure oscillations indicated that three types of pressure behavior defined in Chapter 2 for a horizontal pipe also occurred in the LP case. It was concluded that the existence of the vertical pipe branch will not qualitatively alter the pressure oscillation pattern and maximum peak pressure magnitude as compared to the horizontal pipe cases. The gravity effect on reducing the pressure is obvious only when the initial water column is long and the air release from the vertical pipe is substantial. The comparison between the experimental results and those calculated with the proposed analytical model indicates that the rigid water column method is able to simulate the rapid filling of an LP system when there are air pockets trapped in the pipe.

Further efforts should be made to investigate the wave speed and the junction energy losses in LP systems under rapid filling conditions. More tests with different initial water column lengths and operating heads need to be conducted to validate the conclusions made in the present study.

5.7 References

- Albertson, M.L., and Andrews, J.S. (1971). "Transients caused by air release." *In "Control of Flow in Closed Conduits."* (J.P.Tullis, ed.), pp.315-340. Colorado State University, Fort Collins, Colorado.
- Cardle, J.A and Song, C.C.S. and Yuan, M. (1989). "Measurements of mixed transient flows." *ASCE Journal of Hydraulic Engineering*, Vol.115, No.2, pp.169-181.
- Li, J. and McCorquodale, J.A. (1999). "Modeling mixed flow in storm sewers." *Journal of Hydraulic Engineering*, Vol. 125, No.11, pp.1170-1179.
- Martin, C.S. (1976). "Entrapped air in pipelines." *Proceedings of the second international conference on pressure surges*, London, September 22-24, 1976, BHRA Fluid Engineering, Cranfiled, Bedford, England.
- Yen, B.C. (1986). "Hydraulics of sewers." *Advances in Hydroscience*, Vol. 14, pp.1-122.
- Yevjevich, V. (1964). "Storm-drain networks." *Advances of HydroScience*, pp.669-704.
- Zech, Y. (1985). "Flow instabilities in culverts and storm sewers." *Proceeding of 21st IAHR Congress on Urban drainage Hydraulics*, Australia.

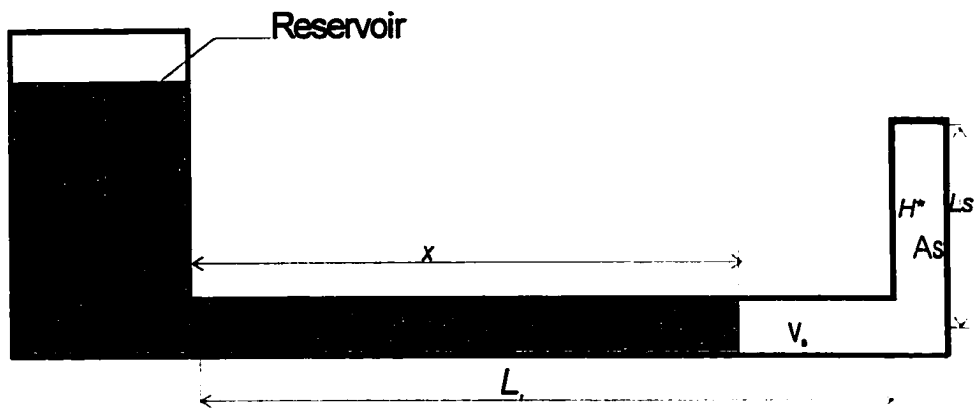


Figure 5.1 Defining sketch for the theoretical analysis.

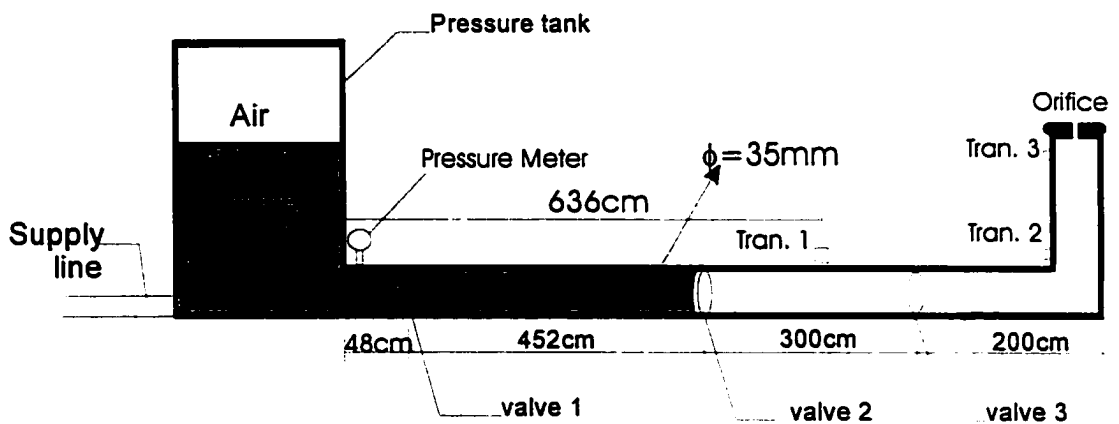
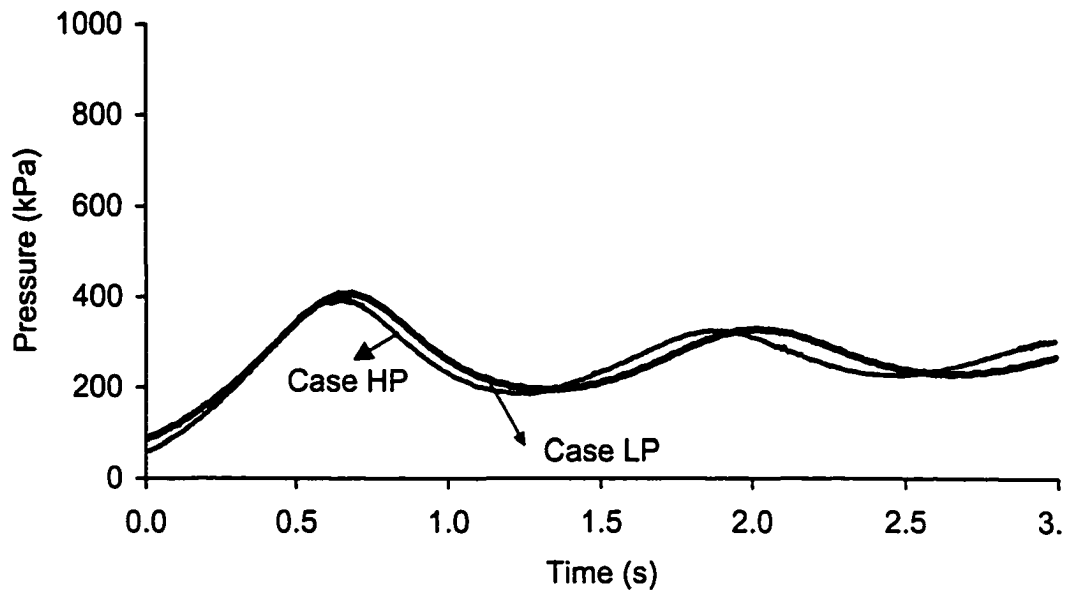
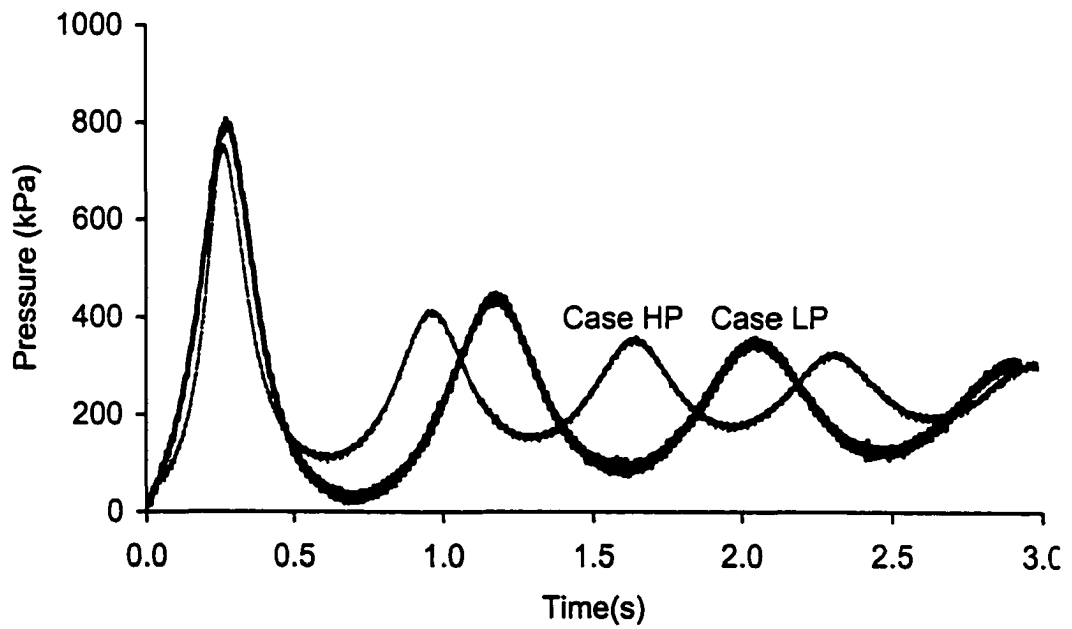


Figure 5-2 Diagram of the experimental apparatus - L pipe (unit of length : cm)

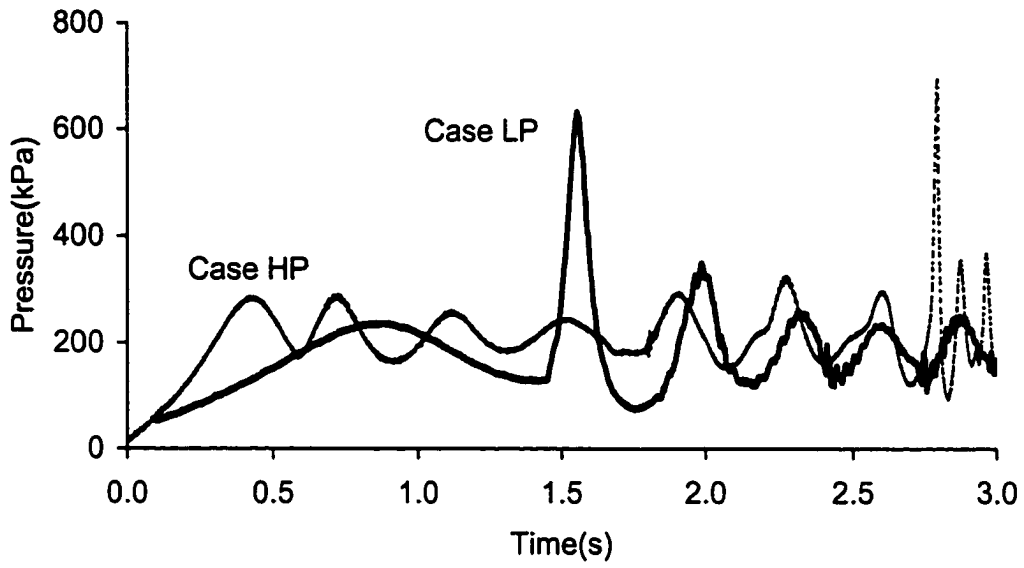


(a) $H_0 = 275$ kPa, $\lambda_0 = 0.048$, $d/D =$

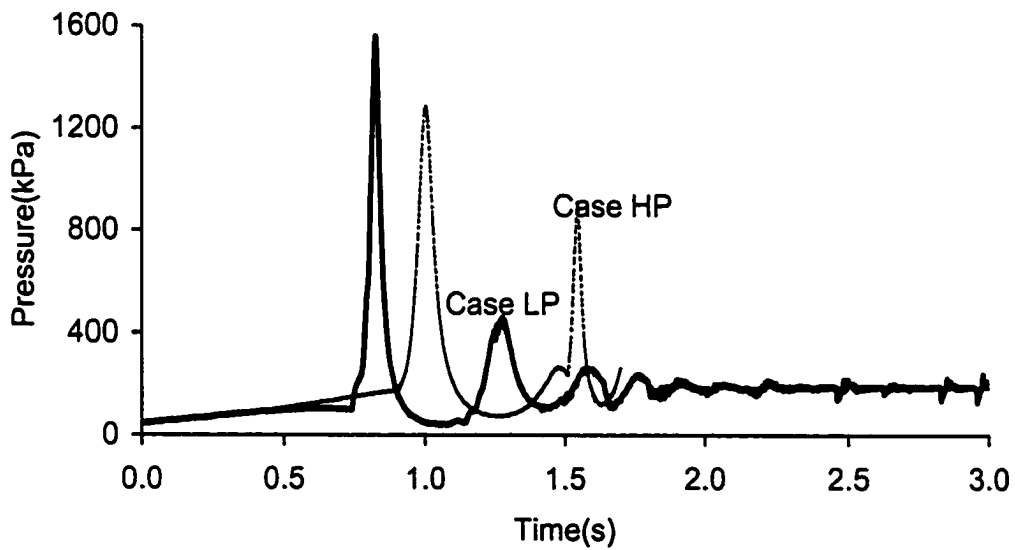


(b) $H_0 = 275$ kPa, $\lambda_0 = 0.8$, $d/D = 0$

Figure 5.3 Pressure Oscillation Patterns



(c) $H_0 = 275 \text{ kPa}$, $\lambda_0 = 0.048$, $d/D = 0.157$



(d) $H_0 = 275 \text{ kPa}$, $\lambda_0 = 0.048$, $d/D = 0.17$

Figure 5.3 Pressure Oscillation Patterns (continued)

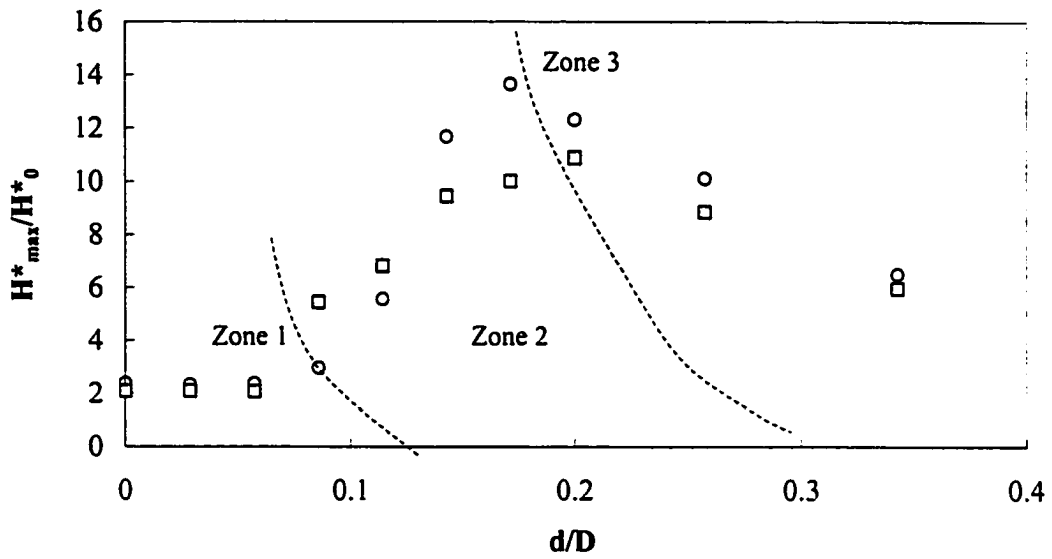


Fig. 5.4a Average maximum pressure magnitude
($H_0 = 275$ kPa, $\lambda_0 = 0.8$)

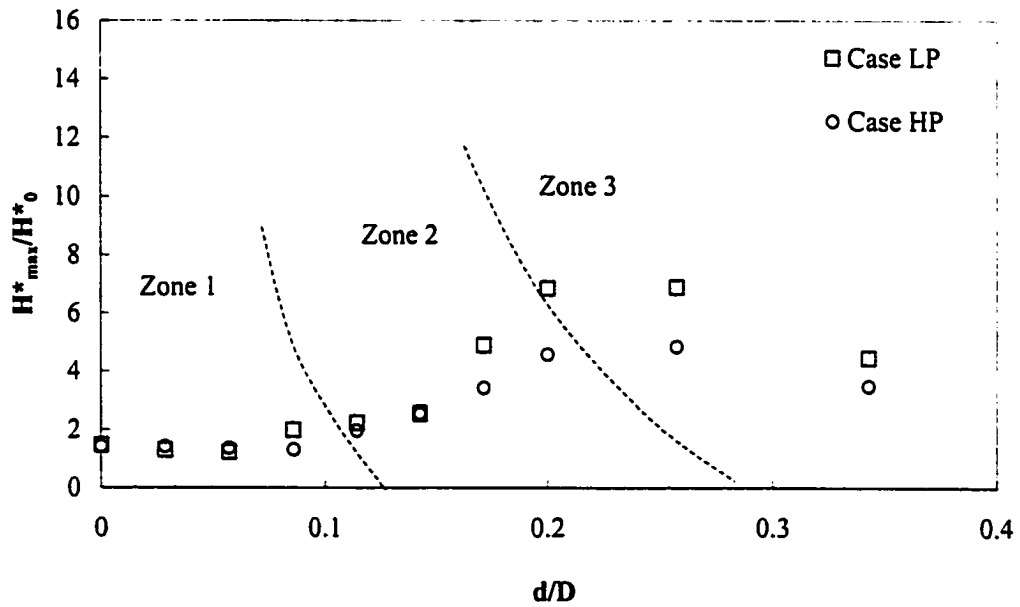


Fig. 5.4b Average maximum pressure magnitude
($H_0 = 275$ kPa, $\lambda_0 = 0.048$)

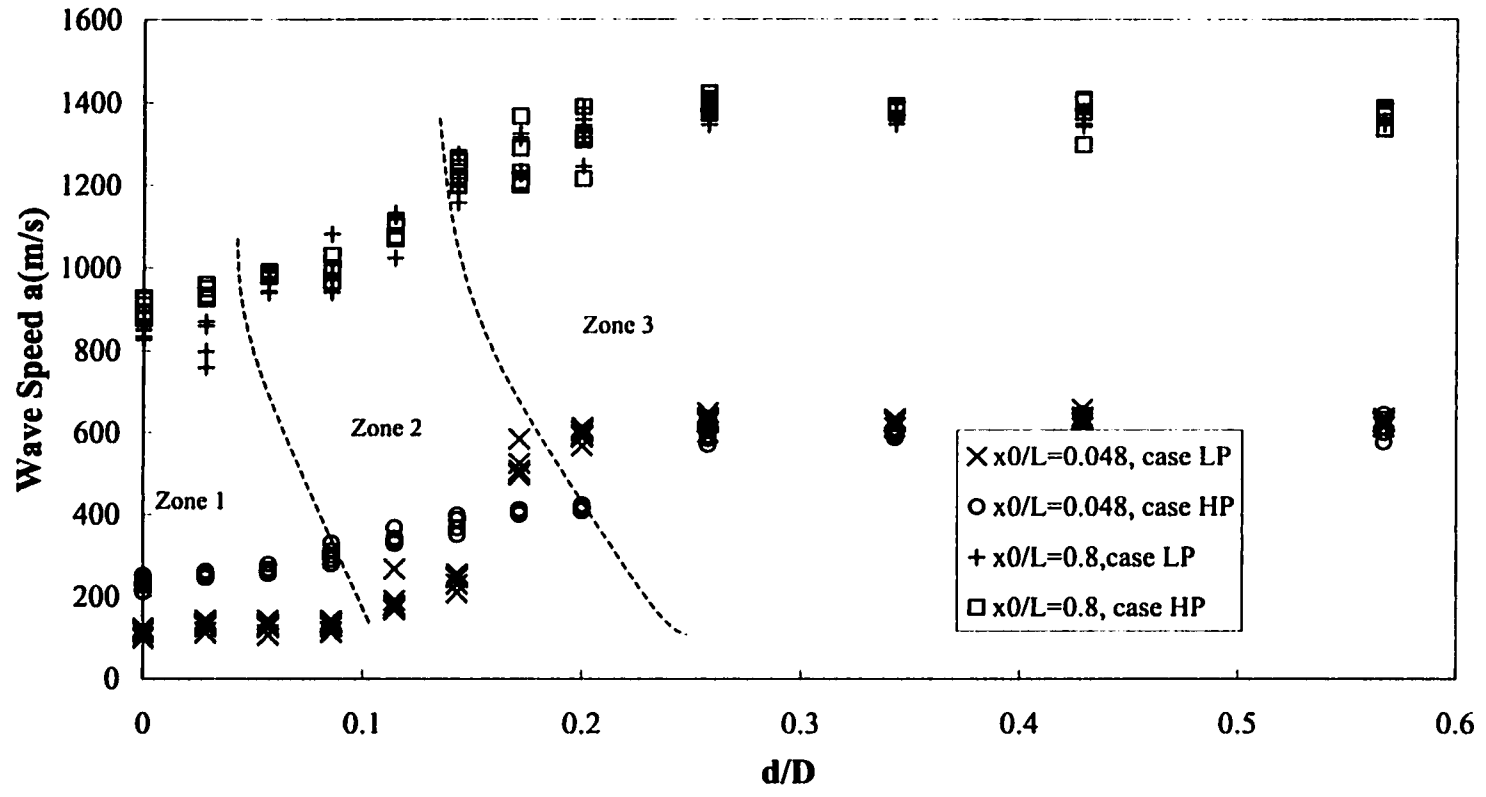
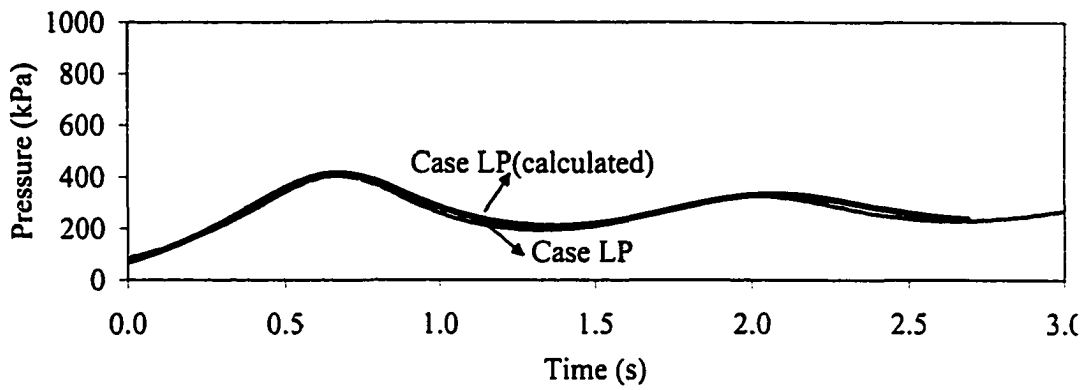
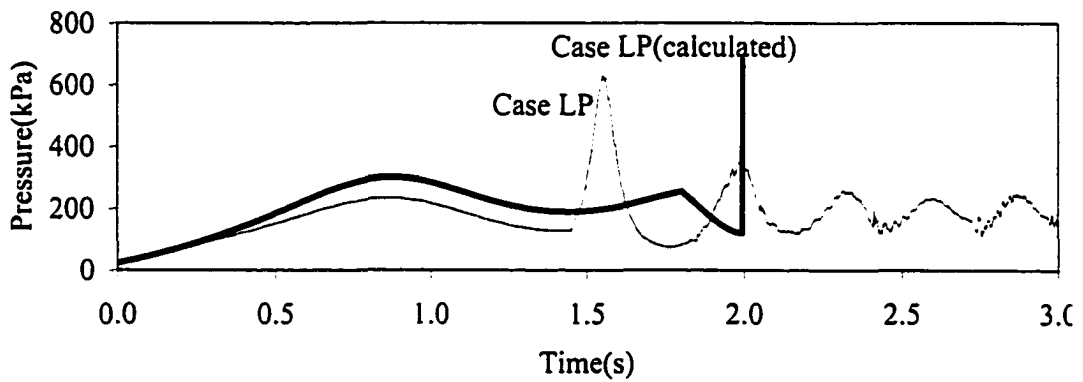


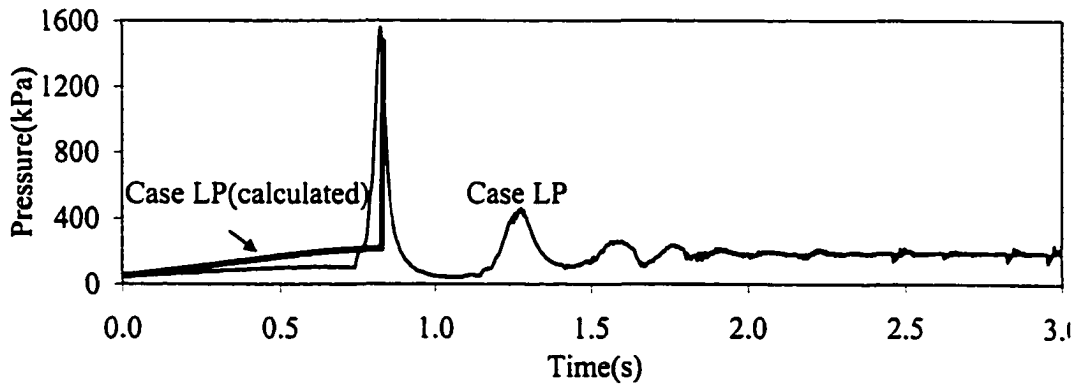
Figure 5.5 Measured speed of pressure wave ($H_0 = 275$ kPa)



(a) $H_0 = 275 \text{ kPa}$, $\lambda_0 = 0.048$, $d/D = 0$



(b) $H_0 = 275 \text{ kPa}$, $\lambda_0 = 0.048$, $d/D = 0.114$



(c) $H_0 = 275 \text{ kPa}$, $\lambda_0 = 0.048$, $d/D = 0.17$

Figure 5.6 A comparison of calculated and measured pressure oscillation patterns

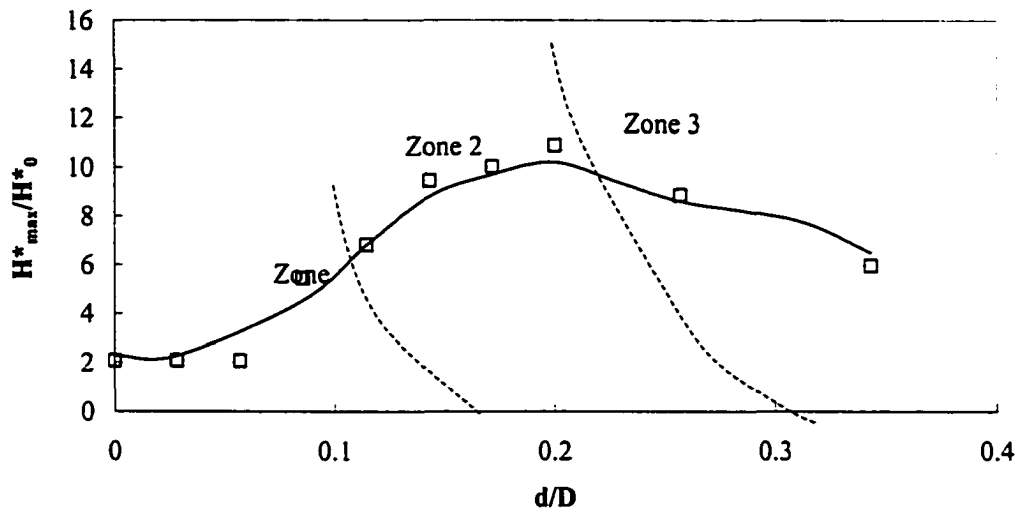


Fig. 5.7a A comparison between calculated and measured maximum pressure magnitudes ($H_0=275$ kPa, $\lambda_0 = 0.8$)

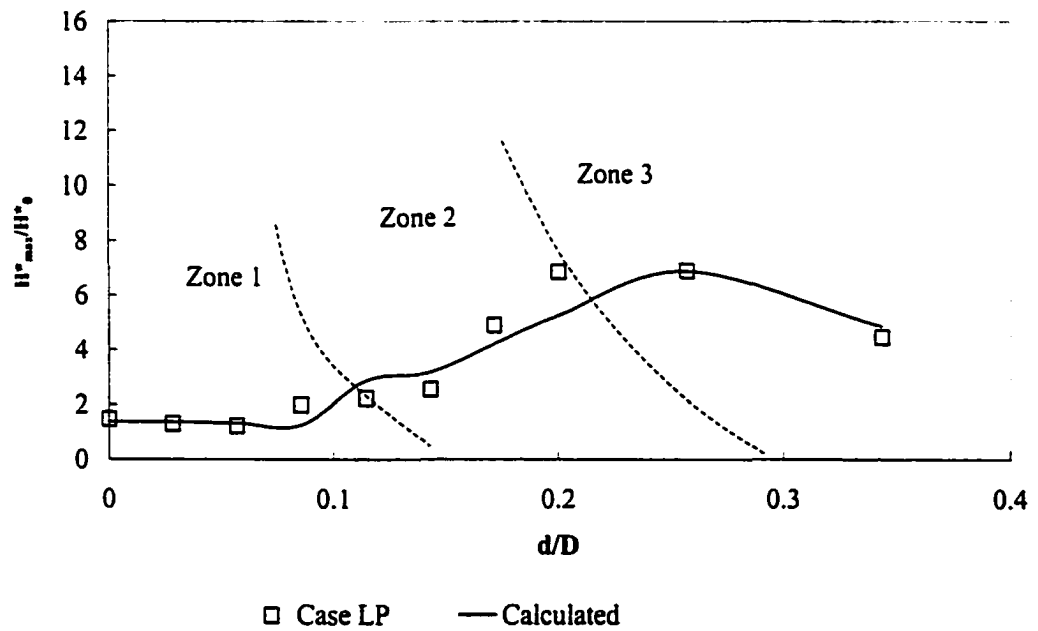


Fig. 5.7b A comparison between the calculated and measured maximum pressure magnitudes ($H_0=275$ kPa, $\lambda_0 = 0.048$)

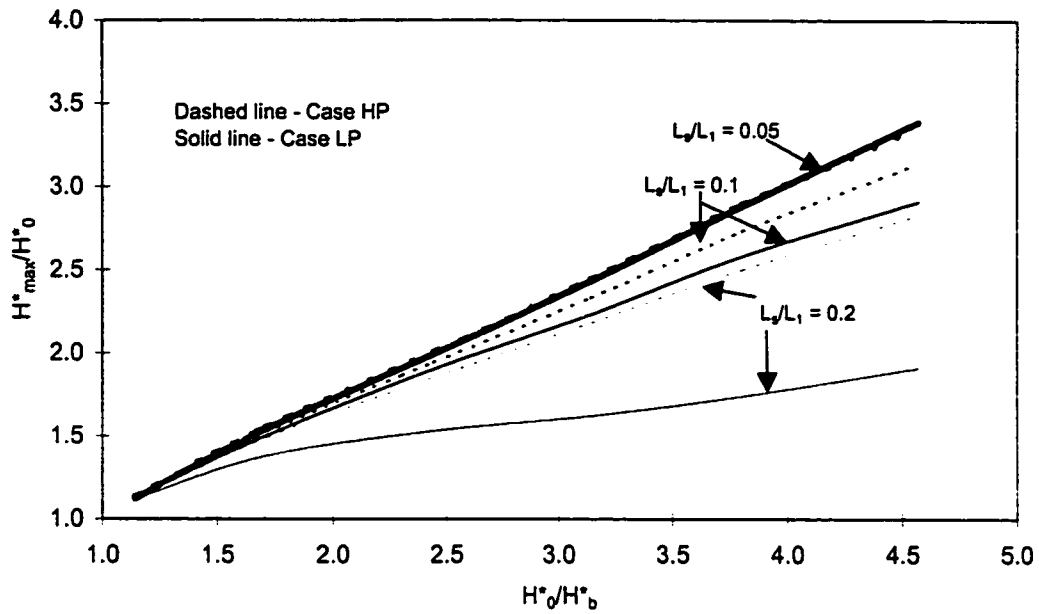


Fig. 5.8 Effects of relative vertical pipe length on the maximum air pressure ($\lambda_0 = 0.8, L/D = 200, f = 0.035$)

Table 5.1 Comparison of calculated maximum pressure magnitudes between LP case and HP case (shown in Fig.5.8)

H^*_0/H^*_b	1.14	1.71	2.44	3.14	3.86	4.57
LP case	H^*_{max}/H^*_0	H^*_{max}/H^*_0	H^*_{max}/H^*_0	H^*_{max}/H^*_0	H^*_{max}/H^*_0	H^*_{max}/H^*_0
$L_s/L_1=0.05$	1.12	1.54	1.99	2.43	2.88	3.39
$L_s/L_1=0.10$	1.12	1.50	1.90	2.23	2.58	2.91
$L_s/L_1=0.20$	1.12	1.38	1.53	1.62	1.74	1.91
$L_s/L_1=0.50$	1.98	1.88	1.77	1.67	1.61	1.55
HP case	H^*_{max}/H^*_0	H^*_{max}/H^*_0	H^*_{max}/H^*_0	H^*_{max}/H^*_0	H^*_{max}/H^*_0	H^*_{max}/H^*_0
$L_s/L_1=0.05$	1.13	1.55	2.00	2.44	2.89	3.36
$L_s/L_1=0.10$	1.13	1.52	1.94	2.33	2.73	3.14
$L_s/L_1=0.20$	1.13	1.49	1.85	2.18	2.50	2.83
$L_s/L_1=0.50$	1.13	1.42	1.68	1.92	2.14	2.36

6.0 PRESSURE SURGES IN A RAPIDLY FILLING T-PIPE WITH A VERTICAL PIPE BRANCH CONTAINING TRAPPED AIR

6.1 Introduction

The investigations of transient pressure in a rapidly filling horizontal pipe, as discussed in Chapter 2, revealed significant pressure oscillations in pipeline systems containing trapped air. Consequently, surge control or mitigation approaches need to be explored to reduce the severe pressures induced by the trapped air. In fact, in real world sewer systems, manholes and drop shafts act as air chambers or surge tanks when the trunk sewer is surcharged; therefore, it is worthwhile to evaluate the ability of manholes and drop shafts on mitigating the pressure peaks in a rapidly filling sewer trunk.

This chapter will present our investigations on the trapped air effects on flow transients in a rapid filling T-pipe configuration, which can be regarded as a simplified sewer trunk-manhole-trunk system. We will explore the mitigation effect of a T-pipe on pressure peaks during the rapid filling period.

6.2 Experimental Program

Fig. 6.1 depicts the experimental apparatus used in this investigation. Here, the same pressure tank used in the experiments described in the previous chapters was employed. The 60cm long vertical pipe used in the L-pipe tests discussed in Chapter 5 was repositioned to a point 836 cm downstream of the pressure tank. The pipe segment downstream of the vertical pipe was 200 cm long and the end of the vertical pipe was

sealed. The end of the horizontal pipe was either sealed to form a dead end, or outfitted with a cap containing a centered, sharp-edged orifice to study the effects of air release on pressure transients in the system. All of the pipe branches had an inner diameter of 35 mm. Two quarter-turn ball valves were installed along the pipe at locations 500 and 800 cm downstream of the tank, respectively, to provide two different initial air volume scenarios.

Three high-frequency-response (100Hz) strain-gauge pressure transducers (PACE, Model kPV5) were installed on the vertical pipe and horizontal pipe branches. Two pressure transducers were on the vertical pipe: one was located 5 cm below the top of the vertical pipe and the other was located 5 cm above the top of the horizontal pipe. The third transducer was installed on the 200 cm horizontal pipe extension, 10 cm from the downstream end. Each transducer was connected to a digital demodulator which was in turn connected to the data acquisition board inside of a computer. The same Labview 4.0 program developed in Chapter 2 was used for automate collection of pressure data. The details of the calibration of transducer, the determination of pipe wall friction factor, and valve losses are provided in Chapter 2.

6.3 Theoretical Analysis

6.3.1 Configuration

The sketch of the theoretical model is shown in Fig. 6.2. At the upstream end (the left hand-side of the figure), there is a reservoir which provides a constant driving head, H_0 . L_1 , L_2 and L_5 are the lengths, A_1 , A_2 , and A_5 are the cross-section areas, and U_1 , U_2 ,

and U_s are the velocities of the upstream, downstream, and vertical pipe branches, respectively, and x is the water column length.

6.3.2 Governing equations

Similar to the L-pipe configuration described in Chapter 5, it is assumed that the continuity equation is satisfied at the junction and the pressures at each branch are equal.

Therefore

$$U_1 A_1 = U_s A_s + U_2 A_2 \quad (6-1)$$

and

$$H_{J1} = H_{J2} = H_{Js} = H_J \quad (6-2)$$

in which H_{J1} , H_{J2} , H_{Js} denote the pressure heads of each branch at the junction, specifically the upstream, downstream, and vertical pipe, respectively.

Throughout this paper, subscript i denotes the branch number, with $i = 1, 2,$ and s denoting the upstream, downstream, and the vertical pipe branches, respectively. When the water column is in the i -th pipe branch, the change of air volume is

$$\frac{dV_{ai}}{dt} = -A_i U_i \quad (6-3)$$

and the momentum equation for the water column i is

$$\frac{dU_i}{dt} = -g \frac{H_i - H_{i-1}}{x_i} - f \frac{U_i |U_i|}{2D_i} - K_i \frac{U_i^2}{2x_i} - gS_i \quad (6-4)$$

in which the notation is the same as described in Chapter 5 for the L-Pipe case.

Similar to the L-pipe case, the junction pressure H_J must be solved in order to solve the momentum equations in the vertical branch and the downstream branch of the

T-junction. Following the same procedure described in Chapter 5, and substituting $S_1 = S_2 = 0$ and $S_3 = 1$, the junction pressure can be expressed as:

$$H_j = \frac{1}{\left(1 + \frac{L_1 A_s}{x_s A_1} + \frac{L_1 A_2}{x_2 A_1}\right)} \left(\begin{array}{l} H_0 + \frac{L_1 A_s}{x_s A_1} H_s + \frac{L_1 A_2}{x_2 A_1} H_s - \frac{fL_1}{2g} \left(\frac{U_1 |U_1|}{D_1} - \frac{L_1 A_s U_s |U_s|}{x_s A_1 D_s} \right) \\ - \frac{L_1 A_2 U_2 |U_2|}{x_2 A_1 D_2} + K_2 \frac{L_1 A_2 U_2^2}{x_2 A_1 2g} \\ - K_1 \frac{U_1^2}{2g} + K_s \frac{L_1 A_s U_s^2}{x_s A_1 2g} + L_1 \frac{A_s}{A_1} g \end{array} \right) \quad (6-5)$$

The governing equations for the air phase are again equations (2-3) to (2-6). The impact pressure induced by the water column impact to the pipe is calculated with Equation (2-7).

6.3.3 Non-dimensional equations

Here, again, the governing equations are normalized using the non-dimensional variables defined in Chapter 5. The non-dimensional equations are

$$\frac{d\eta_i}{d\tau} = -\alpha_i \psi_i \quad (6-6)$$

$$\frac{d\psi_i}{d\tau} = -\frac{1}{\varphi_b} \cdot \frac{\varphi_i - \varphi_{i-1}}{\lambda_i} - \frac{C_0}{2} \sqrt{\frac{1}{\alpha_i}} \psi_i |\psi_i| - \frac{K_i}{2\lambda_i} (1 - \lambda_0) \psi_i^2 - \frac{L_1}{H_b^*} S_i \quad (6-7)$$

$$\varphi_j = \frac{1}{\left(1 + \frac{\alpha_2}{\lambda_2} + \frac{\alpha_s}{\lambda_s}\right)} \left(\begin{array}{l} 1 - \varphi_b \frac{C_0}{2} (\psi_1 |\psi_1| - \sqrt{\alpha_2} \psi_2 |\psi_2| - \sqrt{\alpha_s} \psi_s |\psi_s|) - K_1 \frac{\varphi_b}{2} (1 - \lambda_0) \psi_1^2 \\ + \frac{\varphi_b}{2} (1 - \lambda_0) \frac{\alpha_2}{\lambda_2} K_2 \psi_2 |\psi_2| + \frac{\varphi_b}{2} (1 - \lambda_0) \frac{\alpha_s}{\lambda_s} K_s \psi_s |\psi_s| \\ + \frac{\alpha_s}{\lambda_s} \varphi_s + \varphi_b \alpha_s \frac{L_1}{H_b^*} + \frac{\alpha_2}{\lambda_2} \varphi_2 \end{array} \right)$$

(6-8)

It is straight forward to see that the L-pipe is only a special case of the T-pipe; that is, if we set α_2 , the relative area of downstream pipe to the upstream pipe equal to zero, equation (6-8) will be identical to (5-7). The final governing equations are solved using a Fourth-Order Runge-Kutta scheme as discussed in previous chapters.

6.4 Experimental Observations

In the experiments, two upstream heads of 137 kPa and 275 kPa, and two orifice sizes of 0 and 6mm were used to represent the no air release and the substantial air release cases under different driving heads. Initial water column lengths of 5 m and 8 m were used to study the effect of the initial water column length. Each of the tests was repeated at least three times. For illustration purposes, the experimental peak pressure values shown throughout this chapter are the averaged value for each test.

6.4.1 Magnitude of peak pressures

Fig. 6.3 shows the comparison of measured maximum pressures at the end of the horizontal pipe used in Chapter 2 (called case HP hereafter) and the T-pipe case studied here (called case TP, hereafter). The pipe length for the HP case was the same as the horizontal pipe branches in the TP case. From Fig. 6.3 it is seen that the vertical pipe has the effect of reducing the peak pressures, especially when substantial air release occurs (up to 70% peak pressure reduction). The mitigative effect is much less for the no air release case, where the peak pressure was reduced by less than 15%.

The following reasons may explain the pressure reduction provided by a T-pipe:

1. When the advancing water column approaches the T-junction, the surge front splits between the vertical branch and the downstream branch. Consequently, the kinetic energy carried by the water column in the upstream pipe branch is divided between these two branches. For no or small air release cases, the air pocket trapped in the downstream branch will absorb less energy than in the HP case; therefore the air pocket pressure will be lower than that in the HP case. For large air release situations, the reduced kinetic energy means the water column approaches the pipe end more slowly than it does in a HP case; therefore, after the air is released, the deceleration rate of the water column is low and so the impact pressure is reduced. This reason could not be quantitatively verified by these experiments since the velocity of the water column at the filling stage was not measured.
2. The split surge fronts will trap air in both the vertical and the downstream pipe branches. This means that, after the air pocket in the downstream branch is released, there is still air trapped in the vertical branch. As a result, the air content in the flow is higher than that in a HP case, and the speed of the pressure wave in the T-pipe is lower than that in the HP case and so resulting impact pressure is reduced. This reason was confirmed by the measured wave speed which was observed to be significantly lower compared with that in the HP case. For $x_0 = 8$ m ($\lambda_0 = 0.96$) and $x_0 = 5$ m ($\lambda_0 = 0.60$), the wave speed dropped from about 1000~1200 m/s to 300~500 m/s.

6.4.2 Pressure oscillation patterns

Fig. 6.4 compares the recorded pressure histories at the location of Transducer 1 (shown in Fig. 6.2) for the HP and TP cases, for a filling head of 275 kPa, $\lambda_0 = 0.60$ and $d/D = 0$ (no air release). It is seen that the pressure oscillation for the TP case is slower and the peak amplitude is lower than that observed in the HP case.

Figs. 6.5 through 6.7 present the pressure oscillation patterns at all three locations for various orifice sizes and initial water column lengths. It was found that, for the no air release cases, as illustrated in Fig. 6.5, the pressure oscillation patterns at all three transducer locations were the same, and all were dominated by the trapped air pockets. However, for the substantial air release cases, as illustrated by Figs. 6.6 and 6.7, the pressure oscillation patterns at all three transducer locations were different. At the end of the horizontal pipe (Tran.1), the pressure oscillation pattern had a short period and sharp peaks, due to the rapid air release. On other hand, the pressure oscillation pattern at the top of the vertical pipe (Tran.3) had a long period and flat troughs, characteristic of the cushioning effect of a trapped air pocket. This observation indicates that, when the air in the horizontal pipe is released, there is still trapped air in the vertical pipe. Fig. 6.6 also suggests that the pressure oscillation pattern at the junction (Tran. 2) is similar to that at Tran.3.

A comparison of pressure oscillation patterns between Fig. 6.6 and Fig. 6.7 indicates that the air release occurs later when the initial water column length is shorter ($\lambda_0 = 0.60$ in Fig. 6.7) as compared to a longer initial water column length case ($\lambda_0 = 0.96$ in Fig. 6.6)

Preliminary experiments were also conducted to investigate the effects of air release through an orifice in the top of the vertical pipe. Figs. 6.8 and 6.9 illustrate a comparison of the observed pressure oscillation patterns for both a sealed and an orifice outfitted vertical pipe (orifice size $d_1 = 7\text{mm}$). An orifice was also placed at the downstream end of the horizontal pipe ($d = 6\text{mm}$) for the tests depicted in Fig. 6.9. In all 4 test runs, the initial water column length was $\lambda_0 = 0.6$. Based on the results present in Figs. 6.8 and 6.9, it can be seen that if there is an orifice on top of the vertical pipe, the pressure peak at the end of the horizontal pipe is actually higher, which implies that the sealed vertical pipe is more effective in reducing the pressure peak occurring at the end of the horizontal pipe. More experiments will be conducted to explore the pressure behavior under the situation of air release through the vertical pipe.

6.5 Comparison of Experimental and Analytical Model Results

Fig. 6.10 shows a comparison of measured and calculated maximum pressures at the location of Transducer 1. It is seen that the relative error of the calculated values is within 20% for no air release situations and is within 40% for large air release situations. The significant discrepancy under large air release conditions may be attributed to the difficulty of accurately quantifying the speed of pressure wave, as well as the negligence of the junction energy loss which was difficult to determine in the experiments.

A calculated pressure oscillation pattern is plotted in Fig. 6.11 along with the corresponding experimental observations. The results indicate that the analytical model is able to predict the pressure history for the no air release cases with reasonable accuracy. However, it was found that the model was unable to predict the pressure oscillation

pattern under significant air release conditions. This failure can be attributed to the model's inability to calculate the pressure oscillation behavior in the vertical pipe branch once the water column reaches the downstream pipe end. Also, without further experimental investigations, it is impossible to establish even an empirical expression to quantify the speed of the pressure wave in a T-pipe configuration.

6.6 Conclusions and Suggestions

The mitigative effect of a vertical pipe on pressure transients induced by trapped air pockets in a rapidly filling T-pipe system was investigated and the T-pipe configuration was shown to be able to mitigate the pressure surge during rapid filling, and was found to be especially effective in reducing the impact pressure when the air release was large. A comparison between the calculated and experimental results indicated that the proposed analytical model, based on the rigid water column theory, is able to simulate the rapid filling of pipeline system when there are air pockets trapped inside when no air release occurs. However, the model is unable to predict the pressure oscillation pattern under significant air release conditions because of the difficulty in accurately quantifying the speed of pressure wave.

Further efforts should be made in the following areas: (1) different vertical pipe sizes, lengths, and locations should be tested; (2) the wave speed in T-pipe systems under rapid filling conditions should be intensively investigated; (3) energy losses at T-junctions during rapid filling should be investigated; and (4) mechanisms of air-water release at T-junctions should be explored.

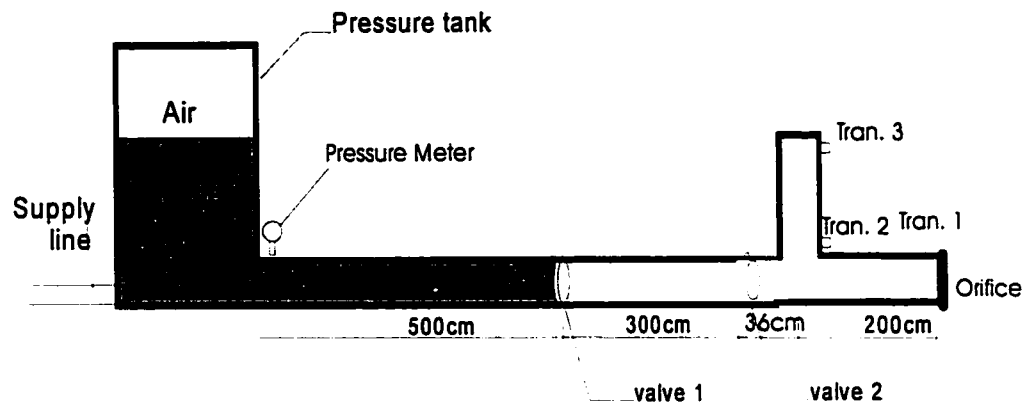


Figure 6.1 Diagram of the experimental apparatus – T-pipe (unit of length: cm)

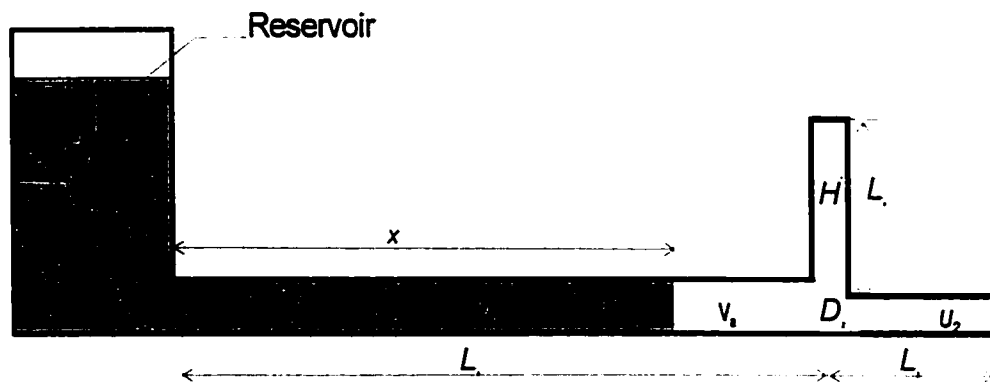
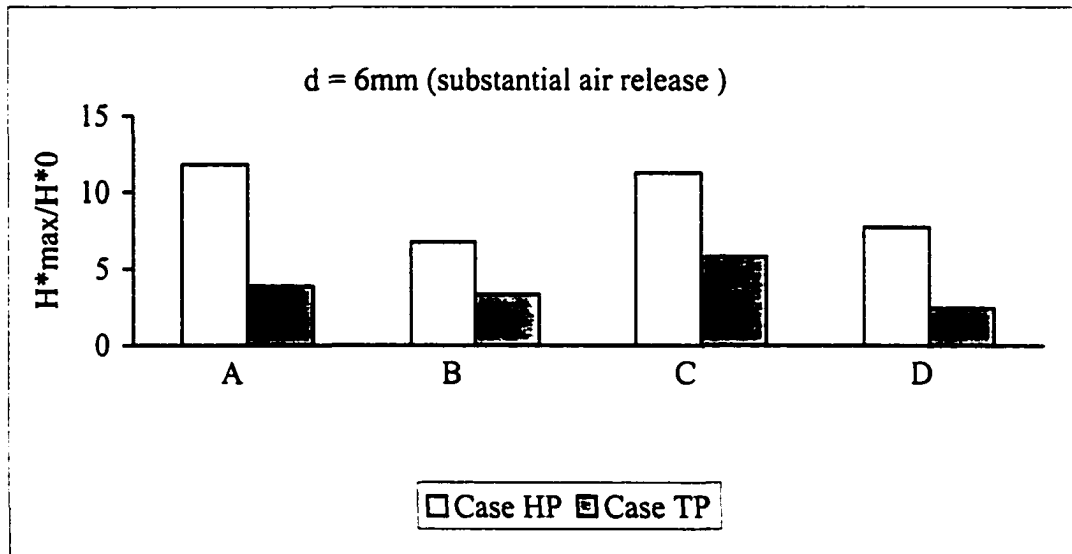
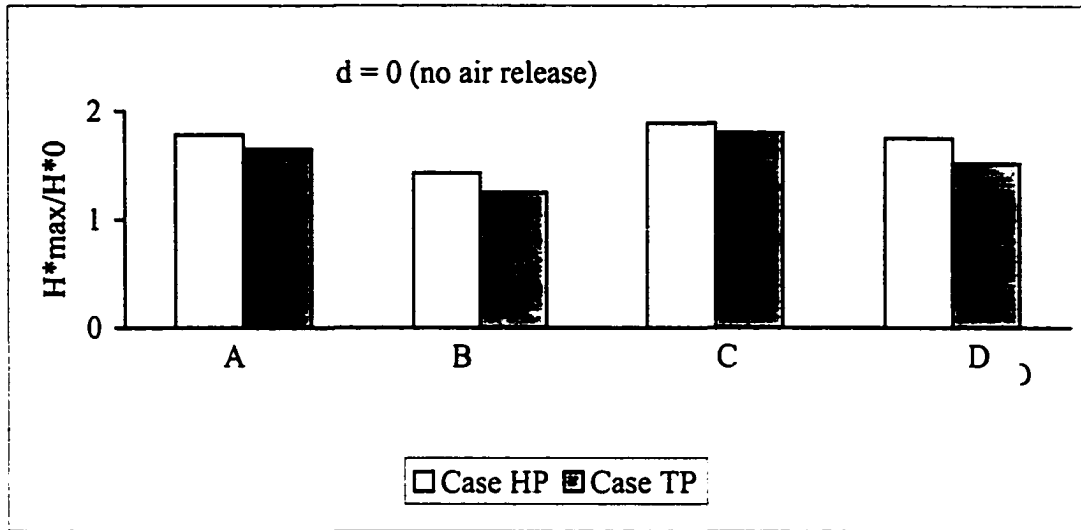


Figure 6.2 Defining sketch for the theoretical analysis



A: $\lambda_0 = 0.96$, $H_0 = 137\text{Kpa}$

B: $\lambda_0 = 0.60$, $H_0 = 137\text{Kpa}$

C: $\lambda_0 = 0.96$, $H_0 = 275\text{Kpa}$

D: $\lambda_0 = 0.60$, $H_0 = 275\text{Kpa}$

Figure 6.3 A comparison of measured maximum pressure magnitude between HP case and TP case

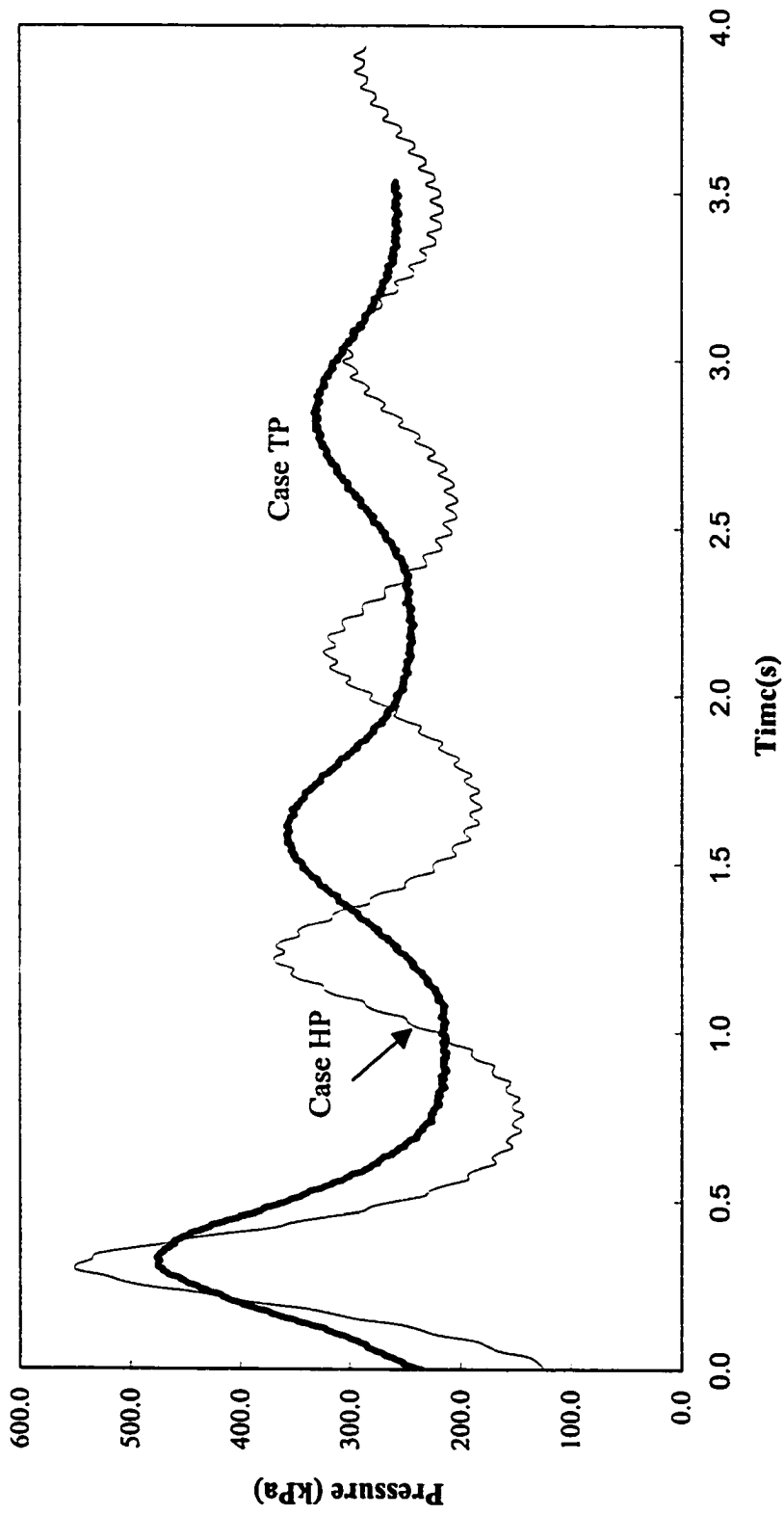


Figure 6.4 A comparison of pressure oscillation patterns between a TP case and a HP case
 ($H_0 = 275$ kPa, $\lambda_0 = 0.60$, $d/D = 0$)

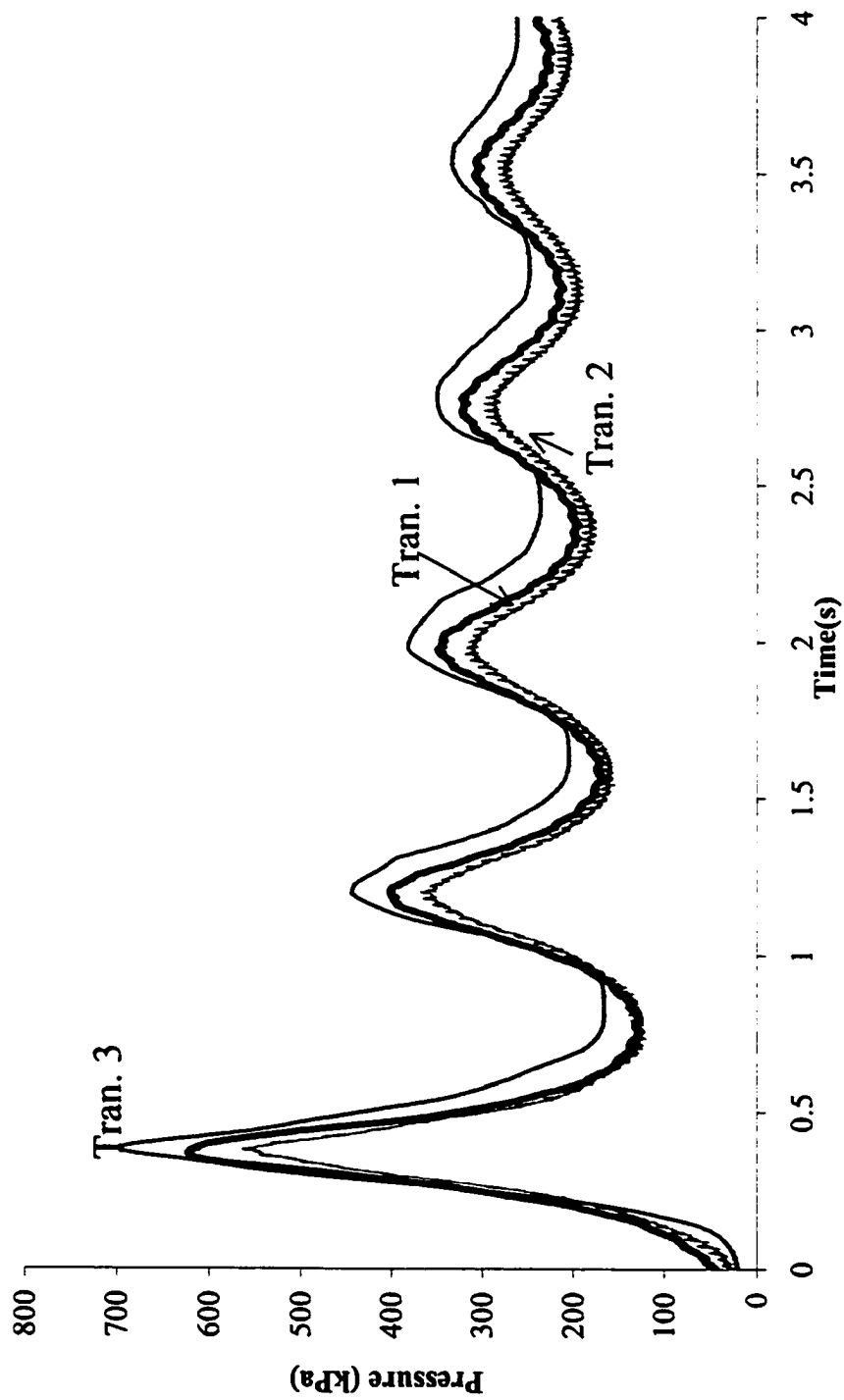


Figure 6.5 Pressure Oscillation Patterns at Three Transducer Locations
 ($H_0 = 275$ kPa, $\lambda_0 = 0.96$, $d/D=0$)

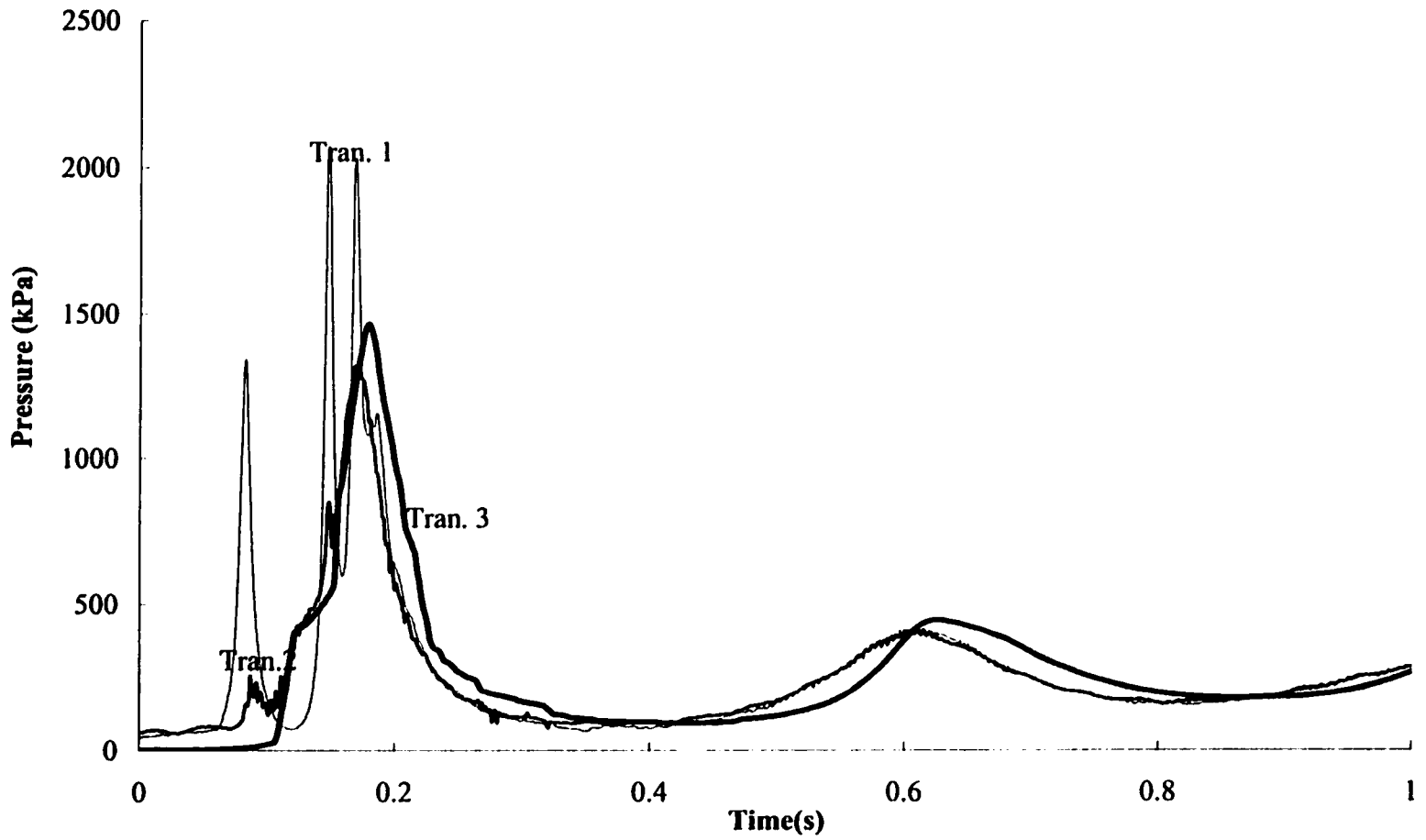


Figure 6.6 Pressure Oscillation Patterns at Three Transducer Locations
($H_0 = 275$ kPa, $\lambda_0 = 0.96$, $d/D = 0.171$)

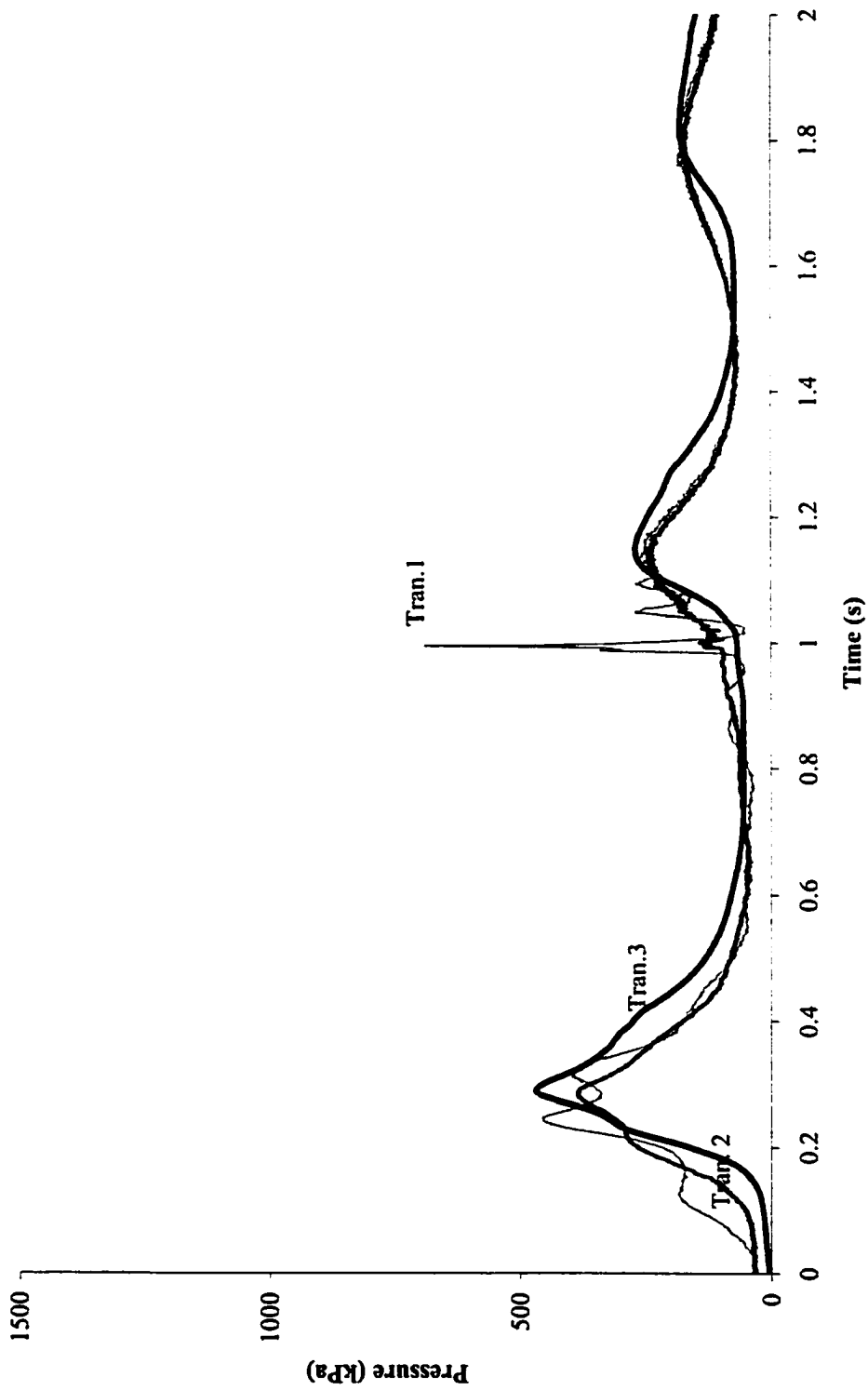


Fig. 6.7 Pressure oscillation patterns at all three locations
 ($H_0 = 137\text{kPa}$, $\lambda_0 = 0.60$, $d/D = 0.171$)

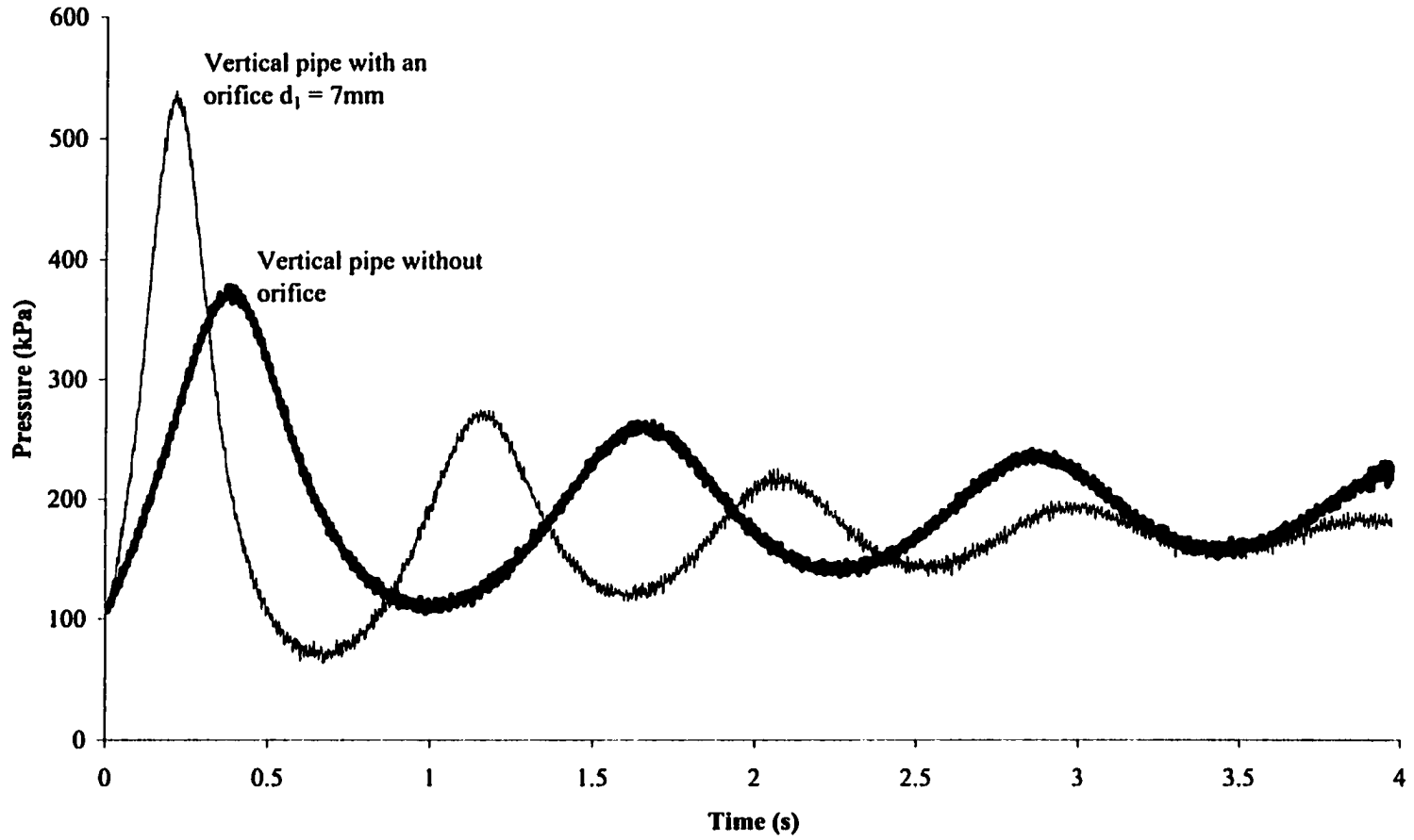


Fig. 6.8 A comparison of pressure history between cases with/without orifice on top of the vertical pipe (at location Tran.1, $H_0 = 275$ kPa, $\lambda_0 = 0.60$, $d/D = 0$)

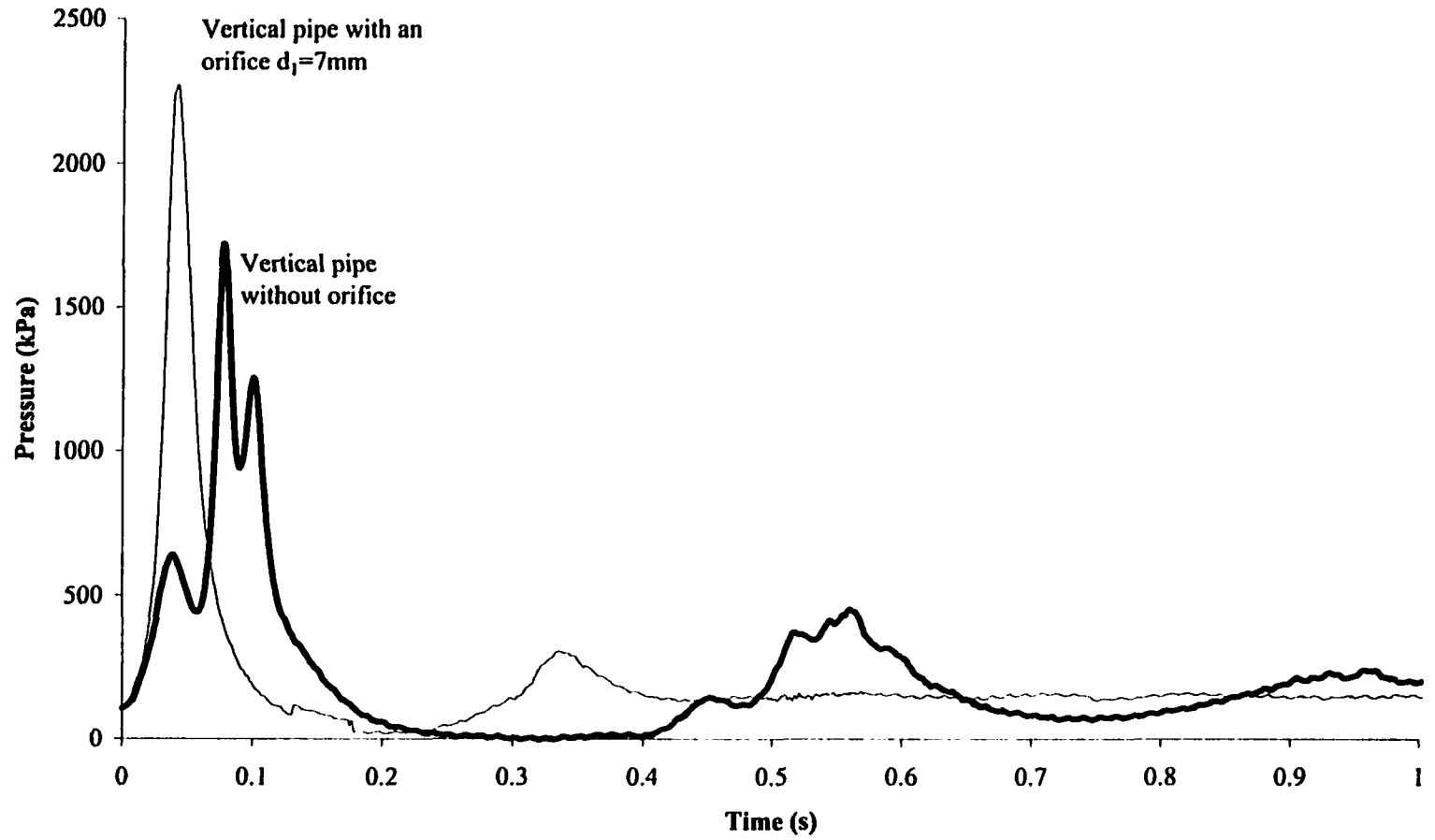
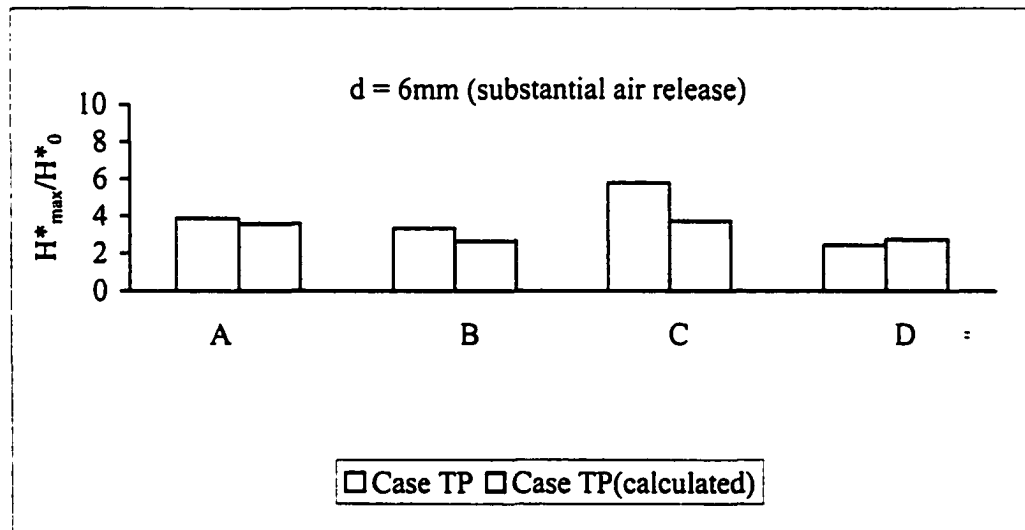
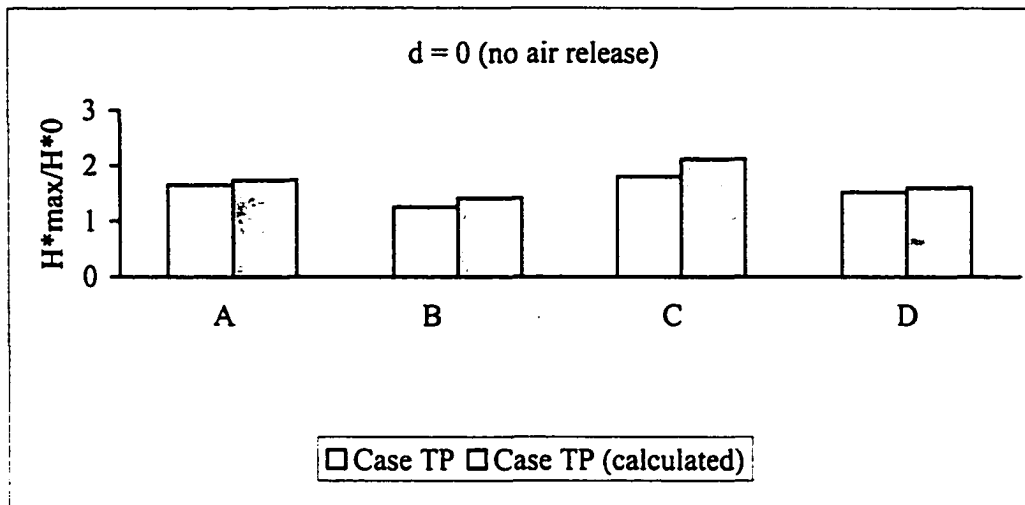


Fig. 6.9 A comparison of pressure history between with/without orifice on top of the vertical pipe (at location Tran.1, $H_0 = 275$ kPa, $\lambda_0 = 0.60$, $d/D = 0.171$)



A: $\lambda_0 = 0.96$, $H_0 = 137\text{Kpa}$

B: $\lambda_0 = 0.60$, $H_0 = 137\text{Kpa}$

C: $\lambda_0 = 0.96$, $H_0 = 275\text{Kpa}$

D: $\lambda_0 = 0.60$, $H_0 = 275\text{Kpa}$

Figure 6.10 A Comparison of calculated and measured maximum pressure magnitud

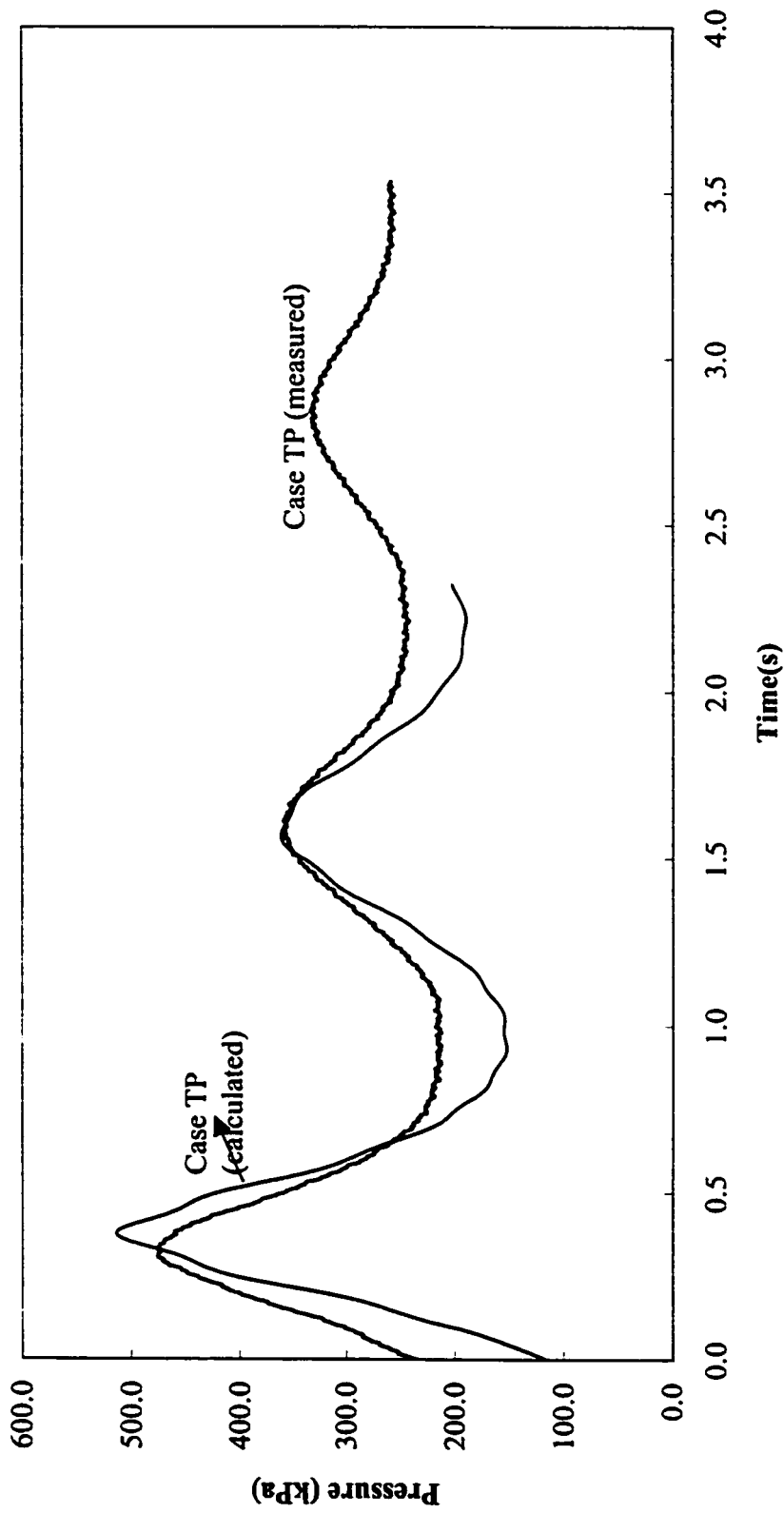


Figure 6.11 A comparison of calculated and measured pressure oscillation patterns
 ($H_0=275$ kPa, $\lambda_0=0.60$, $d/D=0$)

7.0 CONCLUSIONS AND RECOMMENDATIONS FOR FUTURE WORK

7.1 Conclusions

In this thesis, three configurations of rapid filling of a pipeline containing trapped air were investigated: (1) a rapidly filling horizontal pipe which is initially dry; (2) a rapidly filling horizontal receiving pipe which is partially full; and (3) a rapidly filling horizontal-vertical pipeline.

7.1.1 Rapidly filling horizontal pipe which is initially dry

The observations from our physical experiments confirm that air trapped in a rapidly filling pipe can induce high peak pressures, especially when air leakage occurs.

The experiments revealed that there are three types of pressure oscillation patterns in a rapidly filling horizontal pipe, depending on the relative size of the leakage orifice. When no air is released or orifice sizes are small, the cushioning effects of the air pocket prevents the water column from impacting on the pipe end and, from generating high water hammer pressures. However, the maximum pressure experienced may still be up to four times the upstream driving pressure. In this case, the pressure oscillation pattern has a long period, and the peak pressure remains relatively constant for a given initial air volume and upstream driving head. When the orifice size is very large, the air cushioning effect vanishes and the water column can easily impact on the pipe end, inducing a waterhammer impact pressure. In this case, the maximum pressure decreases with increasing orifice size, since for the larger orifice sizes, water escapes and mitigates the

waterhammer effect. For intermediate orifice sizes, the pressure oscillation pattern consists of both long period pressure oscillations (while the air pocket persists) followed by short period pressure oscillations (once waterhammer dominates). In this case, the maximum observed pressures increase rapidly with increasing orifice size, since the cushioning effect of the air pocket decreases as the air release rate increases. The highest maximum pressures (up to fifteen times that of the upstream head) were observed at the upper limit of this intermediate region, which occurs at a fairly consistent orifice size.

The analytical model presented here integrates the computation of air pocket pressure and air release pressure in a rapidly filling horizontal pipe, providing a single model capable of handling all three types of behavior. If the friction factor and the wave speed are known, the model is satisfactory in determining the amplitude of the peak pressure for the entire orifice range and is able to approximately simulate the pressure oscillation pattern of Type 1 behavior, the case of a negligible waterhammer impact effect. Although the model is unable to simulate the pressure oscillation pattern when the air release is substantial, it can predict the type of pressure oscillation behavior and the peak pressure.

A photographic study was conducted to explore the validity of the assumptions made in our analytical model for the simulation of flow transients in a rapidly filling horizontal pipe containing trapped air. The actual air-water interface shape and the nature of the air entrainment, as well as their effects on the pressure oscillation patterns were explored. The observations indicated that, if the pipe end is sealed or the orifice size is small, the water column contains a negligible amount of entrained air and approaches the pipe end along the bottom. The air trapped on top of the water acts as a shock

absorber; therefore, the overall pressure oscillation pattern has a long period. The observations further indicated that, if the orifice is large, the water column is highly air entrained and the water front is steep. In this case, the air release is significant and there is no visible air pocket trapped on top of the flow by the time that the water column reaches the pipe end. Without the trapped air pocket, the air cushioning effect vanishes and the water column can easily slam into the pipe end and induce a sharp and short period waterhammer pressure. It was also observed that, if the orifice is not large enough to allow for a significant air release, the water front contains a moderate amount of air and is steeper than that observed in the small air release case. After the water reaches the pipe end, some air is still trapped within the flow as bubbles or pockets whose random behaviors cause the pressure oscillation to have a long period, irregular pattern. When the last air pocket is released, the sharp and short period water impact pressure dominated, although the peak magnitude was mitigated by the earlier air cushioning effect.

7.1.2 Rapidly filling horizontal pipe which is partially full

For small air release situations, the maximum pressure magnitudes increase with the tailwater depth because the initial air volume is reduced. If the orifice is large, the tailwater is disturbed especially when the initial water column length is short; therefore air pockets are trapped and the orifice may be choked, resulting a lower water impact pressure on the pipe end. Both dry-front and surge models can simulate the maximum pressure magnitudes for the situations in which the tailwater is less disturbed by the filling surge front.

7.1.3 Rapid filling horizontal-vertical pipeline

The mitigative effect of a vertical pipe on pressure transients induced by trapped air pockets in rapidly filling L-pipe was investigated. It was found that the L-pipe system does not qualitatively alter the pressure oscillation pattern and maximum peak pressure magnitude and the gravity effect on reducing the pressure is obvious only when the initial water column is long and the air release from the vertical pipe is substantial. A comparison between the measured and calculated results indicates that the rigid water column method is able to simulate the rapid filling of an L-pipe system when there are air pockets trapped in the pipe.

The mitigative effect of a vertical pipe on pressure transients induced by trapped air pockets in a rapid filling T-pipe system was also investigated and the T-pipe configuration was shown to be able to mitigate the pressure surge during rapid filling, and was found to be especially effective in reducing the impact pressure when the air release was large. The proposed analytical model is able to simulate the maximum pressure magnitude in a T-pipe configuration when air pockets are trapped inside of the pipe. However, the model is unable to predict the pressure oscillation pattern under significant air release conditions because of the difficulty in quantifying the speed of pressure wave.

7.2 Surge Controls for Sewage Systems

The experimental results suggest that the pressure peaks due to trapped air pocket compression and release are certainly high enough to blow off manhole covers and explain sewer ruptures. For most manhole covers, the air leakage is negligible ($d/D \approx$

0.002), so, based on the observed results, a conservative estimate of the peak pressure (3 times the upstream head) would be 400 to 500 kPa (60 to 75 psi). This is at least one order of magnitude greater than the structural loads that typical urban sewer systems are designed for.

There are many ways to reduce or control large pressure transients in drainage systems. It is known from our modeling and experimental studies that the air-induced pressure is severe only when all of the following conditions are satisfied:

- a) The filling is rapid or the flow backup is intensive and fast;
- b) The air is able to be trapped;
- c) There are exits for air release and the size of the exits are intermediate.

Based on these conditions, the following measures are recommended:

To **reduce the risk of flow backup and rapid filling**, the inflow rate should be reduced by appropriate inlet controls. The dimensions of sewer pipes should be enlarged if economically possible. In-line and off-line storage devices should be constructed. Adequate standby power and sump storage for pumped systems should be provided. The design of interceptors and drop-inlets should consider energy dissipation. The systems should be well maintained to prevent clogging.

To **reduce the entrapment in pipelines**, air vents should be placed in the crown of conduits to release the air moving along the crown of the conduit. The variation of pipe section should be smoothly transitioned, and the changes in section areas should not be large (i.e. the difference of pipe sizes of the adjacent segments should not be too big).

To **reduce the air release pressure**, a surge tank or air chamber should be upstream of the surge location. The size of the air release valve should be carefully determined to avoid high impact pressure.

From the planning and design points of view, great attention should be paid to the locations where the air-related pressure surges are likely to occur since air entrapment and air release are local events. Usually the downstream end of the sewer system (Fig. 7.1.a) or dead ends formed by the sewer stubs (Fig. 7.1.b) should be carefully planned and designed since these are the areas in which surge-events are likely. Appropriate junction design in these areas is significant in reducing pressure surges.

With respect to the concern of system response to air pressure transients, drainage sewer systems should be designed in such a manner that small disturbances in one reach will not be amplified upon entering a succeeding reach. The natural periods of adjoining reaches must be sufficiently different from each other.

7.3 Suggestions for Further Studies

In terms of experimental studies, different pipe lengths and sizes should be tested to further verify the analytical model. The experimental investigations have some constraints which may limit the application of the experimental results, such as the use of single pipe diameter and material, which prevented the investigation of the effects of pressure wave speed on the flow transients. Also under larger diameter conditions, the water-air relation may be different from that under small pipe conditions. In addition, the effects of pipe support, pressure head adjustment in the pressure tank, orifice condition, water quality, temperature, etc. should be investigated further.

Further efforts on the study of rapidly filling L-pipe and T-pipe systems should also be made; in particular: (1) different vertical pipe sizes, lengths, and locations should be tested; (2) the variation of the speed of pressure wave during rapid filling conditions should be intensively investigated; (3) energy loss at junctions during rapid filling should be investigated; and (4) mechanisms of air-water release at junctions should be explored.

The proposed rigid water column model is unable to predict the pressure response after the air is released. The remedy is developing a rigid-elastic hybrid method which could use the rigid column method before the water column reaches the orifice and the compressible flow model after that.

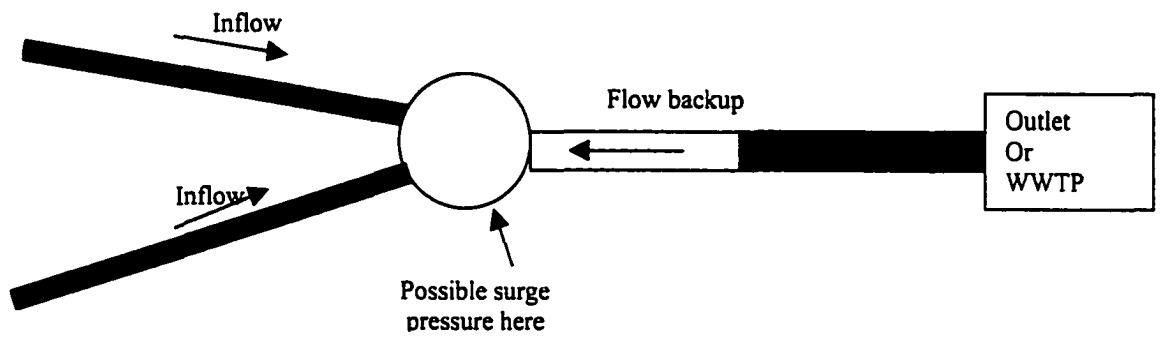


Fig. 7.1.a Possible Scenario of Air Release Pressure – Flow Backup

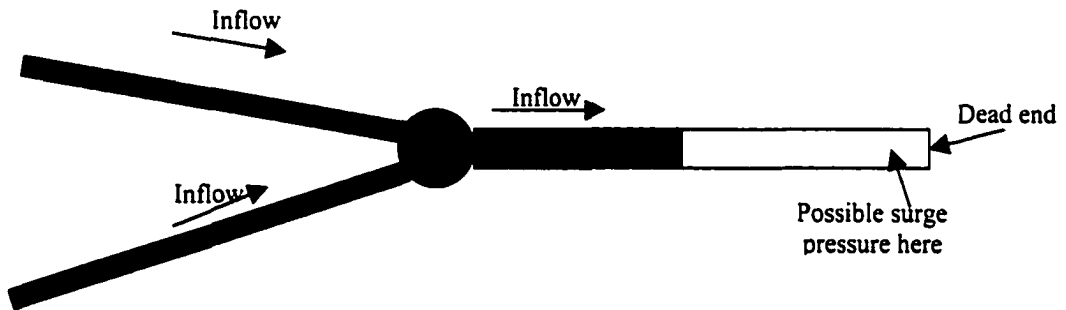
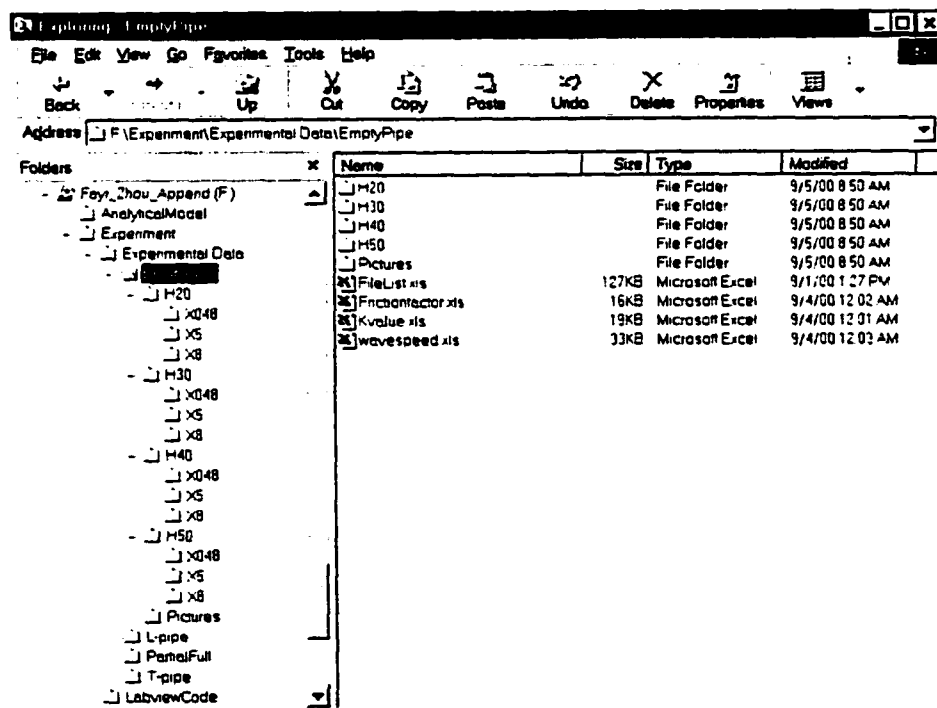


Fig. 7.1.b Possible Scenario of Air Release Pressure – Rapid Filling to a Dead End

8.0 APPENDIX – CD-ROM

8.1 What's on the CD-ROM

This thesis's CD-ROM includes the sources code of analytical model, original data files generated from LabView data acquisition program, as well as the LabView 4.0 program for data acquisition. This appendix provides a brief overview of the contents of the CD-ROM. For a more detailed look at any of these parts, load the CD-ROM and browse the content. The following picture shows the structure of the CD-ROM.



8.2 Analytical Model

The folder *AnalyticalModel* contains some Fortran 77 source code and Microsoft Excel (version 97) spreadsheets which were used to simulate different test

configurations. Please open the 'readme' file using *WordPad* or *Microsoft Word/97* before looking into any of these programs.

8.3 Experimental data

The folder */Experiment* contains two sub-folders: (a) *Experimental Data*, and (b) *LabViewCode*. Each are discussed below. Under '*Experimental Data*', there is complete set of pressure history files collected during the experiments. The files are grouped into subfolders by the tested configurations described in the thesis (e.g. empty pipe, L-pipe, partially full, and T-pipe, etc.). In each subfolder, there is a table (*Microsoft Excel/97* format) which lists the file names and the corresponding test cases. The data files can be opened using *Wordpad*, *Microsoft Word/97*, or *Microsoft Excel/97*.

In the folder entitled '*EmptyPipe*', the file '**FileList.xls**' provides the file names and the corresponding test cases. The file '**Frictionfactor.xls**' provides the measured friction factors. The file '**Kvalue.xls**' provides the measured values of minor loss of the valves. The file '**wavespeed.xls**' provided the measured values of speed of pressure wave. The subfolders '*H20*' through '*H50*' represent upstream driving heads of 20 psi to 50 psi, respectively. Within each driving head folder, there are three subfolders of *x048*, *x5* and *x8*, which represent the different initial water column lengths.

Pictures of air-water interface taken with a high speed camera are provided are listed in the folder entitled '*Pictures*'. The file '**FileNameList**' lists the picture file names and the corresponding test case. These picture files can be opened by *Microsoft Photo Editor 3.0*.

The folder entitled '*LabviewCode*' contains the LabView 4.0 program which was used in these experiment. Because of license restrictions, only the main VI is provided. Users must have Labview 4.0 program installed in their own computers if they want to open this file.

8.4 Declaration

By opening the CD-ROM package, you agree to be bound by the following:

Some of the software with this CD-ROM may be copyrighted; in which case all rights are reserved by the respective copyright holder. You are licensed to use software copyrighted by the author on a single computer.

You may not copy or redistribute the entire CD-ROM as a whole. Copying and redistribution of individual software program on the CD-ROM is governed by terms set by individual copyright holders.

The author states the information in this CD-ROM is true based on the author's actual knowledge. The user should also acknowledge that this is not warranty of any kind by the author.